UNIVERSITY OF CALIFORNIA SAN DIEGO

Cascades, Spectra, Real Space Structure, Inhomogeneous Mixing and Transport in Active Scalar Turbulence

A dissertation submitted in partial satisfaction of the
requirements for the degree
Doctor of Philosophy

in

Physics

by

Xiang Fan

Committee in charge:

Patrick H. Diamond, Chair
Luis Chacón
Alexander Groisman
Stefan G. Llewellyn Smith
Massimo Vergassola
William R. Young

2019

The dissertation of Xiang Fan is approved, and it is acceptable in quality and form for publication on microfilm and electronically:

_____

_____

_____

_____

_____

_____

Chair

University of California San Diego

2019

DEDICATION

To my parents Yongxia Zhou and Junbo Fan.

EPIGRAPH

And God said,

$$\nabla \cdot \mathbf{E} = 4\pi\rho$$

$$\nabla \cdot \mathbf{B} = 0$$

$$\nabla \times \mathbf{E} = -\frac{1}{c}\frac{\partial \mathbf{B}}{\partial t}$$

$$\nabla \times \mathbf{B} = \frac{1}{c}(4\pi\mathbf{J} + \frac{\partial \mathbf{E}}{\partial t})$$

and there was light.

—Physicists

TABLE OF CONTENTS

LIST OF FIGURES

LIST OF TABLES

ACKNOWLEDGEMENTS

This work would not have been possible without the help from my advisor, Prof. Patrick H. Diamond. Pat is extremely knowledgeable in the field of theoretical plasma physics, as well as other areas beyond physics, and he guided me the directions of my studies during my PhD study. Pat has spent an enormous amount of time with me discussing the research results, polishing my papers, and improving my talks. He is very hard-working and has high standard of work, and I see him as my exemplar. I am also grateful that I am given the chance to visit China for one or two months per year because Pat has partnerships with institutes in China. This was very important to me because my wife lived in China during the first 4 years of my PhD journey.

I would like to thank Dr. Luis Chacón and Dr. Hui Li in Los Alamos National Lab for the help with the simulation code. I also thank other committee members, Prof. William R. Young, Prof. Stefan Llewellyn Smith, Prof. Massimo Vergassola, and Prof. Alexander Groisman, for the invaluable comments and suggestions on my thesis research.

I am grateful to all my colleagues and friends discussed research with me. Special thanks goes to Dr. Jiacong Li and Dr. Rongjie Hong, from whom I really learned a lot. My sincere thanks also go to Dr. Mikhail Malkov, Dr. Rima Hajjar, Chang-Chun Chen, Robin Heinonen, Dr. Rameswar Singh, Prof. Zhibin Guo, Prof. Yosuke Kosuga, and Dr. Deng Zhao. I thank you all for supporting my research.

Nobody has been more important to me in the pursuit of the PhD degree than my wife Dr. Jingyi Xi. We lived in two cities that are 6,359 miles away from each other during my first 4 years of PhD journey, but our love is not beaten by the distance. Whenever I was upset or depressed, she can always make me recover. I really appreciate her understanding, support, and encouragement.

Finally, I would like to thank my parents, Yongxia Zhou and Junbo Fan, who are always supportive in my career in academia. I appreciate their understanding of my few visits due to the busy lifestyle as a PhD student.

Chapter 2 is a reprint of the material as it appears in X. Fan, P.H. Diamond, L. Chacón, H. Li, "Cascades and spectra of a turbulent spinodal decomposition in two-dimensional symmetric binary liquid mixtures", *Phys. Rev. Fluids*, 1 (5), 054403, 2016. The dissertation author was the primary investigator and author of this paper.

Chapter 3 is a reprint of the material as it appears in X. Fan, P.H. Diamond, L. Chacón, "Formation and evolution of target patterns in Cahn-Hilliard flows", *Phys. Rev. E (Rap. Comm.)*, 96 (4), 041101, 2017. The dissertation author was the primary investigator and author of this paper.

Chapter 4 is a reprint of the material as it appears in Xiang Fan, P.H. Diamond, L. Chacón, "Spontaneous transport barriers quench turbulent resistivity in two-dimensional magnetohydrodynamics", *Phys. Rev. E (Rap. Comm.)*, 99 (4), 041201, 2019. The dissertation author was the primary investigator and author of this paper.

The research presented in this dissertation was supported by the US Department of Energy, Office of Science, Office of Fusion Energy Sciences, under Award No. DE-FG02-04ER54738 and CMTFO Award No. DE-SC0008378.

VITA

2013	B. S. in Physics, Peking University, Beijing, China
2019	Ph. D. in Physics, University of California San Diego

PUBLICATIONS

Xiang Fan, P.H. Diamond, L. Chacón, H. Li, "Cascades and spectra of a turbulent spinodal decomposition in two-dimensional symmetric binary liquid mixtures", *Phys. Rev. Fluids*, 1 (5), 054403, 2016.

Xiang Fan, P.H. Diamond, L. Chacón, "Formation and evolution of target patterns in Cahn-Hilliard flows", *Phys. Rev. E (Rap. Comm.)*, 96 (4), 041101, 2017.

Xiang Fan, P.H. Diamond, L. Chacón, "CHNS: A case study of turbulence in elastic media", *Physics of Plasmas*, 25 (5), 055702, 2018.

Xiang Fan, P.H. Diamond, L. Chacón, "Spontaneous transport barriers quench turbulent resistivity in two-dimensional magnetohydrodynamics", *Phys. Rev. E (Rap. Comm.)*, 99 (4), 041201, 2019.

ABSTRACT OF THE DISSERTATION

Cascades, Spectra, Real Space Structure, Inhomogeneous Mixing and Transport in Active Scalar Turbulence

by

Xiang Fan

Doctor of Philosophy in Physics

University of California San Diego, 2019

Patrick H. Diamond, Chair

An active scalar system refers to a system with a scalar field that is coupled to the fluid dynamics and gives feedback to the velocity field through local forces. Active scalar turbulence systems are ubiquitous, and the study of these systems is a central focus of research in theoretical plasma physics. As examples, the 2D Cahn-Hilliard Navier-Stokes (CHNS) system and 2D Magnetohydrodynamics (MHD) system are studied in this dissertation.

The similarities and differences between 2D CHNS and 2D MHD are discussed. These are both elastic (i.e., self-restoring) systems, and display a memory, governed by freezing-in laws. The CHNS system supports an elastic wave, which is analogous to Alfven wave in MHD.

Cascades and spectra in 2D CHNS are investigated, with focus on the interaction between inverse and forward cascades. The inverse cascade of mean square concentration $\langle \psi^2 \rangle$, which is closely related to the real space dynamics of blob formation and merger, is found to be the dominant nonlinear transfer process. The spectrum of $\langle \psi^2 \rangle_k$ exhibits a scaling law of $\sim k^{-7/3}$, and this exponent is the same as the corresponding one in 2D MHD. On the other hand, the kinetic energy spectrum follows $E_k \sim k^{-3}$. This exponent is closer to that for 2D Navier-Stokes, instead of that for 2D MHD. We suggest this is because the restoring force is significant only in the interfacial regions. The packing fraction of interfacial regions is small because of the formation and merger of blobs. This suggests that the inverse cascade of $\langle \psi^2 \rangle$ - related to blob coalescence - modifies the forward cascade in 2D CHNS.

The evolution of the concentration field of the Cahn-Hilliard system in the background of a single eddy is studied. This is analogous to the flux expulsion phenomenon in 2D MHD. Though the system is simple, complex evolution is observed. 3 stages are observed: the "jelly roll" pattern stage, the stage of topological evolution, and the "target" pattern stage. The target pattern is metastable, as the bands gradually merge with time.

We also study turbulent transport in active scalar systems. We intended to first explore the classic problem of the suppression of turbulent transport in 2D MHD as an exercise in code verification, and then move to 2D CHNS. However, novel blob-and-barrier real space structures were observed with higher magnetic Reynolds number Rm in 2D MHD. We argue that the conventional approach of mean field theory is not applicable for the case without an external large scale magnetic field. The magnetic energy is observed to be concentrated in the intermittent, thin transport barrier regions, which located in the interstices between blobs of magnetic potential. The turbulent transport is quenched primarily because of these barriers. Barrier formation is linked to the inverse cascade of mean square magnetic potential $\langle A^2 \rangle$ and negative turbulent resistivity. For small scale forcing, spontaneous formation of layering occurs.

More generally, we demonstrate that synergistic studies of related but different systems

– 2D CHNS and 2D MHD – can lead to improved understanding. These studies can provide insights for all active scalar turbulence systems, since these systems share important common properties such as memory, elastic waves, and conservation laws.

Chapter 1

Introduction

1.1 Turbulence

Turbulence is a ubiquitous phenomenon occurring in continua (gas, liquid, or plasma). In contrast to the case of a laminar flow, a marker particle in a turbulent flow moves in a seemingly irregular way. Turbulence is generally considered as *the* major unsolved problems of classical physics. The Navier-Stokes Equation is the governing equation for the motion of viscous gas and liquid, and is the most fundamental and intensively studied equation that can exhibit turbulence phenomenon. Before discussing the turbulence in active scalar systems, let us first review some of the basics of the turbulence in the Navier-Stokes system.

The Navier-Stokes Equation is:

$$\partial_t \mathbf{v} + \mathbf{v} \cdot \nabla \mathbf{v} = -\frac{1}{\rho} \nabla p + \nu \nabla^2 \mathbf{v} + \mathbf{f} \tag{1.1}$$

where $\mathbf{v}$ is velocity, ρ is density, p is pressure, ν is viscosity, and $\mathbf{f}$ is an external forcing term. Reynolds Number Re is the dimensionless number which characterizes the state of the system, and is defined by $\mathrm{Re} \equiv lv/\nu$ where l is the relevant length scale and v is characteristic velocity. When Re is greater than a threshold, the flow becomes turbulent.

The Navier-Stokes Equation may seem simple at first glance, yet mathematicians still can not even prove whether or not the 3D Navier-Stokes Equation always has a smooth solution, given an initial velocity field. Indeed, this is one of the seven Millennium Prize Problems stated by the Clay Mathematics Institute in 2000 [14]. Whoever can prove it can win the $1 Million prize - which should be increased, on account of inflation. One reason why this problem is so hard is because a solution of the Navier-Stokes Equation generally involves turbulence.

Although there is no rigorous mathematical tool with which to fully understand turbulence, physicists still made progress in understanding some of its properties [35]. In 1941, Kolmogorov developed a model (the so called K41 theory) of a fluid with high Re, based on Richardson's idea of "cascade" [58]. Kolmogorov made two assumptions for turbulent flows satisfying 3D Navier-Stokes Equation with high Re, namely that: (1) the eddies are statistically isotropic on small scales, and (2) the small scale physics is determined by only viscosity ν and energy dissipation rate ε. The dissipation length scale is then calculated to be $\eta = (\nu^3/\varepsilon)^{1/4}$. Turbulent flows contain a broad dynamic range of eddies. In a cascade, a larger size eddy decays into smaller ones. These eddies then break up into even smaller ones, and so on, until they reach the dissipation scale η. The range between dissipation scale η and relevant characteristic length scale L is referred to as inertial range $\eta < l < L$. The energy passes from large scale eddies to small scale ones in the inertial range, and only dissipates on the scale of η. This transfer process is called the energy cascade. Based on the assumptions and model above, Kolmogorov obtained the energy spectrum:

$$E_k = C\varepsilon^{2/3}k^{-5/3} \tag{1.2}$$

where C is a universal constant. This famous result - the spectral exponent $-5/3$ - was later verified by simulations and experiments. Another great achievement in K41 theory is the $4/5$ law: in the limit of infinite Re, the third order structure function in a fully developed turbulence is given by $\langle(\delta v_{\parallel}(l)^3\rangle = -\frac{4}{5}\varepsilon l$. This is one of the few results in 3D Navier-Stokes turbulence that is both exact (i.e. no adjustable parameter) and nontrivial. Of course, there is more physics beyond

K41 theory, such as intermittency phenomena.

The 2D Navier-Stokes system has many features in common with systems in strongly magnetized plasmas, and therefore is of particular interest for plasma physicists. It is interesting that, turbulent flows in the 2D Navier-Stokes system behave significantly differently from those in 3D [61, 10]. There are two quadratic conserved quantities: energy $E = \frac{1}{2}\int \mathbf{v}^2 \, \mathrm{d}x^2$ and enstrophy $\Omega = \frac{1}{2}\int |\nabla \times \mathbf{v}|^2 \, \mathrm{d}x^2$. As a result, coexisting (dual) cascades occur in 2D, in contrast to only one forward energy cascade in 3D. One 2D cascade is the inverse energy cascade. It is called "inverse" because the energy is transferred from small scale to large scale, opposite to the direction of that in 3D. The other cascade is the direct/forward enstrophy cascade. If the external forcing is injected at intermediate scale k, then the energy spectrum contains two parts: the inverse cascade range and the forward cascade range. For the inverse cascade range $k \ll k_f$, the energy spectrum is $\sim k^{-5/3}$, assuming a scale-independent energy flux as in 3D; and for the forward cascade range $k \gg k_f$, the energy spectrum is $\sim k^{-3}$, assuming a constant enstrophy flux.

Turbulence can be studied by simulations. In order to obtain the complete information of the velocity field, a direct numerical simulation (DNS) is required for a turbulent flow, which refers to a simulation directly solving Navier-Stokes without further modelling. DNS is computationally expensive due to the large range of length scales and time scales involved. The whole inertial range, from dissipation scale η to system size L, needs to be resolved in DNS. This requires the minimum number of mesh points to be $N^3 \geq \mathrm{Re}^{9/4}$ for 3D DNS, and $N^2 \geq \mathrm{Re}^{3/2}$ for 2D DNS. Considering the time resolution requirement, the total CPU hours needed for a DNS is $\propto \mathrm{Re}^3$ for 3D and $\propto \mathrm{Re}^{9/4}$ for 2D. Therefore, it is usually very costly to do DNS for fluids with large Re, and large scale parallel computing is usually involved [82].

1.2 Active Scalar Turbulence

A passive scalar turbulent system refers to a scalar field which evolves according to the flow's motion, but does not give feedback to the flow [91]. In contrast, an active scalar turbulent system is a system where the scalar field can affect the fluid motion via feedback. Active scalar turbulence systems can exhibit more interesting properties as compared with the pure Navier-Stokes turbulence. This is because in active turbulence, *waves* usually play an important role, in addition to eddies.

Active scalar turbulence is one of the central topics in theoretical plasma physics. Examples of active scalar system in plasma include: 2D Magnetohydrodynamics (MHD) and its close relative, reduced MHD. Many important models in strongly magnetized plasmas are generalizations of reduced MHD, including: ballooning coupling [22, 48], the Hasegawa-Wakatani system, and related system for drift wave and ITG turbulence [43, 44, 63, 64, 69]. In plasma physics, active scalar systems are natural results of the modelling process to simplify the Braginsky system [11] for case of strong magnetization and weak compression. These systems are widely used to model the plasmas in Tokamaks, so the understanding of these systems is important in fusion energy researches. The equations for 2D MHD, as an example, is shown in the next subsection. These active scalar systems have the generic structure of: (1) a vorticity equation, with a coupling to the scalar because of $\mathbf{j} \times \mathbf{B}$ force; (2) one or more scalar advection equations. Many of the active scalar systems in plasma physics exhibit elasticity, due to a *memory*, which originates from the freezing-in law for magnetic fields. Apart from plasma physics, active systems are also ubiquitous elsewhere. Examples include the Cahn-Hilliard Navier-Stokes (CHNS) system, flow with polymers, flow with bubbles, and many other systems.

2D MHD and 2D CHNS will be discussed in introduced in the following subsections. Then we will discuss some physics questions in active scalar turbulence systems.

1.2.1 2D MHD

One of the simplest but important active scalar system in plasma physics is 2D Magnetohydrodynamics (MHD). MHD describes the macroscopic behavior of plasmas, and is widely used to model the plasmas in Tokamak, in astrophysics (in the sun, in interplanetary medium, etc.), and in geophysics (for example, in the Earth's magnetic field).

The 2D MHD equations read:

$$\partial_t A + \mathbf{v}\cdot\nabla A = \eta\nabla^2 A \tag{1.3}$$

$$\partial_t \omega + \mathbf{v}\cdot\nabla\omega = \frac{1}{\mu_0\rho}\mathbf{B}\cdot\nabla\nabla^2 A + \nu\nabla^2\omega \tag{1.4}$$

$$\mathbf{v} = \hat{\mathbf{z}}\times\nabla\phi,\ \omega = \nabla^2\phi \tag{1.5}$$

$$\mathbf{B} = \hat{\mathbf{z}}\times\nabla A,\ j = \frac{1}{\mu_0}\nabla^2 A \tag{1.6}$$

where A is the scalar magnetic potential (note that A is a scalar in 2D but is a vector in 3D), $\mathbf{B}$ is magnetic field, j is current, ϕ is stream function, ω is vorticity, η is resistivity, ν is viscosity, and $\mu_0\rho$ is magnetic permeability and density. The first equation is a simple diffusion equation for A, and the scalar A affects the motion of the fluid via the $\frac{1}{\mu_0\rho}\mathbf{B}\cdot\nabla\nabla^2 A$ term, which comes from the $\mathbf{j}\times\mathbf{B}$ force. The two characteristic dimensionless parameters in MHD are the Reynolds number Re and the Magnetic Reynolds number $\mathrm{Rm}\equiv lv/\eta$.

The basic elements in MHD turbulence are eddies and waves, in contrast to the Navier-Stokes system which only contains eddies but not waves. The most important wave in MHD turbulence is the Alfvén wave, with the dispersion relation $\omega_{\mathbf{k}} = k_{\|}v_A$ where $v_A = \sqrt{B^2/4\pi\rho}$.

In MHD, in the limit of $\eta = 0$, magnetic field lines are frozen into the fluid and have to move along with it. This constraint is called Alfvén's Theorem, i.e. "freezing-in law". This has profound impact on the evolution of the fields and renders MHD distinct from the Navier-Stokes system, because "memory" appears due to Alfvén's Theorem. A system is said to have "memory"

if the instantaneous value of the field reflects the *time history* of the fluid motions acting on it, in contrast to the situation of a Markov process, where the present is affected by only 1 time step's worth of the past.

In 3D MHD, if the magnetic field is strong and almost uniform along one direction, i.e. $\mathbf{B_0} = -B_0\hat{\mathbf{z}}$, then the 3D MHD equations can be reduced to a 2D system with an externally imposed magnetic field. This is called reduced MHD [27]:

$$\partial_t A + \mathbf{v}\cdot\nabla A = \eta\nabla^2 A + B_0\frac{\partial\phi}{\partial z} \tag{1.7}$$

$$\partial_t \omega + \mathbf{v}\cdot\nabla\omega = \frac{1}{\mu_0\rho}\mathbf{B}\cdot\nabla\nabla^2 A + B_0\frac{\partial}{\partial z}\nabla^2 A + \nu\nabla^2\omega \tag{1.8}$$

$$\mathbf{v} = \hat{\mathbf{z}}\times\nabla\phi,\ \omega = \nabla^2\phi \tag{1.9}$$

$$\mathbf{B} = \hat{\mathbf{z}}\times\nabla A,\ j = \frac{1}{\mu_0}\nabla^2 A \tag{1.10}$$

Reduced MHD is an important system in the field of magnetically confined plasmas. It is evident that reduced MHD and 2D MHD have similar structures - indeed, identical nonlinear structure. The study of 2D MHD can therefore gain insights into reduced MHD as well as other models in plasma physics based on reduced MHD.

1.2.2 2D CHNS

The Cahn-Hilliard Navier-Stokes (CHNS) equations describe the motion of a binary fluid undergoing spinodal decomposition. Spinodal decomposition is a second order phase transition for a binary fluid, which evolves from a miscible phase (such as water+alcohol) to an immiscible phase (such as water+oil). See Fig. 1.1 for illustration. Spinodal decomposition has applications in alloy manufacturing, because it provides a way to produce micro structure which enhances physical properties of the alloy [104]. More importantly, CHNS system is also of interest theoretically, because (1) it is one of the few phase transitions in solids for which there is

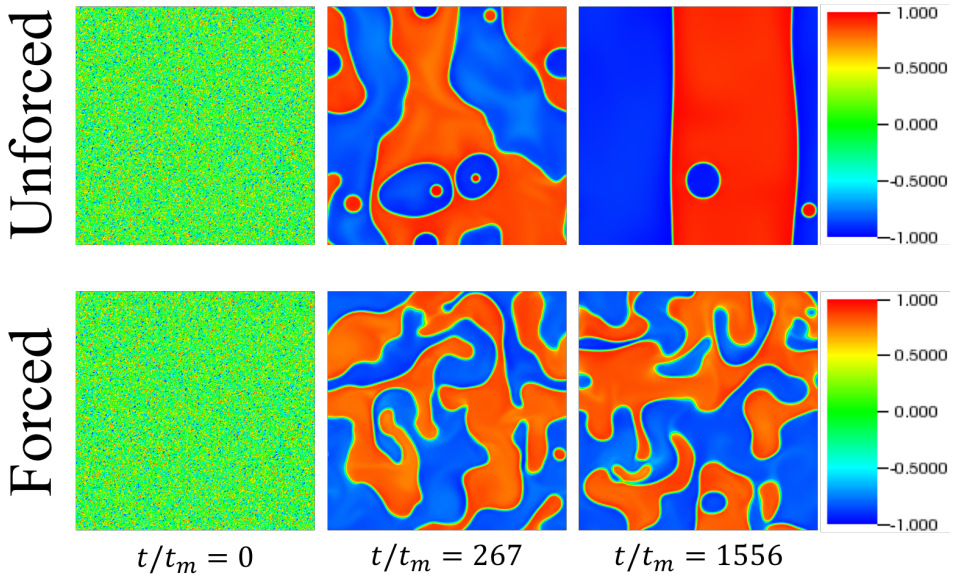

Figure 1.1: Some typical screenshots for the ψ field in the 2D CHNS system. Reprint from [30].

any plausible quantitative theory [104]; (2) it is an active scalar system which provides insights to related but different systems.

Let $\psi(\mathbf{x},t)$ be the relative concentration field $\psi \equiv \frac{\rho_1-\rho_2}{\rho_1+\rho_2}$ of the binary fluid ($\rho 1$ and $\rho 2$) undergoing spinodal decomposition, and its governing equation is the CHNS equations:

$$\partial_t \psi + \mathbf{v}\cdot\nabla\psi = D\nabla^2(-\psi+\psi^3-\xi^2\nabla^2\psi) \tag{1.11}$$

$$\partial_t \omega + \mathbf{v}\cdot\nabla\omega = \frac{\xi^2}{\rho}\mathbf{B}_\psi\cdot\nabla\nabla^2\psi + \nu\nabla^2\omega \tag{1.12}$$

$$\mathbf{v} = \hat{\mathbf{z}}\times\nabla\phi,\ \omega = \nabla^2\phi \tag{1.13}$$

$$\mathbf{B}_\psi = \hat{\mathbf{z}}\times\nabla\psi,\ j_\psi = \xi^2\nabla^2\psi \tag{1.14}$$

where D is diffusivity, ξ is a coefficient describing the strength of the surface tension interaction. Note that ψ ranges from -1 to 1 assuming the binary fluid is symmetric. The ψ field affects the fluid motion via the $\frac{\xi^2}{\rho}\mathbf{B}_\psi\cdot\nabla\nabla^2\psi$ term, which comes from the surface tension force.

In 2D, MHD and CHNS have many similarities. Here are the correspondences: the scalar

field $A \leftrightarrow \psi$ (and their derived quantities), the diffusion coefficient $\eta \leftrightarrow D$, and coupling strength $\frac{1}{\mu_0} \leftrightarrow \xi^2$. Apart from these obvious correspondences, these two systems are also analogous in deeper ways. The quadratic conserved quantities in 2D MHD are energy, mean square magnetic potential $\langle A^2 \rangle$, and cross helicity. In 2D CHNS, they are energy, mean square concentration $\langle \psi^2 \rangle$, and cross helicity, analogous to the ones in 2D MHD. These two systems both support a linear wave that is "springy". They are both elastic (i.e., self-restoring) systems, and both systems exhibit memory due to freezing-in laws. Of course, there are important differences as well. The range of ψ is limited, but there is no physics restriction on A. The real space structure is different, and the packing fraction for CHNS is significantly smaller, since the back reaction on fluid motion is limited to interfacial regions. The two systems are compared in detail in Chapter 2.

1.3 Some Challenges

There are many challenges to understanding active scalar turbulence. Some of the most prominent physics issues include: (1) the physics of dual (or multiple) cascades, (2) the nature of "blobby" turbulence, (3) the effects of negative diffusion/resistivity, and (4) the understanding of turbulent transport. They are discussed below.

The energy cascade is rather simple in the most familiar turbulence system, the 3D Navier-Stokes system. There is only one cascade, the energy cascade, in that system. If energy is injected at large scales, the energy cascades to small scale. However, there can be more than one cascades in active scalar turbulence systems, with forward or inverse directions. For example, in MHD, it is known that there are a forward energy cascade, and an inverse cascade of $\langle A^2 \rangle$ (2D) or $\langle \mathbf{A} \cdot \mathbf{B} \rangle$ (3D). The question is, which cascade is more fundamental? Can one cascade affect another? How? Previous studies focus mainly on the energy cascade in the inertial range, partly due to its being the natural extension of the K41 theory in the 3D Navier-Stokes system. However, the other cascade, the inverse cascade of $\langle A^2 \rangle$, may be at least equally important. In CHNS, we will show

there are also two cascades: a forward energy cascade, and an inverse cascade of $\langle \psi^2 \rangle$. Note that 2D CHNS and 2D MHD are analogous with respect to cascades and spectra. The inverse cascade in 2D CHNS is more robust, and can alter the forward energy cascade. Note that many important models of electromagnetic turbulence in magnetized plasmas are based on 2D MHD (or its close relative, reduced MHD), therefore such systems also support dual (or multiple) cascades and are relevant to the questions mentioned above.

"Blobby" turbulence refers to turbulence in which meso scale real space structures resemble blobs. Blobby turbulence is observed in the Scrap-Off Layer (SOL) in Tokamak and stellarator devices [9, 28, 36], and plays an important role in terms of dynamics and transport in SOL. There are numerous simulation studies of these, which yield many impressive color view graphs. However, some fundamental questions still remain to be investigated, such as: "What makes a blob a blob?" What sets the scale of the blobs? How do the blobs co-exist or interact with cascade processes? The CHNS system is a naturally blobby turbulent system. As we will show in later chapters, size of blobs in 2D CHNS grows, until limited by the balance of kinetic and elastic energy. As blobs grow, the active regions of elastic feedback on fluid reduce, and the power law of the energy spectrum is thus modified. The study of how the concentration field in the Cahn-Hilliard system evolves in the background of a single eddy can also give us insights into how blobs form and interact in that system. The blobby real space structures can also occur in 2D MHD, as will be discussed in Chapter. 4. We argue that the blob-and-barrier real space structure is closely related to the important phenomenon of why turbulent transport in 2D MHD is quenched, absent an external large scale magnetic field.

Negative diffusion (or negative resistivity) describes how the gradient of a field increases, instead of decays in a diffusive system [95]. It is usually related to bistability. Negative diffusion is a mechanism for the formation of macroscopic flow in turbulence. Zonal flow formation is one of the most important example of negative diffusion phenomenon in geophysics and plasma physics [25, 45]. The formation of zonal flow has some similarity to phase separation in

CHNS, see Fig. 1.2. The CHNS system is a natural system for the study of negative diffusion phenomena. In CHNS, a negative diffusion term appears explicitly in the original equations, along with a nonlinear term and a positive hyper-diffusion term. In 2D MHD, negative turbulent resistivity can also appear (for a short transition period), and lead to the formation of a large scale blob-and-barrier real space structure, and even layering.

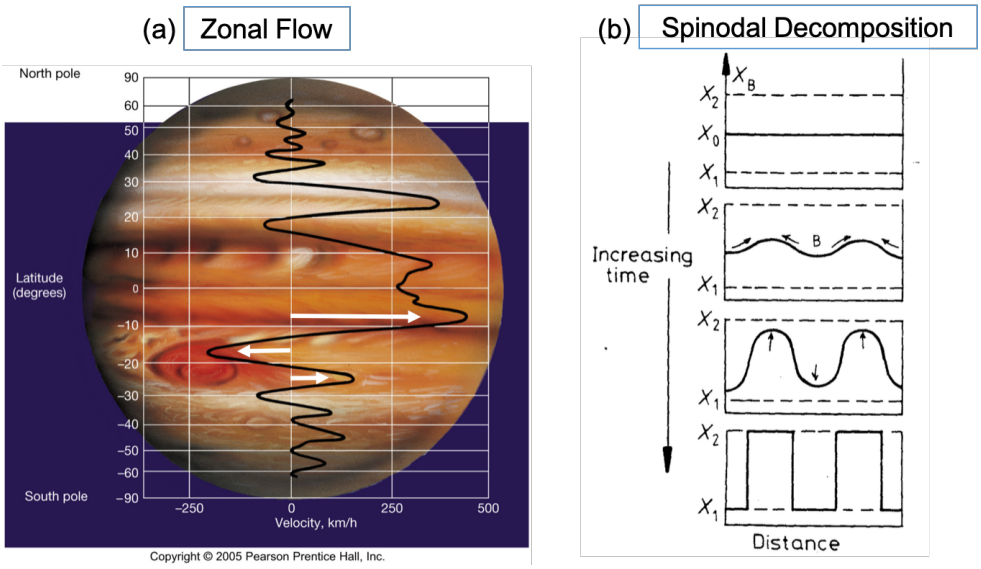

Figure 1.2: Zonal flow vs Spinodal Decomposition. (a) Zonal flow. The white arrows refer to the directions of flow. Copyright ©2005 Pearson Prentice Hall, Inc. (b) Spinodal Decomposition. The black arrows refer to the directions of ψ evolution. Reprint from [83]

Turbulent transport is an important topic for turbulent systems. In 2D MHD, the effect of small scale magnetic field on transport coefficients is found to be significant even for a very weak large scale magnetic field [16]. Turbulent transport of magnetic potential is suppressed, relative to the kinematic prediction. This type of analysis was extended to 3D MHD in order to understand the dynamo effect [25] (note that, strictly speaking, dynamo action does not exist in 2D MHD). However, the conventional mean field approach is not applicable to a newly discovered blob-and-barrier real space structure, as discussed in Chapter 4. How to understand this highly intermittent, inhomogeneous mixing is challenging.

Although 2D MHD and CHNS are simple, idealized systems, the study of the turbulence

in these systems illuminates all the challenges mentioned above, and provides general insights useful for the study of many other active scalar turbulent systems.

1.4 Overview of the Remaining Chapters

In this dissertation, we focus on three main topics: cascades and spectra in 2D CHNS, the evolution of Cahn-Hilliard system in the background of a single eddy, and the mechanism of transport suppression in 2D MHD. They will be discussed in Chapter 2-4, respectively. A summary and future work are discussed in Chapter 5.

In Chapter 2, cascades and spectra in turbulent 2D CHNS system are investigated. 2D MHD and 2D CHNS systems are compared in detail. The similarities include ideal quadratic conserved quantities and the directions of cascades. The $\langle \psi^2 \rangle$ inverse cascade in 2D CHNS is analogous to the $\langle A^2 \rangle$ inverse cascade in 2D MHD. The $\langle \psi^2 \rangle_k$ and $\langle A^2 \rangle_k$ spectra have the same $-7/3$ exponents in the two systems. However, the kinetic energy spectra have different scaling. The spectrum in 2D CHNS is more like that for 2D Navier-Stokes turbulence, than that for 2D MHD. We resolve this apparent puzzle by observing that the blob merger process tends to make the region of active feedback decrease, so the back reaction of surface tension is reduced. The evolution of packing fraction is studied.

In Chapter 3, the evolution of Cahn-Hilliard system in the background of a single eddy is analyzed. This study is inspired by, and is an analogue of, the classic study of flux expulsion in 2D MHD. It offers insights of how a scalar field with a negative diffusion, a nonlinear term, and a positive hyper-diffusion term interact with flow shear. A complex evolution process is observed. There are 3 stages: the "jelly roll" pattern stage, the stage of topological evolution, and a "target" pattern stage. The results indicate the target pattern is metastable: bands in the target pattern merge with time. The band merger process resembles the step merger in staircase models in plasma physics and elsewhere.

In Chapter 4, the suppression of turbulent transport in 2D MHD is studied. This topic is a classic problem, however, we found that the conventional approach, mean field theory, is not applicable to the case without an external large scale magnetic field. A novel blob-and-barrier structure is observed. Barriers are located in the interstices of blobs of magnetic potential field. Magnetic fields are highly concentrated in these one dimensional barrier regions. We call these regions barriers because we argue these regions are where transport is heavily suppressed. We propose that the formation of these barriers is due to negative resistivity which is originated from the inverse cascade of $\langle A^2 \rangle$. It is also observed that, for small scale forcing, a staircase (or layering) of the A field can spontaneously form in 2D MHD.

In Chapter 5, the key results of the chapters above are summarized, and possible future directions of study are discussed.

Chapter 2

Cascades and Spectra of a Turbulent Spinodal Decomposition in 2D Symmetric Binary Liquid Mixture

We study the fundamental physics of cascades and spectra in 2D Cahn-Hilliard-Navier-Stokes (CHNS) turbulence, and compare and contrast this system with 2D MagnetoHydroDynamic (MHD) turbulence. The important similarities include basic equations, ideal quadratic invariants, cascades and the role of linear elastic waves. Surface tension induces elasticity, and the balance between surface tension energy and turbulent kinetic energy determines a length scale (Hinze scale) of the system. The Hinze scale may be thought of as the scale of emergent critical balance between fluid straining and elastic restoring forces. The scales between the Hinze scale and dissipation scale constitute the elastic range of the 2D CHNS system. By direct numerical simulation, we find that in the elastic range, the mean square concentration spectrum H_k^{Ψ} of the 2D CHNS system exhibits the same power law $(-7/3)$ as the mean square magnetic potential spectrum H_k^A in the inverse cascade regime of 2D MHD. This power law is consistent with an inverse cascade of H^{Ψ}, which is observed. The kinetic energy spectrum of the 2D CHNS system

is $E_k^K \sim k^{-3}$ if forced at large scale, suggestive of the direct enstrophy cascade power law of 2D Navier-Stokes (NS) turbulence. The difference from the energy spectra of 2D MHD turbulence implies that the back reaction of the concentration field to fluid motion is limited. We suggest this is because the surface tension back reaction is significant only in the interfacial regions. The interfacial regions fill only a small portion of the 2D CHNS system, and their interface packing fraction is much smaller than that for 2D MHD.

2.1 Introduction

Binary liquid mixtures can pass spontaneously from one miscible phase to two coexisting immiscible phases following a temperature drop. This second-order phase transition is called a spinodal decomposition. The Cahn-Hilliard-Navier-Stokes (CHNS) model [13, 12] is the standard model for binary liquid mixture undergoing spinodal decomposition. The 2D CHNS system is as follows: (the definitions and derivation are discussed below)

$$\partial_t \psi + \mathbf{v} \cdot \nabla \psi = D\nabla^2(-\psi + \psi^3 - \xi^2 \nabla^2 \psi) \tag{2.1}$$

$$\partial_t \omega + \mathbf{v} \cdot \nabla \omega = \frac{\xi^2}{\rho} \mathbf{B}_\psi \cdot \nabla \nabla^2 \psi + \nu \nabla^2 \omega \tag{2.2}$$

$$\mathbf{v} = \hat{\mathbf{z}} \times \nabla \phi, \ \omega = \nabla^2 \phi \tag{2.3}$$

$$\mathbf{B}_\psi = \hat{\mathbf{z}} \times \nabla \psi, \ j_\psi = \xi^2 \nabla^2 \psi \tag{2.4}$$

Table 2.1: Comparison of 2D MHD and the 2D CHNS system.

	2D MHD	2D CHNS
Ideal Quadratic Conserved Quantities	Conservation of E, H^A and H^C	Conservation of E, H^Ψ and H^C
Role of elastic waves	Alfven wave couples $\mathbf{v}$ with $\mathbf{B}$	CHNS linear elastic wave couples $\mathbf{v}$ with $\mathbf{B}_\psi$
Origin of elasticity	Magnetic field induces elasticity	Surface tension induces elasticity
Origin of the inverse cascades	The coalescence of magnetic flux blobs	The coalescence of blobs of the same species
The inverse cascades	Inverse cascade of H^A	Inverse cascade of H^Ψ
Power law of spectra	$H_k^A \sim k^{-7/3}$	$H_k^\Psi \sim k^{-7/3}$

The definitions of the variables are discussed later in the paper. It is evident that this system is closely analogous to the 2D MagnetoHydroDynamics (MHD) model for plasmas:

$$\partial_t A + \mathbf{v}\cdot\nabla A = \eta\nabla^2 A \tag{2.5}$$

$$\partial_t \omega + \mathbf{v}\cdot\nabla\omega = \frac{1}{\mu_0\rho}\mathbf{B}\cdot\nabla\nabla^2 A + \nu\nabla^2\omega \tag{2.6}$$

$$\mathbf{v} = \hat{\mathbf{z}}\times\nabla\phi,\ \omega = \nabla^2\phi \tag{2.7}$$

$$\mathbf{B} = \hat{\mathbf{z}}\times\nabla A,\ j = \frac{1}{\mu_0}\nabla^2 A \tag{2.8}$$

Since 2D MHD turbulence has been well studied [27, 26, 84, 85, 17, 18, 8, 7, 6, 60, 50, 90, 68], it provides us with potential insight and guidance for exploring the physics of 2D CHNS turbulence. The comparison of 2D MHD and the 2D CHNS system is shown in Table 2.1, the details are discussed later in this paper.

The similarity between binary liquid mixture and 2D MHD was first discussed by Ruiz and Nelson [89]. They addressed only the regime when the binary liquid mixture is miscible, i.e. *above* the critical temperature. The governing equation for this regime is

$$\partial_t\psi + \mathbf{v}\cdot\nabla\psi = D\nabla^2\psi \tag{2.9}$$

In this limit, basically there is no difference from 2D MHD. However, the more interesting and challenging regime occurs when the binary liquid mixture undergoes spinodal decomposition, i.e.

below the critical temperature.

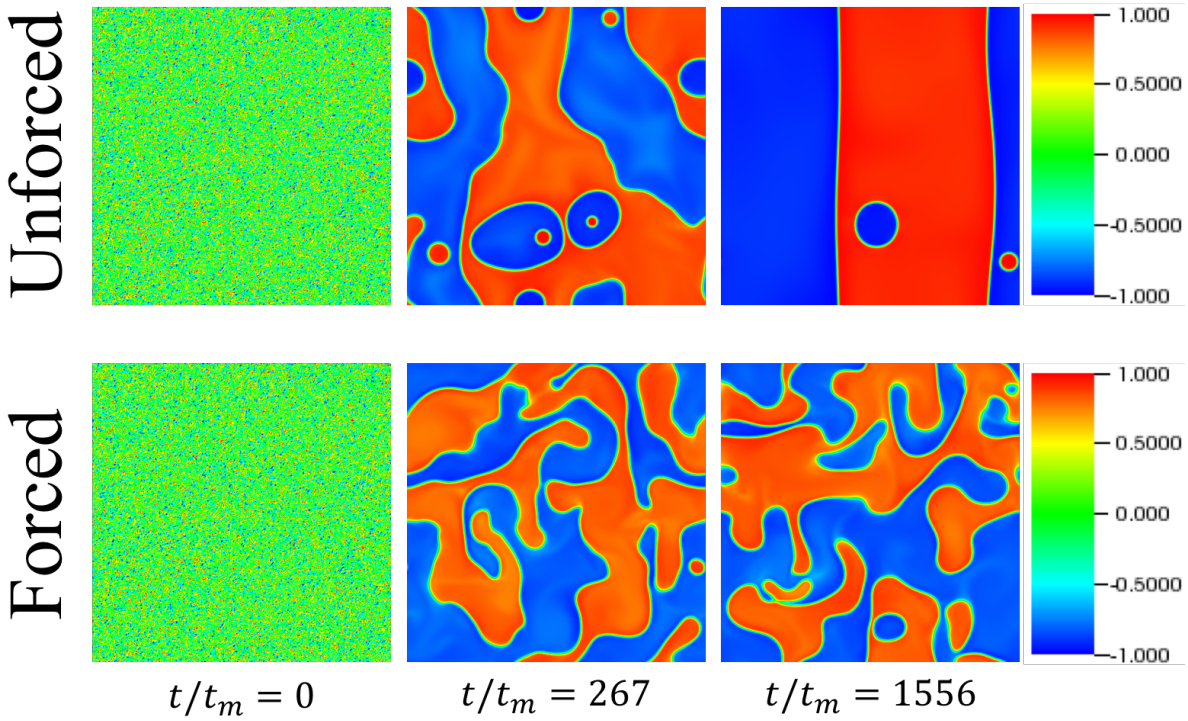

Figure 2.1: Top panels are pseudo color plots of ψ field for an unforced run (Run1) at various times; bottom panels are the ones for a forced run (Run4). Time t is normalized by the diffusive mixing time $t_m = \xi^2/D$.

When the binary liquid mixture is quenched below the critical temperature, spinodal decomposition occurs. Small scale blobs tend to coalesce and form larger blobs [55, 54, 4, 92], see Fig. 2.1 (top panel) for an illustration. The blob size grows as $L \sim t^{2/3}$ if unforced [37]. The length scale growth can be arrested by external fluid forcing, and an emergent characteristic length scale of the blob size is formed by the critical balance between turbulent kinetic energy and surface tension energy in 2D CHNS turbulence [5]. In 3D, the length scale growth is also arrested when proper external forcing is applied, and the emergent characteristic length scale of blob size is consistent with the Hinze scale: $L_H \sim (\frac{\rho}{\sigma})^{-3/5}\varepsilon^{-2/5}$ where ρ is density, σ is surface tension, and ε is the energy dissipation rate per unit mass [78, 79]. In the inverse energy cascade regime of the 2D CHNS system, the characteristic length scale is also consistent with the Hinze

scale [80].

Previous studies did not adequately separate the Hinze scale from the dissipation scale. We define the elastic range as the range of scales from the Hinze scale down to the dissipation scale. This is where the surface tension induced elasticity is important to the dynamics. The 2D CHNS system is more MHD-like in the elastic range. The power laws of the turbulent spectra in the elastic range were not investigated by previous studies.

In this study, we first describe the fundamental theory of spinodal decomposition in Sec. 2.2. In Sec. 2.3, we compare and contrast 2D CHNS with 2D MHD in terms of basic equations, ideal quadratic conserved quantities, cascades, and linear elastic wave. The concepts of the Hinze scale and the elastic range are explained in detail in Sec. 2.4. Next we use the PIXIE2D code [20, 19] to simulate the 2D CHNS system in Sec. 2.5. We focus on the turbulent spectra and cascades in the elastic range, and compare them with 2D MHD. Conclusions and discussions are presented in Sec. 2.6.

2.2 Governing Equations for Spinodal Decomposition

We consider spinodal decomposition in a symmetric (50%-50%) binary liquid mixture of equal density. Spinodal decomposition is a second-order phase transition, and so can be modeled by Landau theory.

The corresponding order parameter is the local relative concentration $\psi(\mathbf{x},t)$:

$$\psi = \frac{\rho_A - \rho_B}{\rho_A + \rho_B} \tag{2.10}$$

where ρ_A and ρ_B are the local densities of the two species. When $\rho_B = 0$, $\psi = +1$ implies an A-rich phase; when $\rho_A = 0$, $\psi = -1$ implies a B-rich phase. The range of ψ is thus $\psi \in [-1,1]$.

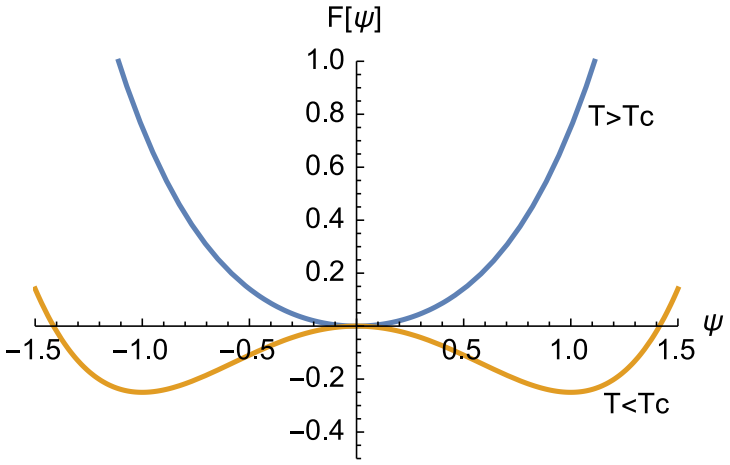

Figure 2.2: Free energy functional $F[\psi]$ for $T > T_c$ and $T < T_c$.

The free energy functional reads as:

$$F[\psi] = \int (\frac{1}{2}A\psi^2 + \frac{1}{4}B\psi^4 + \frac{\xi^2}{2}|\nabla\psi|^2)\,\mathrm{d}\mathbf{r} \tag{2.11}$$

where A and B are coefficients of a Taylor expansion, and ξ is a coefficient describing the strength of the surface tension interaction. ξ also characterizes the interfacial thickness. The first two terms characterize the second-order phase transition dynamics, while the last term is the curvature penalty. In Landau theory, B must always be greater than 0 for the system to be thermodynamically stable, while A can be either positive or negative, i.e.:

$$A = A_0(T - T_c) \tag{2.12}$$

where A_0 is some temperature independent constant, T is the temperature and T_c is the critical temperature for spinodal decomposition. As shown in Fig. 2.2, when $T > T_c$, $A > 0$, the free energy $F[\psi]$ has a "V" shape, so there is only one minimum at $\psi = 0$. When $T < T_c$, $A < 0$, the free energy $F[\psi]$ has a "W" shape, so there is one unstable maximum at $\psi = 0$, and two minima at $\psi = \pm\sqrt{-\frac{A}{B}}$. When the homogeneous phase of the binary liquid mixture is quenched down to below the critical temperature, the $\psi = 0$ phase becomes unstable because the system tends to

reach its minimal energy, and the system now prefers the $\psi = \pm\sqrt{-\frac{A}{B}}$ phases, implying phase separation. Because of the definition of ψ, the minimal energy should be reached when $\psi = \pm 1$, so we have $B = -A$. For simplicity, we study the isothermal case when the temperature is fixed below T_c, i.e. A is constant. Without loss of generality, we set $B = -A = 1$:

$$F[\psi] = \int (-\frac{1}{2}\psi^2 + \frac{1}{4}\psi^4 + \frac{\xi^2}{2}|\nabla\psi|^2)\,\mathrm{d}\mathbf{r} \tag{2.13}$$

The dynamics of the binary liquid mixture under spinodal decomposition is fully determined by this free energy functional. The chemical potential is

$$\mu = \frac{\delta F}{\delta \psi} = -\psi + \psi^3 - \xi^2\nabla^2\psi \tag{2.14}$$

According to Fick's Law $\mathbf{J} = -D\nabla\mu$ (where D is diffusivity) and the continuity equation $\mathrm{d}\psi/\mathrm{d}t + \nabla\cdot\mathbf{J} = 0$, we obtain the Cahn-Hilliard Equation:

$$\mathrm{d}\psi/\mathrm{d}t = D\nabla^2(-\psi + \psi^3 - \xi^2\nabla^2\psi) \tag{2.15}$$

The total derivative is $\mathrm{d}/\mathrm{d}t = \partial\psi/\partial t + \mathbf{v}\cdot\nabla$ when flow is present, where $\mathbf{v}$ is velocity. The fluid motion satisfies Navier-Stokes Equation, with an additional force term due to surface tension:

$$\partial_t\mathbf{v} + \mathbf{v}\cdot\nabla\mathbf{v} = -\frac{1}{\rho}\nabla p - \frac{\xi^2}{\rho}\nabla^2\psi\nabla\psi + \nu\nabla^2\mathbf{v} \tag{2.16}$$

Here ν is viscosity, p is pressure, and $\rho = \rho_A + \rho_B$ is density. The second term on the R.H.S. comes from the surface tension force, which has the from $-\frac{1}{\rho}\psi\nabla\mu$. This means that the force pushes two species in opposite directions, with a strength proportional to the gradient of the chemical potential. This surface tension force can be written in the form $-\frac{1}{\rho}\nabla(-\frac{1}{2}\psi^2 + \frac{3}{4}\psi^4 - \xi^2\psi\nabla^2\psi) - \frac{\xi^2}{\rho}\nabla^2\psi\nabla\psi$. The first part can be absorbed into the definition of pressure p, leaving the second part as in

Eq. (2.16). Finally, for 2D incompressible flow, $\nabla \cdot \mathbf{v} = 0$, so it is more convenient to take the curl of Eq. (2.16) and work with the vorticity equation.

To summarize, the governing equations for spinodal decomposition in 2D symmetric binary liquid mixture are the Cahn-Hilliard-Navier-Stokes (CHNS) equations: Eqs. (2.1) - (2.4), where ϕ is the stream function, ω is vorticity, and $\mathbf{B}_\psi$ and j_ψ are analogous to magnetic field and current in MHD, respectively, which will be discussed in the next section.

2.3 Comparison and contrast of 2D CHNS Turbulence and 2D MHD Turbulence

2.3.1 Basic Equations

The 2D CHNS system is an analogue to 2D Magnetohydrodynamics (MHD) in plasma physics. MHD turbulence is comparatively better understood due to several decades of extensive study. By comparison and contrast of 2D CHNS turbulence and 2D MHD turbulence, we can understand each more clearly.

The 2D MHD equations are Eqs. (2.5) - (2.8), where A is the scalar magnetic potential in 2D, $\mathbf{B}$ is magnetic field, j is current, η is resistivity, and μ_0 is magnetic permeability. Comparing Eqs. (2.1) - (2.4) and Eqs. (2.5) - (2.8), we immediately grasp the correspondence between these two systems, which is summerized in Table 2.2. Note that the surface tension force $\frac{\xi^2}{\rho}\mathbf{B}_\psi \cdot \nabla\nabla^2\psi$ in Eq. (2.2) and the $\mathbf{j} \times \mathbf{B}$ force $\frac{1}{\mu_0\rho}\mathbf{B} \cdot \nabla\nabla^2 A$ in Eq. (2.6) have the same structure.

The major difference is between the dissipation terms in Eq. (2.1) and Eq. (2.5). The CHNS equations contain a negative diffusivity term $-D\nabla^2\psi$, self nonlinear diffusivity term $D\nabla^2\psi^3$ and a hyper-diffusivity term $-\xi^2 D\nabla^2\nabla^2\psi$. The MHD equations only contain one (positive) resistivity term $\eta\nabla^2 A$. Another difference to notice is that the concentration ψ ranges from -1 to 1, limited by physics definition $\psi = \frac{\rho_A - \rho_B}{\rho_A + \rho_B}$. The magnetic potential A has no such

Table 2.2: The correspondence between 2D MHD and the 2D CHNS system.

	2D MHD	2D CHNS
Magnetic Potential	A	ψ
Magnetic Field	$\mathbf{B}$	$\mathbf{B}_\psi$
Current	j	j_ψ
Diffusivity	η	D
Interaction strength	$\frac{1}{\mu_0}$	ξ^2

restriction.

The CHNS system is more similar to MHD in 2D than in 3D, because magnetic potential A is a scalar in 2D, but is a vector in 3D. The concentration ψ is always a scalar, regardless of dimension.

2.3.2 Ideal Quadratic Conserved Quantities

The quadratic conserved quantities in the ideal system, which means $D, \eta = 0$ and $\nu = 0$ here, are important to the study of turbulent cascades. The real turbulent systems with finite dissipation are different from ideal systems, nevertheless, the ideal conserved quantities are still important constraints imposed on the nonlinear dynamics. In particular, the study of absolute equilibrium distributions of the ideal systems provides us indications of cascade directions.

It is known that there are 3 ideal quadratic conserved quantities in 2D MHD: total energy E (which is the sum of kinetic energy E^K and magnetic energy E^B), mean square magnetic potential H^A, and cross helicity H^C:

$$E = E^K + E^B = \int (\frac{\rho \mathbf{v}^2}{2} + \frac{\mathbf{B}^2}{2\mu_0}) \, \mathrm{d}^2 x \tag{2.17}$$

$$H^A = \int A^2 \, \mathrm{d}^2 x \tag{2.18}$$

$$H^C = \int \mathbf{v} \cdot \mathbf{B} \, \mathrm{d}^2 x \tag{2.19}$$

Note that H^A is not a conserved quantity in 3D MHD; instead, the magnetic helicity $H^B = \int \mathbf{A} \cdot \mathbf{B} \, \mathrm{d}^3 x$ is conserved.

When the dissipation is set to 0, the difference between the 2D CHNS system and 2D MHD disappears, so the ideal quadratic conserved quantities in the 2D CHNS system are the direct analogues of those in MHD, namely: total energy E, mean square concentration H^ψ, and cross helicity H^C:

$$E = E^K + E^B = \int (\frac{\rho \mathbf{v}^2}{2} + \frac{\xi^2 \mathbf{B}_\psi^2}{2}) \, \mathrm{d}^2 x \tag{2.20}$$

$$H^\psi = \int \psi^2 \, \mathrm{d}^2 x \tag{2.21}$$

$$H^C = \int \mathbf{v} \cdot \mathbf{B}_\psi \, \mathrm{d}^2 x \tag{2.22}$$

Note that some previous works [5, 80] use another definition of energy: $E' = E^K + F = \int (\frac{\rho \mathbf{v}^2}{2} - \frac{1}{2}\psi^2 + \frac{1}{4}\psi^4 + \frac{\xi^2}{2} |\nabla \psi|^2) \, \mathrm{d}^2 x$. This is also an ideal conserved quantity, but it is not *quadratic*. In this paper, we focus on *quadratic* conserved quantities, because higher-order conserved quantities are not strictly conserved when the k space is discretized and truncated at large k. Since discretization and truncation are unavoidable when doing statistical physics and numerical simulation, only *quadratic* conserved quantities are robust enough to be meaningful.

The physical meaning of cross helicity in the CHNS equations is not clear, as it is in MHD. The role of cross helicity is an interesting question, but it is beyond the scope of this paper. It will be investigated further in future works.

In addition, recall that there are only two ideal quadratic conserved quantities in 2D Navier-Stokes (NS) turbulence: kinetic energy E^K and enstrophy Ω:

$$E^K = \int \frac{\mathbf{v}^2}{2} \, \mathrm{d}^2 x \tag{2.23}$$

$$\Omega = \int \frac{\omega^2}{2} \, \mathrm{d}^2 x \tag{2.24}$$

It is clear that the constraints on the dynamics of the CHNS system are more like those for 2D MHD than 2D NS. The conservation of enstrophy is broken in the 2D CHNS system by the surface tension force, just as it is broken by the $\mathbf{j} \times \mathbf{B}$ force in 2D MHD. Although enstrophy is not a strict ideal conserved quantity in 2D CHNS system, it is still useful to retain this concept, for reasons discussed below.

2.3.3 Cascades

Turbulence cascade directions of various physics systems are suggested by the absolute equilibrium distributions, i.e. the Gibbs distribution [8, 34]. The peak of the absolute equilibrium distribution for each quadratic conserved quantity is a good indicator of the corresponding cascade direction. This approach only depends on the ideal quadratic conserved quantities of the system. Because the ideal quadratic conserved quantities of 2D CHNS and 2D MHD are direct analogues, we can then obtain an indication of the cascade directions in 2D CHNS by changing the name in variables. The summary of cascade directions of relevant physics systems are shown in Table 2.3.

The Gibbs distribution for 2D MHD is

$$\rho_G = Z^{-1} \exp(-\alpha E - \beta H^A - \gamma H^C) \tag{2.25}$$

where α, β and γ are Lagrangian multipliers and Z is the partition function. Similarly, the Gibbs distribution for 2D CHNS is

$$\rho_G = Z^{-1} \exp(-\alpha E - \beta H^\psi - \gamma H^C) \tag{2.26}$$

By calculating each ideal spectral density from the above absolute equilibrium distribution, suggested cascade directions can be extracted. The second-order moment for a Gaussian distribution

$\rho = Z^{-1} \exp -\frac{1}{2} \sum_{i,j} A_{ij} x_i x_j$ is:

$$\langle x_i x_j \rangle = A_{ij}^{-1} \tag{2.27}$$

Write the ideal quadratic conserved quantities in terms of Fourier modes and in the discrete form, and restrict the index of summation $\mathbf{k}$ within the band $k_{min} < k < k_{max}$:

$$E = \frac{1}{2} \sum_{\mathbf{k}} k^2 (|\phi_{\mathbf{k}}|^2 + |\psi_{\mathbf{k}}|^2) \tag{2.28}$$

$$H^{\psi} = \sum_{\mathbf{k}} |\psi_{\mathbf{k}}|^2 \tag{2.29}$$

$$H^{C} = \sum_{\mathbf{k}} k^2 \phi_{\mathbf{k}} \psi_{-\mathbf{k}} \tag{2.30}$$

Plugging the above expressions into Eq. (2.26) and Eq. (2.27) (set $\rho = 1$ and $\xi^2 = 1$ for simplicity), it is then straightforward to obtain the expressions for ideal spectral densities:

$$E_k^K = \frac{1}{2} k^2 \langle |\phi_{\mathbf{k}}^2| \rangle = \frac{2\pi k}{\alpha} (1 + \frac{k^2 \tan^2 \theta}{k^2 + (\beta/\alpha) \sec^2 \theta}) \tag{2.31}$$

$$E_k^B = \frac{1}{2} k^2 \langle |\psi_{\mathbf{k}}^2| \rangle = \frac{2\pi k}{\alpha} \frac{k^2 \sec^2 \theta}{k^2 + (\beta/\alpha) \sec^2 \theta} \tag{2.32}$$

$$H_k^{\psi} = \langle |\psi_{\mathbf{k}}^2| \rangle = 2k^{-2} E_k^B \tag{2.33}$$

$$H_k^C = k^2 \langle \phi_{\mathbf{k}} \psi_{-\mathbf{k}} \rangle = -\frac{2\gamma}{\alpha} E_k^B \tag{2.34}$$

where $\sin\theta = \gamma/(2\alpha)$. The requirement that E_k^K, E_k^B and H_k^{ψ} are always positive definite implies that $\alpha > 0$, $k_{min}^2 + (\beta/\alpha) \sec^2 \theta > 0$, and $|\gamma| < 2\alpha$. If the spectrum is peaked at high k, and excitation is injected at intermediate scales, we expect the spectrum to relax towards high k [8]. The trend suggests a direct cascade. Similarly, an inverse cascade is suggested if a spectrum is peaked at small k. So for the 2D CHNS system, we predict a *direct* energy cascade and an *inverse* cascade of H_k^A. The spectral transfer of cross helicity spectral density H_k^C needs more consideration and is beyond the scope of this paper.

Table 2.3: The cascade directions for 2D MHD, CHNS and NS turbulences.

Physics System	Conserved Quantity	Cascade Direction
2D MHD	E_k	Direct
	H_k^A	Inverse
2D CHNS	E_k	Direct
	H_k^ψ	Inverse
2D NS	E_k^K	Inverse
	Ω_k	Direct

In 2D MHD, the inverse cascade of H^A can be understood as the process of magnetic flux coalescence [26]. Similarly, in 2D CHNS, the inverse cascade of H^ψ can be related to the coalescence of blobs of the same species.

2.3.4 Linear Elastic Wave

Since Alfven waves play a crucial role in MHD turbulence, it is meaningful to examine the similar linear elastic wave in CHNS system. Recall that in the limit of small damping, the dispersion relation for the Alfven wave in 2D MHD is:

$$\omega(\mathbf{k}) = \pm\sqrt{\frac{1}{\mu_0\rho}}|\nabla A_0 \times \mathbf{k}| - \frac{1}{2}i(\eta+\nu)k^2 \tag{2.35}$$

It is straightforward to linearize the CHNS equations and obtain a similar linear elastic wave:

$$\omega(\mathbf{k}) = \pm\sqrt{\frac{\xi^2}{\rho}}|\nabla\psi_0 \times \mathbf{k}| - \frac{1}{2}i(CD+\nu)k^2 \tag{2.36}$$

where $C = [-1-6\psi_0\nabla^2\psi_0/k^2 - 6(\nabla\psi_0)^2/k^2 - 12\psi_0\nabla\psi_0\cdot i\mathbf{k}/k^2 + 3\psi_0^2 + \xi^2k^2]$ is a dimensionless coefficient. The 2D CHNS system spontaneously leads to a state of phase separation. Inside a blob of the same species, the concentration field ψ_0 is homogeneous, so $\nabla\psi_0 \to 0$. $\nabla\psi_0$ *is large only along the interface of blobs*, as shown in Fig. 2.3. The CHNS linear elastic wave propagates

along the interface of the two species where $\nabla\psi_0 \neq 0$, so it is much like a capillary wave.

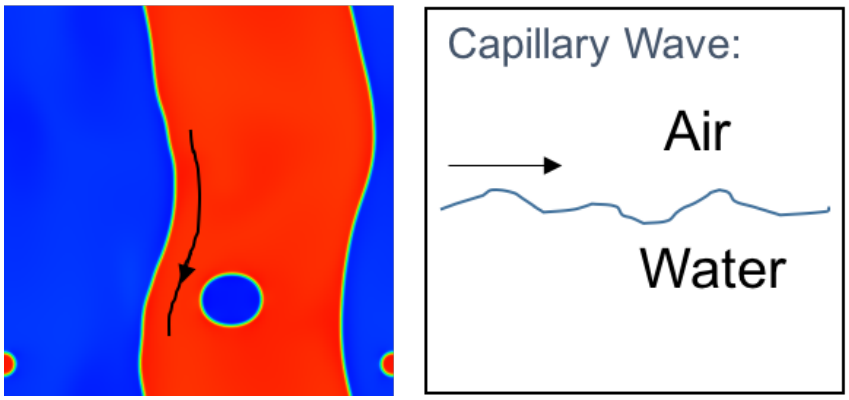

Figure 2.3: The linear elastic wave (left) in the 2D CHNS system propagates only along the interface, similar to capillary wave (right).

Alfven waves and CHNS linear elastic waves are similar, not only due to the resemblance of the dispersion relations, but also because both wave propagate along $\mathbf{B}_0$ or $\mathbf{B}_{\psi 0}$ field lines. Both waves are elastic waves, in which magnetic tension and surface tension generate restoring forces that act as elasticity. The Alfvenization process in MHD turbulence couples $\mathbf{v}$ with $\mathbf{B}$, and even a weak mean magnetic field can spontaneously convert fluid eddies into Alfven waves [26]. The Alfvenization process leads to Alfvenic equipartition $\rho\langle\mathbf{v}^2\rangle \sim \frac{1}{\mu_0}\langle\mathbf{B}^2\rangle$ of the fields. A similar elasticization process can also occur in the 2D CHNS system, because of the presence of linear elastic waves. The corresponding elastic equipartition for the 2D CHNS system is as follows:

$$\rho\langle\mathbf{v}^2\rangle \sim \xi^2\langle\mathbf{B}_\psi^2\rangle \tag{2.37}$$

An interesting difference between Alfven wave and the CHNS linear elastic wave is that, the non-ideal part of the dispersion relation for CHNS linear elastic wave can be either positive or negative depending on k: if $CD+\nu > 0$, then the wave is damped; but if $CD+\nu < 0$, growth is possible. This wave growth is physical, and is responsible for the pattern formation during the linear phase, and the sustainment of sharp interfaces that separate phases during the dynamical evolution of the physical system in the nonlinear phase. It is important to note that treating this

anti-diffusive term numerically is non-trivial, and requires unconditionally energy-stable temporal update schemes that ensure energy is either conserved or slightly dissipated. In this work, we have employed the MP-BDF2 energy-stable scheme proposed in Ref. [42], which in addition to being energy-stable, is unconditionally uniquely solvable.

2.4 Important Length Scales and Ranges of 2D CHNS Turbulence

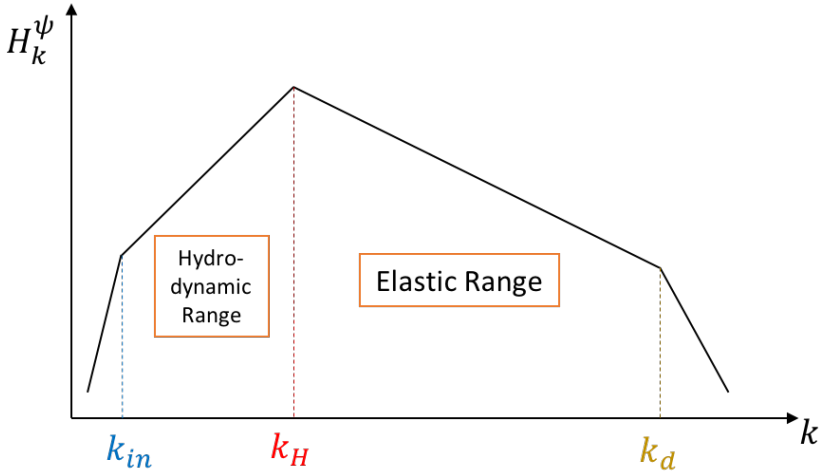

Figure 2.4: The Hinze scale, hydrodynamic range and elastic range.

In the forced 2D CHNS system, large blobs in the binary liquid mixture tend to be broken up by turbulent fluid straining, while small blobs tend to stick together due to surface tension. From this competition, a statistically stable length scale for the blob size, the Hinze scale L_H, emerges. L_H is defined by balancing turbulent kinetic energy and surface tension energy [49, 78]:

$$\frac{\rho\langle \mathbf{v}^2\rangle}{\sigma/L_H} \sim 1 \tag{2.38}$$

where σ is surface tension. According to [55, 54], the surface tension is $\sigma = \sqrt{\frac{8}{9}}\xi$. The surface

tension energy can also be expressed in terms of B_ψ^{rms} ($B_\psi^{rms} = \langle \mathbf{B}_\psi^2 \rangle^{1/2}$). The key is to identify the relevant length scale for $\nabla\psi$. We propose to use the geometric mean of the blob size L_H and the interface width ξ, because they are the longest and shortest gradient length scales, respectively, as shown in Fig. 2.5. Assuming the length scale for B_ψ^{rms} is the geometric mean of L_H and ξ, i.e. $B_\psi^{rms} \sim \sqrt{\frac{\Delta\psi}{L_H}\frac{\Delta\psi}{\xi}} \sim \sqrt{\frac{1}{L_H\xi}}$, then the original expression for surface tension energy σ/L_H is consistent with our expression $\xi^2\langle \mathbf{B}_\psi^2 \rangle$ in Eq. (2.20). It is interesting to note that the critical balance Eq. (2.38) is then consistent with elastic equipartition ($\rho\langle \mathbf{v}^2 \rangle \sim \xi^2\langle \mathbf{B}_\psi^2 \rangle$).

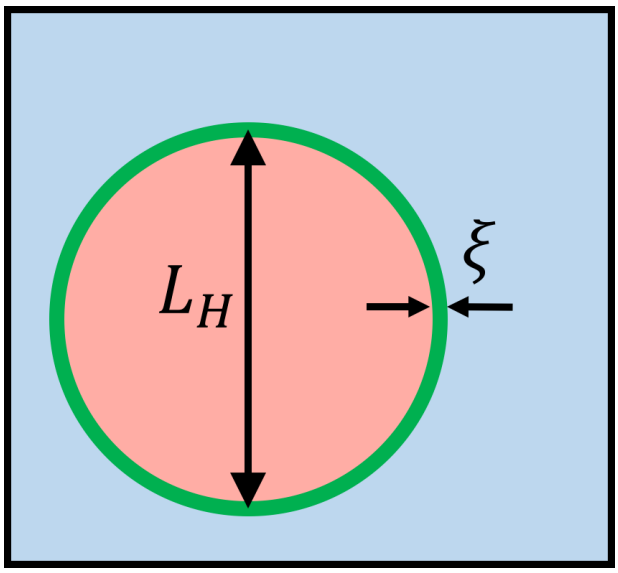

Figure 2.5: The gradient length scales.

The expression for the Hinze scale was originally derived for the 3D NS direct energy cascade regime [49]. The velocity was estimated using the Kolmogorov energy distribution law, $\langle \mathbf{v}^2 \rangle / k_H \sim \varepsilon^{2/3} k_H^{-5/3}$ where $\varepsilon = \nu \int \omega^2 \, dx^2$ is the kinetic energy dissipation rate per unit mass and $k_H = 2\pi/L_H$. We then obtain the expression:

$$L_H \sim (\frac{\rho}{\xi})^{-3/5} \varepsilon^{-2/5} \tag{2.39}$$

However, in the 2D NS direct enstrophy cascade regime, the velocity distribution is $\langle \mathbf{v}^2 \rangle / k_H \sim \varepsilon_\Omega^{2/3} k_H^{-3}$ where $\varepsilon_\Omega = \nu \int (\nabla \times \omega \hat{\mathbf{z}})^2 \, dx^2$ is the enstrophy dissipation rate per unit mass. Therefore,

in 2D:

$$L_H \sim (\frac{\rho}{\xi})^{-1/3}\varepsilon_\Omega^{-2/9} \tag{2.40}$$

Note that the Hinze scale depends on the magnitude of the external forcing via ε_Ω, and it does not depend on the scale of the external forcing. The Hinze scale separates the k space into two ranges: the scales larger than L_H form the hydrodynamic range, where the usual eddy break-up process dominates. The range of scales between L_H and dissipation scale L_d is the *elastic range*, where the blob coalescence process dominates, as shown in Fig. 2.4. Separation between the Hinze scale L_H and dissipation scale L_d is critical to defining an elastic range. The dissipation scale here should be related to the direct enstrophy cascade. By simple dimensional analysis, we obtain $L_d = (\nu^3/\varepsilon_\Omega)^{1/6}$. Defining a dimensionless number for the ratio of L_H to L_d gives:

$$L_H/L_d = Hd = (\frac{\rho}{\xi})^{-1/3}\nu^{-1/2}\varepsilon_\Omega^{-1/18} \tag{2.41}$$

$Hd \gg 1$ is required to form a large enough elastic range. It is clear that reducing ν is an efficient way to obtain a longer elastic range.

The A blobs in 2D MHD and ψ blobs in the 2D CHNS system are shown side by side in Fig. 2.6. In the elastic range of the 2D CHNS system, the blob coalescence process is analogous to the magnetic flux blob coalescence process in 2D MHD. The former leads to the inverse cascade of H^ψ, and the latter leads to the inverse cascade of H^A. In the elastic range of the 2D CHNS system, surface tension induces elasticity and plays a major role in defining a restoring force. Similarly, in 2D MHD, the magnetic field induces elasticity and make MHD different from a pure fluid. The 2D CHNS system is more MHD-like in the elastic range.

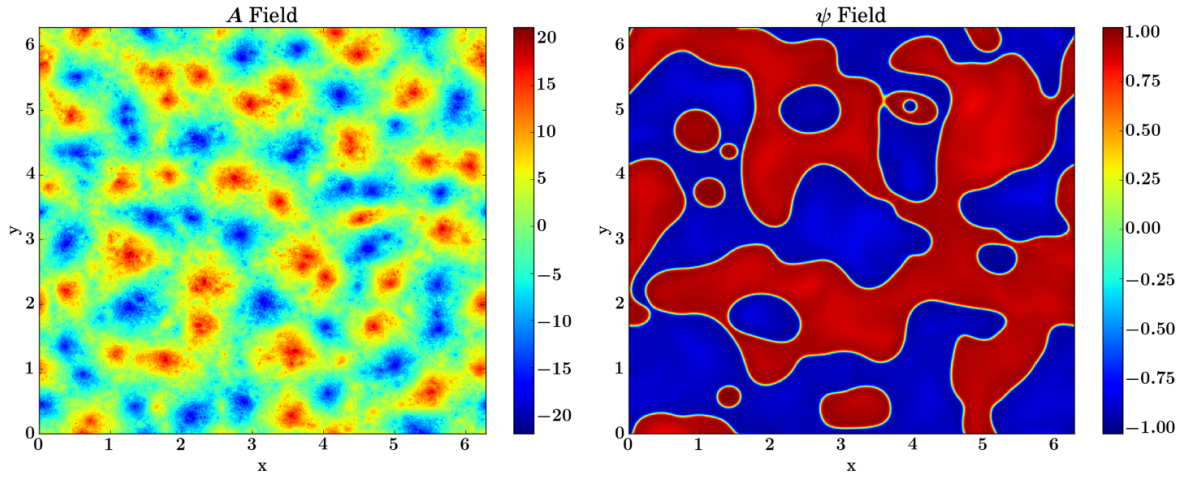

Figure 2.6: The A blobs in 2D MHD (Run6) and the ψ blobs in the 2D CHNS system (Run2).

2.5 Numerical Results

2.5.1 Basic Setup

We solve 2D CHNS Eqs. (2.1) - (2.4) and 2D MHD Eqs. (2.5) - (2.8) with the PIXIE2D code [20, 19]. The simulation box size is $L_0 \times L_0 = 2\pi \times 2\pi$, and the resolution is 1024×1024. External forcing is applied to the A and ϕ field with the sinusoidal form $f_{A,\phi}(x,y) = f_{0A,\phi} \sin[x * \text{int}(k_{fA,\phi} \cos\theta_{A,\phi}) + y * \text{int}(k_{fA,\phi} \sin\theta_{A,\phi}) + \varphi_{A,\phi}]$, where f_0 is the forcing magnitude, k_f is the forcing scale, and $\theta, \varphi \in [0, 2\pi)$ are random angle and random phase that change at each time step, respectively. This kind of external forcing keeps the system isotropic and homogeneous.

The free parameters in the equations are ξ (or μ_0), D (or η), ν, and ρ. In addition, the external forcing properties $f_{0A,\phi}$, and $k_{fA,\phi}$ are also adjustable. Important dimensionless numbers here are as follows [80, 75]:

- $L_H/L_d = Hd$, the ratio of the Hinze scale to dissipation scale.
- $Re_\lambda = \sqrt{10}E^K/\rho\sqrt{\varepsilon\nu}$, the Taylor microscale Reynolds number.
- $Sc = \nu/D$, the Schmidt number; or $Pr = \nu/\eta$, the Prandtl number.

- $Ch = \xi/L_0$, the Cahn number, which is the ratio of the interfacial thickness to the system size.

- $We = \rho L_f f_{0\phi}/\sigma$ (where $L_f = 2\pi/k_f$), the forcing scale Weber number, which characterizes the relative importance of the external forcing compared to the surface tension.

- $Gr = L_0^2 f_{0\phi}/\nu^2$, the Grashof number, which approximates the ratio of the external forcing to viscosity.

We keep $Sc = Pr = 1$ in all our runs, and other parameters are listed in Table 2.5.

The system is periodic in both directions. The initial condition for the concentration field ψ (or magnetic potential field A) is a random distribution of $+1$ and -1, while the stream function field ϕ is 0 everywhere initially. Although the range of ψ is $[-1,1]$ from its physics definition $\psi = \frac{\rho_A - \rho_B}{\rho_A + \rho_B}$, we don't enforce this restriction in our simulation and let it freely evolve according to Eqs. (2.1) - (2.4). This approach is valid because the Probability Density Function (PDF) of ψ lies mostly in the range $[-1,1]$ spontaneously, as shown in Fig. 2.7. This PDF is consistent with previous studies [73].

2D simulations are sufficient to capture much of the important physics of the CHNS turbulence. The length scale growth, the arrest of the length scale growth, the emergence of the Hinze scale, and the inverse cascade of H^ψ appear both in 3D and 2D simulations [78]. It is well known that 2D and 3D Navier-Stokes turbulence have totally different cascades and spectra, but 2D and 3D MHD turbulence are rather more similar. So as an analogy, 2D and 3D CHNS turbulence also should not differ much.

2.5.2 Benchmark

In the simulation, we verified that, if unforced, the blob coalescence progresses, and the blob size grows until it reaches the system size. If ϕ field is forced at large scale, blob size growth

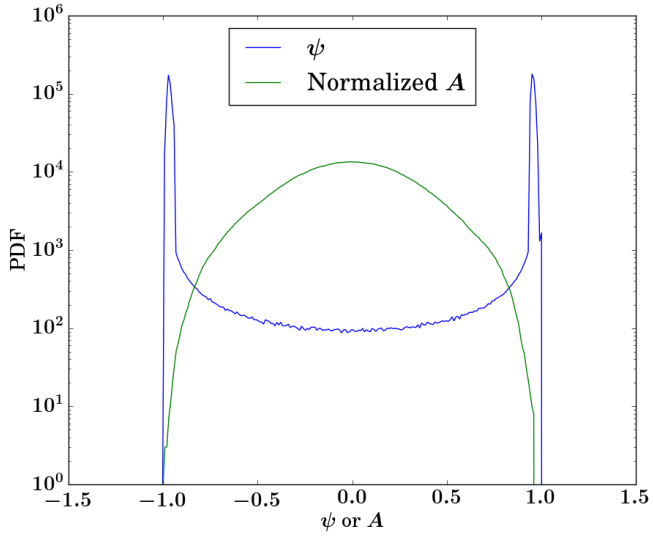

Figure 2.7: The Probability Density Function (PDF) of ψ (Run2) and normalized A (Run6). The PDF of ψ falls into the range $[-1, 1]$ spontaneously.

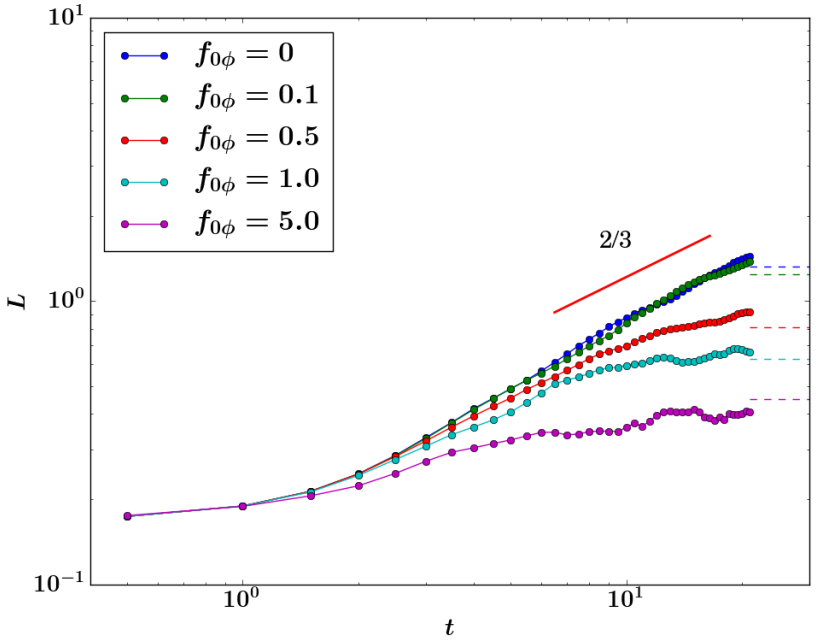

Figure 2.8: Blob size growth for Run1 - Run5. Dashed lines are corresponding the Hinze scales.

can be arrested. See Fig. 2.1 as an illustration. Define the blob size L as the following:

$$L(t) = 2\pi \frac{\int S_k(k,t)\,\mathrm{d}k}{\int k S_k(k,t)\,\mathrm{d}k} \tag{2.42}$$

where $S_k(k,t) = \langle |\psi_{\mathbf{k}}(\mathbf{k},t)|^2 \rangle$ is the structure function. This definition essentially picks the peak of the structure function, if it has a clear peak.

Earlier numerical studies [55, 54] observed that, if the system is unforced, the blob size L grows such that $L \sim t^{2/3}$ at the late stage of the blob coalescence process. This exponent can be obtained dimensionally by balancing the advection term $\mathbf{v}\cdot\nabla\omega$ and the surface tension force term $\frac{\xi^2}{\rho}\mathbf{B}_\psi \cdot \nabla\nabla^2\psi$ in Eq. (2.2) and assuming the velocity can be estimated by $\mathbf{v} \sim \dot{L}$. The presence of external forcing can arrest the length scale growth [5]. Larger forcing leads to a larger enstrophy dissipation rate ε_Ω, and thus a smaller Hinze scale. Fig. 2.8 supports this finding. The peak of the H_k^ψ spectrum moving towards larger scale in Fig. 2.10 is consistent with the blob size L growth shown in Fig. 2.8.

2.5.3 The H_k^ψ Flux

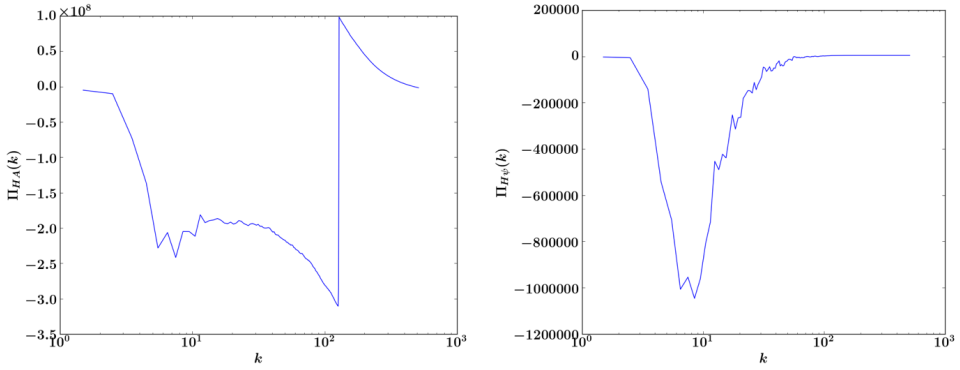

Figure 2.9: The H_k^A flux (left) for MHD (Run6), and the H_k^ψ flux (right) for CHNS (Run2).

The directions of cascades are suggested by the sign of the corresponding spectral fluxes.

We define the H_k^ψ flux and the H_k^A flux as follows:

$$\Pi_{HA}(k) = \sum_{k<k'} T_{HA}(k'), \text{ where } T_{HA}(k) = \langle A_k^*(\mathbf{v}\cdot\nabla A)_k\rangle \tag{2.43}$$

$$\Pi_{H\psi}(k) = \sum_{k<k'} T_{H\psi}(k'), \text{ where } T_{H\psi}(k) = \langle \psi_k^*(\mathbf{v}\cdot\nabla \psi)_k\rangle \tag{2.44}$$

If a flux is negative, then the corresponding transfer is inverse, suggestive of an inverse cascade. See Fig. 2.9 for our simulation results. For the MHD case (left), an external forcing on the magnetic potential A is applied on $k = 128$. The small scale A forcing drives an inverse transfer of H^A. For the CHNS case (right), no forcing on ψ is necessary for the appearance of an inverse transfer of H^ψ. The negative diffusion term in the CHNS equations leads to small scale instability. Thus it plays a similar role to forcing of ψ.

2.5.4 The H_k^ψ Spectrum Power Law

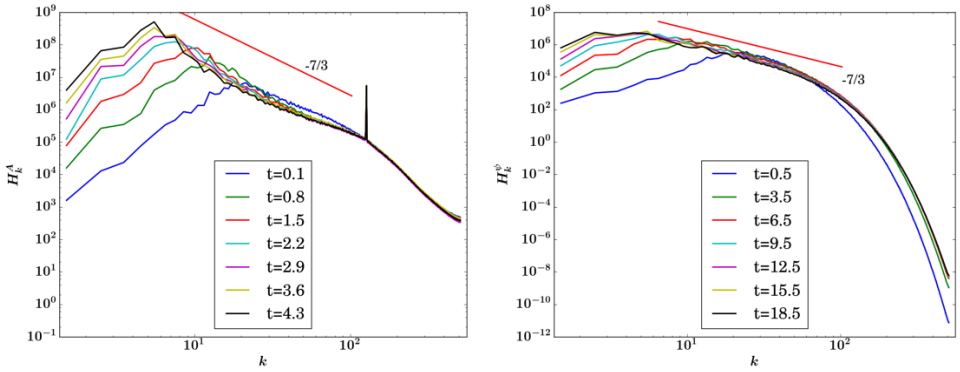

Figure 2.10: The H_k^A spectrum in 2D MHD for Run6 at various times (left), and the H_k^ψ spectrum in 2D CHNS for Run2 (right).

It is known that the dynamics of 2D MHD turbulence is dominated by the inverse cascade of H^A, if H^A is injected at small scales. The corresponding power law of the H_k^A spectrum is $-7/3$:

$$H_k^A \sim \varepsilon_{HA}^{2/3} k^{-7/3} \tag{2.45}$$

Here ε_{HA} is the H^A dissipation rate, and see Fig. 2.10 (left) for the simulation result. Note that in order to obtain a 2D MHD setup similar to the 2D CHNS system, small scale external forcing of the A field and large scale external forcing of the ϕ field are imposed.

The scaling argument for the power of $-7/3$ for 2D MHD is as follows. Assuming there is a constant mean square magnetic potential dissipation rate ε_{HA}, according to the Alfvenic equipartition ($\rho\langle \mathbf{v}^2\rangle \sim \frac{1}{\mu_0}\langle \mathbf{B}^2\rangle$), the time scale for the decay of H^A ($\varepsilon_{HA} \sim H^A/\tau$) can be estimated by $\tau \sim (v^{rms}k)^{-1} \sim (B^{rms}k)^{-1}$. Define the spectrum to be $H^A = \sum_k H^A_k \sim kH^A_k$, so $B^{rms} \sim kA \sim k(H^A)^{1/2} \sim (H^A_k)^{1/2}k^{3/2}$. Therefore, $\varepsilon_{HA} \sim H^A/\tau \sim (H^A_k)^{2/3}k^{7/2}$, leading to Eq. (2.45).

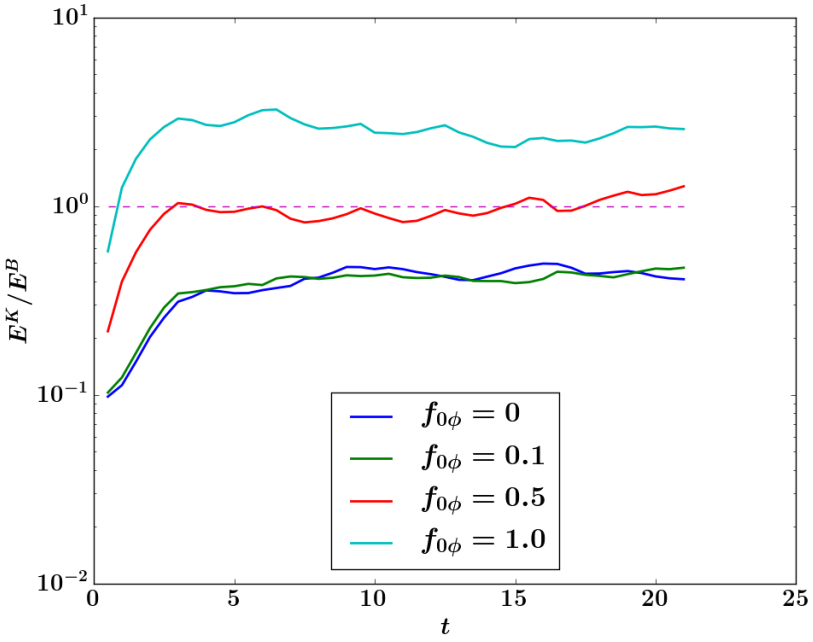

Figure 2.11: The ratio of E^K to E^B for Run1 - Run4 supports the assumption of elastic equipartition ($\rho\langle \mathbf{v}^2\rangle \sim \xi^2\langle \mathbf{B}^2_\psi\rangle$). If the forcing intensity is too strong, then the elastic forcing term in the ω equation becomes negligible, and the system does not significantly differ from the 2D NS equation. In our study, though we tried a broad range of forcing intensity, larger forcing (than Run5) may break the equipartition of the kinetic and magnetic energy.

The same argument can be applied to 2D CHNS turbulence to get a (similar) H_ψ spectrum. Assuming that elastic equipartition applies to the 2D CHNS system ($\rho\langle \mathbf{v}^2\rangle \sim \xi^2\langle \mathbf{B}^2_\psi\rangle$) (see Fig. 2.11), the time scale for the decay of H^Ψ is $\tau \sim (v^{rms}k)^{-1} \sim (B^{rms}_\psi k)^{-1}$. Then by repeating

the above argument for MHD, it is easy to obtain the H_k^ψ spectrum:

$$H_k^\psi \sim \varepsilon_{H\psi}^{2/3} k^{-7/3} \tag{2.46}$$

The simulation result for the H_k^ψ spectrum in 2D CHNS turbulence in Fig. 2.10 (right) verifies the similarity to the H_k^A spectrum in 2D MHD turbulence. The peak of the H_k^ψ spectrum, which gives the approximate blob size according to Eq. (2.42), moves towards larger scale, as shown in Fig. 2.10. The blob coarsening process is consistent with the inverse cascade of H^ψ. Moreover, the H_k^ψ spectrum with power law $-7/3$ is indeed a good fit, as predicted by the inverse cascade of H^ψ argument. Again, we assumed (marginally satisfied) elastic equipartition in order to obtain the $-7/3$ power law. The result fits the simulation very well. These findings suggest that the dynamics of the fluctuating concentration field is governed by the inverse cascade of H^ψ.

The $-7/3$ power is robust. It does not change with the magnitude of external forcing, as long as the separation between the Hinze scale and the dissipation scale is maintained, so the elastic range is long enough ($Hd \gg 1$). Fig. 2.12 gives the H_k^ψ spectra for different external forcing strengths. It shows that the power $-7/3$ remains unchanged. Note that larger external forcing leads to a smaller Hinze scale according to Eq. (2.40), so the elastic range is shorter. If the Hinze scale is close to or even smaller than the dissipation scale, there will be no clear elastic range, and thus no power law spectrum for H_k^ψ. Thus, a sufficient separation between the Hinze scale and the dissipation scale ($Hd \gg 1$) is critical to uncovering elastodynamic phenomena.

2.5.5 The Energy Spectrum Power Law

When the ϕ field is forced at large scale, the kinetic energy spectrum is $E_k^K \sim k^{-3}$, as shown in Fig. 2.13. This spectrum is the same as that for the direct enstrophy cascade in 2D NS Turbulence. This result is initially surprising, because enstrophy is *not* a conserved quantity in the 2D CHNS system. The kinetic energy spectrum for 2D CHNS turbulence is different

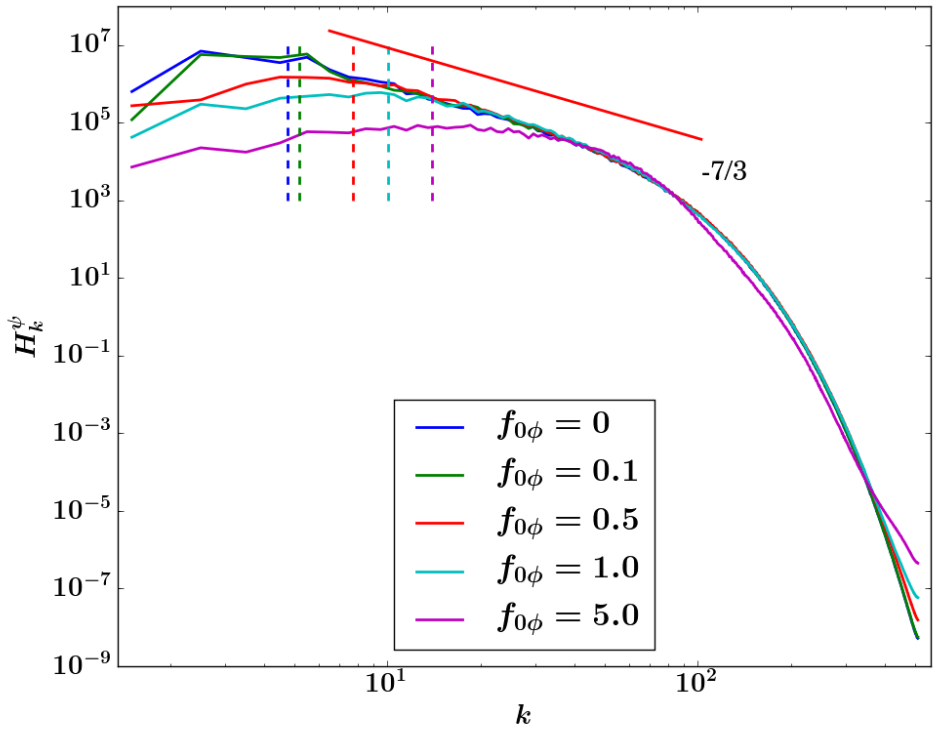

Figure 2.12: H^Ψ spectra for Run1 - Run4, with different magnitudes of external forcing $f_{0\phi}$ thus different Hinze scales. The Hinze scale for each run is marked by a dashed line with the same color.

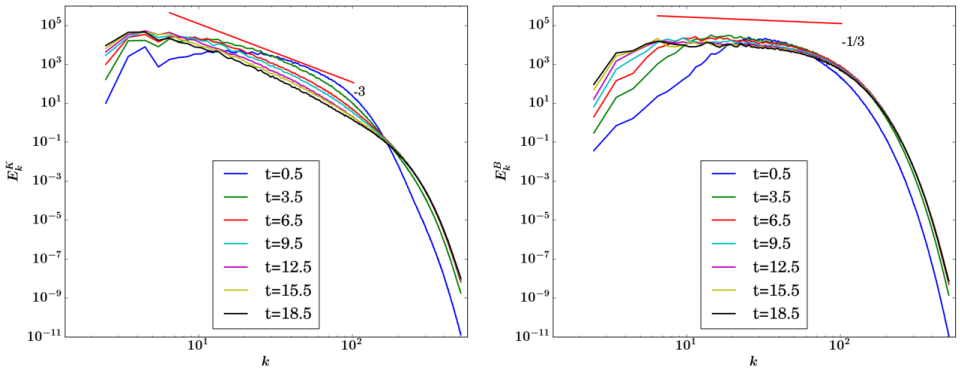

Figure 2.13: Kinetic energy spectrum (left) and magnetic energy spectrum (right) for Run2. The kinetic energy spectrum indicates a direct enstrophy cascade of 2D NS turbulence.

from that for 2D MHD turbulence. It is well known that in the direct energy cascade regime of 2D MHD, the energy spectrum is $E_k^K \sim k^{-3/2}$, which is called the Iroshnikov-Kraichnan (IK) spectrum [60, 50]. The IK spectrum is the consequence of the interaction between Alfven waves propagating in opposite directions. The result that the kinetic energy spectrum for the 2D CHNS system is significantly different from the IK spectrum for MHD suggests that the back reaction of surface tension on the fluid motion is limited.

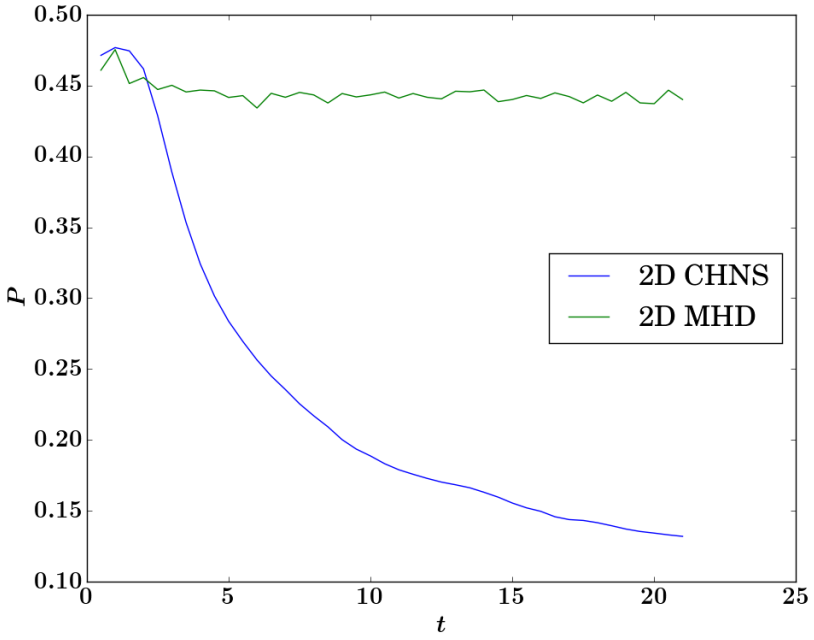

Figure 2.14: The time evolution for the interface packing fraction P, the ratio of mesh grid number where $|\mathbf{B}_\psi| > B_\psi^{rms}$ (or $|\mathbf{B}| > B^{rms}$) over total mesh grid number.

This initially surprising result is plausible because in the 2D CHNS system, $\mathbf{B}_\psi$ vanishes in most of the space. $\mathbf{B}_\psi$ is large only in the interfacial regions, and the interfacial regions fill only a small portion of the system, as shown in Fig. 2.15. On the other hand, the magnetic fields in MHD are not localized to specific regions, so Alfven waves can propogate everywhere. Define the interface packing fraction P to be the ratio of mesh grid number where $|\mathbf{B}_\psi| > B_\psi^{rms}$ (or $|\mathbf{B}| > B^{rms}$) to the total mesh grid number. This definition of interface packing fraction is a rather simple choice of a figure of merit, but one for which we can easily grasp the underlying physics. In the

2D CHNS system, $P = 13.9\%$ for Run2; while for 2D MHD, $P = 44.0\%$ for Run6. This notable difference shows that only a small portion of the 2D CHNS system is strongly affected by the $\mathbf{B}_\psi$ field, as compared to MHD. The time evolution for the interface packing fraction P is shown in Fig. 2.14. In the 2D CHNS system, as time progresses, the blob coalescence process drives the interfacial region to a smaller and smaller interface packing fraction, and thus suppresses the elastic effects on fluid motion. If there is a larger number of blobs, there will be a larger interfacial region, and thus the velocity field will be more heavily influenced by the $\mathbf{B}_\psi$ field. In that case, the kinetic energy spectrum will be more MHD-like.

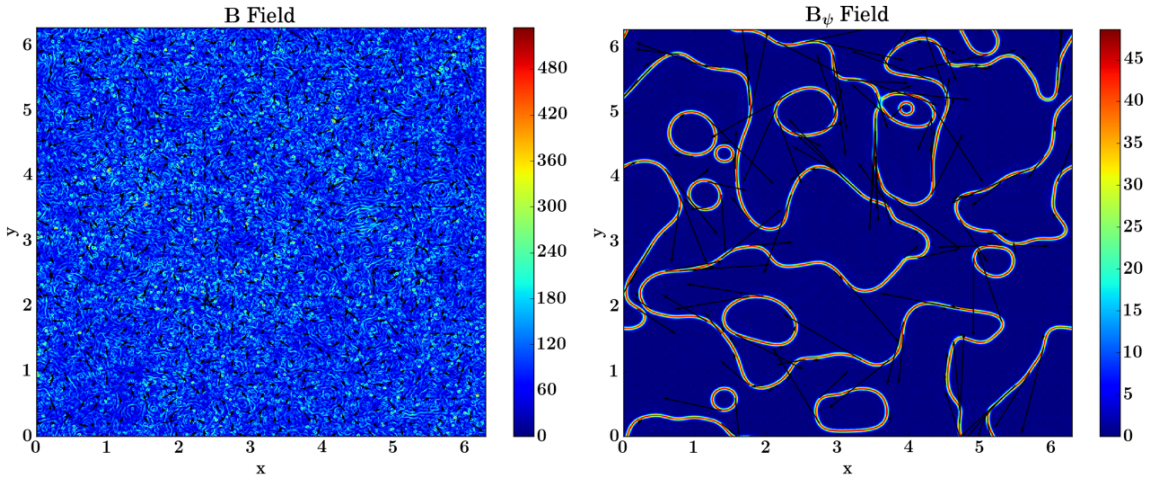

Figure 2.15: **B** field for Run6 (left) and $\mathbf{B}_\psi$ field for Run2 (right). From the color map we can see that the structures look quite different.

2.6 Conclusion and Discussion

2D CHNS turbulence is an analogue to 2D MHD turbulence. The two systems have some common features and also some important differences. See Table 2.1 for comparison and Table 2.4 for contrasts. The theories of 2D MHD turbulence give us inspiration and guidance for the study of 2D CHNS turbulence.

From the basic equations, it is easy to notice similarities between 2D CHNS and 2D

Table 2.4: Contrast of 2D MHD and the 2D CHNS system.

	2D MHD	2D CHNS
Diffusion	A simple positive diffusion term	A negative, a self nonlinear, and a hyper-diffusion term
Range of potential	No restriction for range of A	$\psi \in [-1,1]$
Interface Packing Fraction	Not far from 50%	Small
Back reaction	$\mathbf{j}\times\mathbf{B}$ force can be significant	Back reaction is apparently limited
Kinetic energy spectrum	$E_k^K \sim k^{-3/2}$	$E_k^K \sim k^{-3}$
Suggestive cascade by E_k^K	Suggestive of direct energy cascade	Suggestive of direct enstrophy cascade

MHD. Most clear is that the surface tension force is a direct analogue of the $\mathbf{j}\times\mathbf{B}$ force. The ideal quadratic conserved quantities of these two systems have the same form, and this leads to the same cascade directions. The linear elastic wave from the 2D CHNS system has a similar dispersion relation to the Alfven wave from 2D MHD. The linear elastic wave plays an important role in the dynamics through the elasticization process, which is analogous to the Alfvenization process.

The scales between the Hinze scale and dissipation scale in the 2D CHNS system form the elastic range. Separation of the Hinze scale and the dissipation scale ($Hd \gg 1$) is critical to allow an elastic range. In the elastic range, the surface tension interaction induces an elastic effect critical to the nonlinear dynamics, so the system is more MHD-like.

By direct numerical simulation, we find that in the elastic range, the mean square concentration spectrum is $H_k^\psi \sim k^{-7/3}$. This power law scaling can be recovered theoretically by assuming elastic equipartition (which is at best marginally satisfied). The $-7/3$ power law is the same as the H_k^A spectrum in the inverse cascade regime of 2D MHD. The $-7/3$ power law is robust and independent of the forcing strength. This result suggests that the dynamics of the fluctuating concentration field is governed by the inverse cascade of H_k^ψ. The inverse cascade of H^ψ is consistent with the blob coalescence process.

The kinetic energy spectrum for the 2D CHNS system is $E_k^K \sim k^{-3}$ when forced at large scale. This spectrum is different from the IK spectrum in MHD, and is the same as the kinetic energy spectrum in the 2D NS turbulence direct enstrophy cascade regime. This result suggests

that the back reaction of surface tension on the fluid motion is limited. This is plausible because the back reaction is only significant in the interfacial regions, which fill only a small part of the system. This is an important difference between 2D CHNS turbulence and 2D MHD turbulence. In order to make the kinetic energy spectrum more MHD-like, we need to increase the interface packing fraction. We will obtain larger interfacial regions if we have a large number of small blobs instead of a small number of large blobs. Thus the apparent next step is to increase the forcing strength or change the form of forcing in order to increase the interface packing fraction. However, a larger forcing strength leads to a smaller Hinze scale, and thus a shorter elastic range. If we want to keep a broad enough elastic range, we have to decrease the dissipation scale at the same time, i.e. decrease ν. This requires higher resolution and more computing resources, and so we will perform runs with higher resolution in future works. The definition of interface packing fraction we use in this paper is rather crude, and more study about how to characterize the interface, what physics controls the interface packing fraction, and how to increase the interface packing fraction would be interesting. The statistics of $|\mathbf{B}_\psi|$ and how it is related to the interface packing fraction is also a relevant interesting problem to study.

The theories of 2D MHD turbulence can also inspire the study of turbulent transport and memory effects in 2D CHNS turbulence. Even a weak mean magnetic field can result in a large mean square fluctuation. Such small scale magnetic fields will result in enhanced memory, so turbulent transport in MHD with even a weak large scale magnetic field is suppressed [16, 98, 99, 27]. This effect may also appear in 2D CHNS turbulence. It is also interesting to investigate the possible change of momentum transport in the elastic range of CHNS, due to elastic wave effects. 2D CHNS turbulence also has similarities to elastic turbulence in polymer solutions [96, 24]. The comparison and contrast among MHD, CHNS and polymer hydrodynamic turbulence will be discussed in future works.

Table 2.5: Simulation parameters. Note that for 2D MHD runs, ξ means $\mu_0^{-1/2}$, and D means η.

Run	System	ξ	D	ν	ρ	$f_{0\phi}$	$k_{f\phi}$	f_{0A}	k_{fA}	Re_λ	Hd	We	Gr	ξ^2/ρ
Run1	CHNS	0.015	10^{-3}	10^{-3}	1.0	0	–	–	–	5.5	39	0	0	$2.25*10^{-4}$
Run2	CHNS	0.015	10^{-3}	10^{-3}	1.0	0.1	4	–	–	6.1	39	11	$3.9*10^{6}$	$2.25*10^{-4}$
Run3	CHNS	0.015	10^{-3}	10^{-3}	1.0	0.5	4	–	–	25	35	56	$2.0*10^{7}$	$2.25*10^{-4}$
Run4	CHNS	0.015	10^{-3}	10^{-3}	1.0	1.0	4	–	–	59	33	110	$3.9*10^{7}$	$2.25*10^{-4}$
Run5	CHNS	0.015	10^{-3}	10^{-3}	1.0	5.0	4	–	–	719	30	550	$2.0*10^{8}$	$2.25*10^{-4}$
Run6	MHD	0.015	10^{-3}	10^{-3}	1.0	1.0	4	10^3	128	18	-	-	-	$2.25*10^{-4}$

Acknowledgments

We thank David Hughes and Steve Tobias for useful conversations. P. H. Diamond thanks Annick Pouquet for a fascinating discussion of competing cascades in MHD turbulence. We acknowledge the hospitality of Peking University where part of this research was performed. Xiang Fan thanks Los Alamos National Laboratory for its hospitality and help with computing resources. We thank the participants at the 2015 Festival de Théorie for discussions and comments. This research was supported by the U.S. Department of Energy, Office of Science, Office of Fusion Energy Sciences, under Award Number DE-FG02-04ER54738 and CMTFO.

Chapter 2 is a reprint of the material as it appears in X. Fan, P.H. Diamond, L. Chacón, H. Li, "Cascades and spectra of a turbulent spinodal decomposition in two-dimensional symmetric binary liquid mixtures", *Phys. Rev. Fluids*, 1 (5), 054403, 2016. The dissertation author was the primary investigator and author of this paper.

Chapter 3

Formation and Evolution of Target Patterns in Cahn-Hilliard Flows

We study the evolution of the concentration field in a single eddy in the 2D Cahn-Hilliard system to better understand scalar mixing processes in that system. This study extends investigations of the classic studies of flux expulsion in 2D MHD and homogenization of potential vorticity in 2D fluids. Simulation results show that there are three stages in the evolution: (A) formation of a 'jelly roll' pattern, for which the concentration field is constant along spirals; (B) a change in isoconcentration contour topology; and (C) formation of a target pattern, for which the isoconcentration contours follow concentric annuli. In the final target pattern stage, the isoconcentration bands align with stream lines. The results indicate that the target pattern is a metastable state. Band merger process continues on a time scale exponentially long relative to the eddy turnover time. The band merger process resembles step merger in drift-ZF staircases; this is characteristic of the long-time evolution of phase separated patterns described by the Cahn-Hilliard equation.

3.1 Introduction

Spinodal decomposition is a process by which a binary liquid mixture can evolve from a miscible phase (e.g., water+alcohol) to two co-existing phases (e.g., water+oil). When the binary liquid mixture is cooled below the critical temperature in the absence of external forcing, initially small blobs coalesce and become larger blobs until their size grows to the system size [13]. If large scale external forcing is imposed, blob size growth is arrested. The competition between the elastic energy and the turbulent kinetic energy leads to a statistically stable blob size. The Hinze scale $L_H \sim (\frac{\rho}{\sigma})^{-3/5}\varepsilon^{-2/5}$ is an estimate of the stable blob size. Here, ρ is density, σ is surface tension, and ε is the energy dissipation rate per unit mass [76, 81, 79, 78, 23, 97, 42]. In our previous work [30], we defined the elastic range to be the scales in the range $L_d < l < L_H$, where L_d is the dissipation scale. The elastic range scales are those for which the surface tension-induced elasticity is important to dynamics.

The Cahn-Hilliard equation is a standard model for spinodal decomposition. When considering the back reaction of the surface tension on to fluid motion, we need to couple the Cahn-Hilliard with Navier-Stokes (CHNS). 2D CHNS has analogies to 2D Magnetohydrodynamics (MHD) [89]. The concentration ψ in 2D CHNS is the analogue of the magnetic potential A in 2D MHD. Both models consist of a vorticity equation and a diffusion equation for an active scalar. 2D CHNS differs from 2D MHD by the appearance of negative diffusivity for potential and a nonlinear dissipative flux. A linear elastic wave, the analogue of the Alfven wave, exists in the 2D CHNS system and introduces the crucial element of memory. This wave propagates along the *interface* of the blobs, thus resembles a capillary wave. The two systems have identical ideal quadratic conserved quantities, and they both exhibit dual cascades. Our previous work [30] showed that the mean square concentration spectrum for the 2D CHNS system in the elastic range is $\sim k^{-7/3}$, and it is associated with an inverse cascade of mean square concentration. Note that the power $-7/3$ is the same as the power for the mean square magnetic potential spectrum in

2D MHD. On the other hand, the kinetic energy spectrum is proportional to k^{-3}, which is the same power law as for a 2D Navier-Stokes fluid in the forward enstrophy cascade regime. The kinetic energy power law -3 in 2D CHNS is far from $-3/2$ in 2D MHD, and the difference can be explained by the difference in the physics of back reaction. Unlike the case in MHD where the magnetic fields fill the whole space, the CHNS analogue of the magnetic fields, which are the blob interfaces, have a much smaller spatial packing fraction (i.e., relative spatial "active volume"). Thus, in CHNS, the back reaction is only significant in the interfaces of the blobs, because the waves propagate along the interfaces, like surface waves. This implies that for CHNS, the interfaces of the blobs are crucial to the mixing dynamics.

In order to better understand the dynamics in the CHNS turbulence, we examine the evolution of the concentration field in the background of a single convective eddy in the Cahn-Hilliard system. Since the system tends to evolve to a state of a few large blobs, the simplest problem which emerges is that of understanding the competition of shearing and dissipation in the context of a single cell structure. This goal leads us to a study which re-visits the classic problems of flux expulsion in 2D MHD [101, 38, 71, 72] and potential vorticity homogenization in 2D fluids [88, 87]. Weiss (1966) studied the evolution of an initial uniform magnetic field $\mathbf{B}_0$ in the background of a single eddy in 2D MHD [101]. Because the magnetic field was expelled to a layer at the boundary of the eddy, this phenomenon was named "flux expulsion". The eddy was observed to stretch the initial field, and the final value of average magnetic field was estimated to be $\langle B^2 \rangle \sim \mathrm{Rm}^{1/2} \langle B_0^2 \rangle$, where Rm is the magnetic Reynolds number ($\mathrm{Rm} \gg 1$). The time scale for the magnetic field to reach a steady state was found to scale as $\tau_{\mathrm{MHD}} \sim \mathrm{Rm}^{1/3} \tau_0$. Rhines and Young (1983) studied the time scale of the homogenization of a passive scalar in 2D fluids with closed streamlines [87]. A rapid stage and a later slow stage are observed. In the rapid stage, shear-augmented diffusion dominates, and the initial values of the passive scalar approach an average about a streamline. The time scale for the rapid stage is proportional to $\mathrm{Pe}^{1/3}$, where Pe is the Péclet Number. In the slow stage, the passive scalar homogenizes within the eddy over the

full diffusion time, which is proportional to Pe. A system of a few blobs can be viewed as an array of such eddies. Thus, we hope that understanding the physics of a single eddy can promote understanding of the turbulent system.

3.2 Simulation System

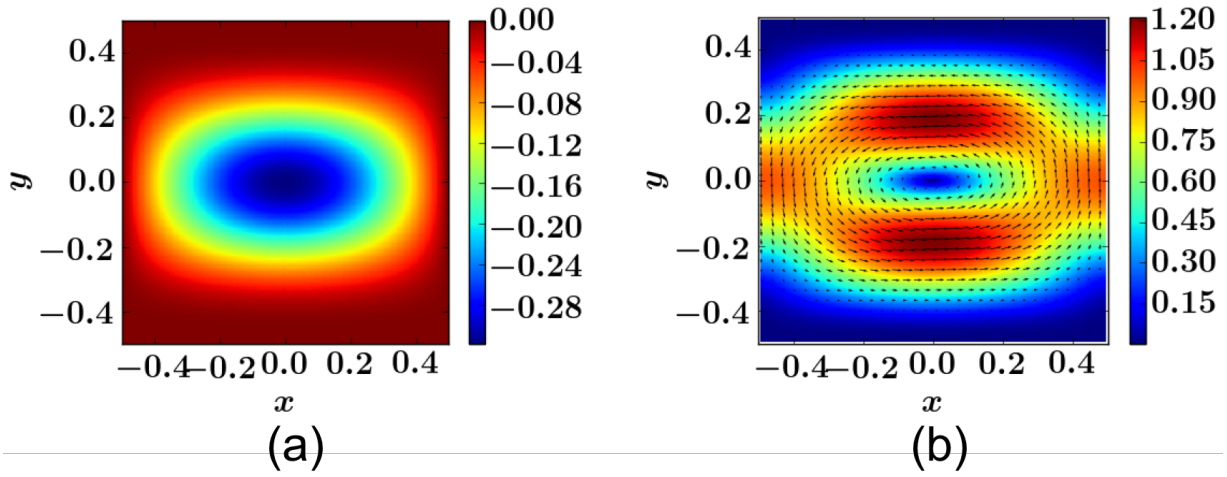

Figure 3.1: The background stream function ϕ (a) and velocity field $\mathbf{v}$ (b).

In this Rapid Communication, we report on solutions of the 2D Cahn-Hilliard system by PIXIE2D [20, 21] in the background of a single eddy, which is an analogue to the flux expulsion problem. The basic equation is:

$$\partial_t \psi + \mathbf{v} \cdot \nabla \psi = D\nabla^2(-\psi + \psi^3 - \xi^2 \nabla^2 \psi) \tag{3.1}$$

where $\psi = \frac{\rho_1 - \rho_2}{\rho_1 + \rho_2}$ is the local relative concentration and satisfies $-1 \leq \psi \leq 1$, D is the diffusivity, ξ is the parameter for interaction strength, and $\mathbf{v}$ is a background velocity field which does not change with time. We use the following background velocity field as a model of single eddy [101]:

$$\phi = -\frac{\phi_0}{\pi}(1 - 4y^2)^4 \cos(\pi x) \tag{3.2}$$

where ϕ is the stream function, see Fig. 3.1. Our simulation is defined on a box of size L_0^2 with 256^2 points, $x, y \in [-L_0/2, L_0/2]$. The initial condition is $\psi_0(x,y) = B_0(x + L_0/2)$, where B_0 is a coefficient analogous to the magnitude of the external magnetic field in MHD. We set $B_0 = 1.0 * 10^{-2}$ in our runs to compare with Weiss's study [101] (B_0 should be a small number considering the allowed range of ψ: $\psi \in [-1, 1]$). The boundary conditions are Dirichlet in both directions: $\psi = \psi_0$ and $\nabla^2\psi = \nabla^2\psi_0$ at boundaries. Without losing generality, we normalize the system as follows: let length scale $L_0 = 1.0$ and time scale $t_0 = L_0/v_0 = L_0^2/\phi_0 = 1.0$. The absolute value of the velocity does not change the physics as long as it is nonzero, because we can always re-scale the time scale to make the system identical to the case where $v_0 = 1.0$. In this Letter, we focus on the competition between shearing and dissipation, so the $v_0 = 0$ cases are excluded. Thus, there are only two independent parameters: D and ξ. The range of parameters used in our simulations are summarized in Table. 3.1.

The dimensionless parameters are:

1. The Péclet Number $\mathrm{Pe} = L_0 v_0 / D$, the analogue of magnetic Reynolds number Rm in MHD, is the advective transport rate to the diffusive transport rate. In our simulation, $\mathrm{Pe} = D^{-1}$.

2. The Cahn Number $\mathrm{Ch} = \xi / L_0$ is the characteristic length scale of the interface width over the system size. In our simulation, $\mathrm{Ch} = \xi$.

Table 3.1: The parameters used in our simulations.

Runs	D	ξ
Run1	$3.16 * 10^{-4}$	$1.0 * 10^{-2}$
Run2	$1.0 * 10^{-4}$	$1.0 * 10^{-2}$
Run3	$3.16 * 10^{-5}$	$1.0 * 10^{-2}$
Run4	$1.0 * 10^{-5}$	$1.0 * 10^{-2}$
Run5	$3.16 * 10^{-5}$	$1.2 * 10^{-2}$
Run6	$3.16 * 10^{-5}$	$1.5 * 10^{-2}$
Run7	$3.16 * 10^{-5}$	$1.8 * 10^{-2}$

3.3 Time Evolution of the Concentration Field

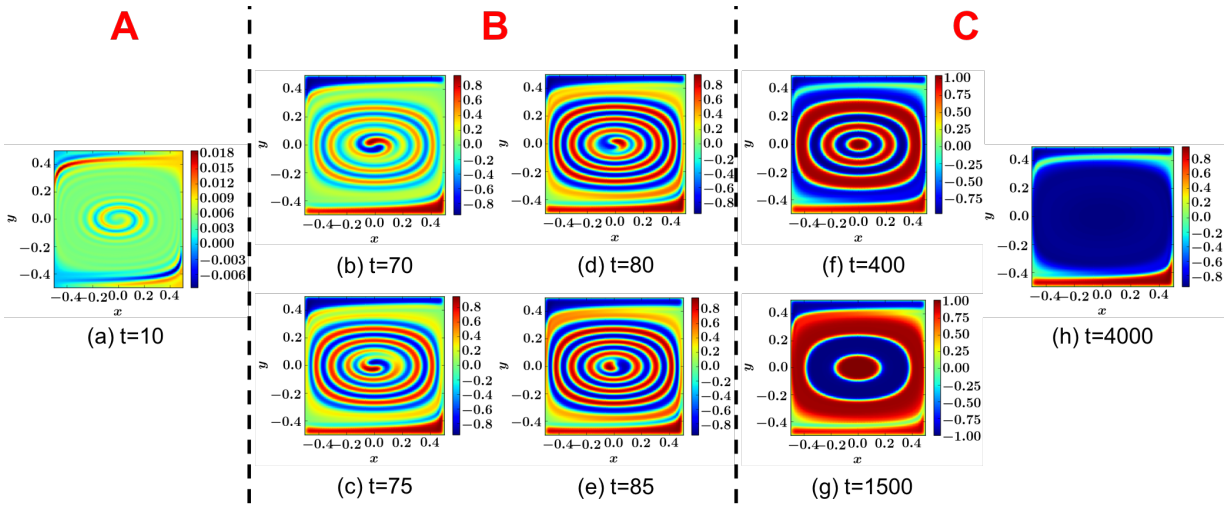

Figure 3.2: The evolution of the ψ field, represented by Run2. (a) The 'jelly roll' stage, in which the stripes are spirals. (b) - (e) The topological evolution stage, in which the topology evolves from spirals to concentric annuli in the center of the pattern. (f) & (g) The target pattern stage, in which the concentration field is composed of concentric annuli. The band merger progress occurs on exponentially long time scales; see (f) → (g) as an example. (h) The final steady state.

We observe three stages in the evolution of the concentration field: (A) formation of a 'jelly roll' pattern, (B) a change in topology, and (C) formation of target pattern (Fig. 3.2).

(A) In the 'jelly roll' pattern stage, the magnitude of $|\psi|$ remains close to zero. Stripes form gradually, and are then wound up into spirals by the fluid motion. See Fig. 3.2 (a) for a typical concentration field plot in the 'jelly roll' pattern stage. This wind-up process also occurs in the early stage of the expulsion problem in MHD.

(B) In the topological evolution stage, the ψ field inside the stripes quickly approaches $\pm \sim 1$, demonstrating that phase separation has occurred. In this stage, stripes break up and reconnect with adjacent stripes. The spirals evolve to concentric annuli, with topology change proceeding from outside to inside, one annulus at a time. Fig. 3.2 (b) - (e) show the

topology evolution of the stripe in the center of the pattern. Fig. 3.3 illustrates this process: the stripes break in the middle, while the outer parts reconnect to form a circle.

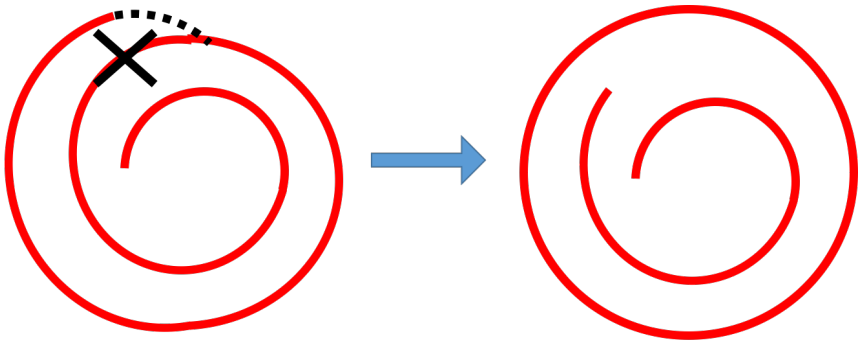

Figure 3.3: An illustration of the topological evolution from the 'jelly roll' pattern to the target pattern: the stripes break in the middle, and the outer parts reconnect into a circle.

(C) In the target pattern stage, the bands form concentric annuli, in contrast to spirals. See Fig. 3.2 (f) and (g) for typical concentration field plots in the target pattern stage. The bands are aligned with the stream lines. This structure is caused by shear flows. Shears can stabilize the bands against their intrinsic surface tension instabilities. Previous studies that investigated how the Cahn-Hilliard system behaves in a shear flow noted that the formation of band patterns aligned along the flow direction [66, 47, 46]. Shear flow with closed stream lines leads to the target pattern.

The target patterns are metastable. They persist on time scales that are exponentially long relative to the eddy turnover time. During their life, the bands merge with each other very slowly, and the number of bands tends to decrease over time (see Fig. 3.2 (f) and (g)). The merger time scales will be discussed in more detail below, after Fig. 3.5. Fig. 3.4 shows how the concentration field along the y axis at $x = 0$ evolves with time. The merger process is shown as the corner of the "$>$" shape in the plot. The band merger process is similar to step merger in drift-ZF staircases [1, 2]. The formation and coalescence of meso-steps is analogous to the formation and merger of the target bands in the Cahn-Hilliard system. Because the Cahn-Hilliard system does not

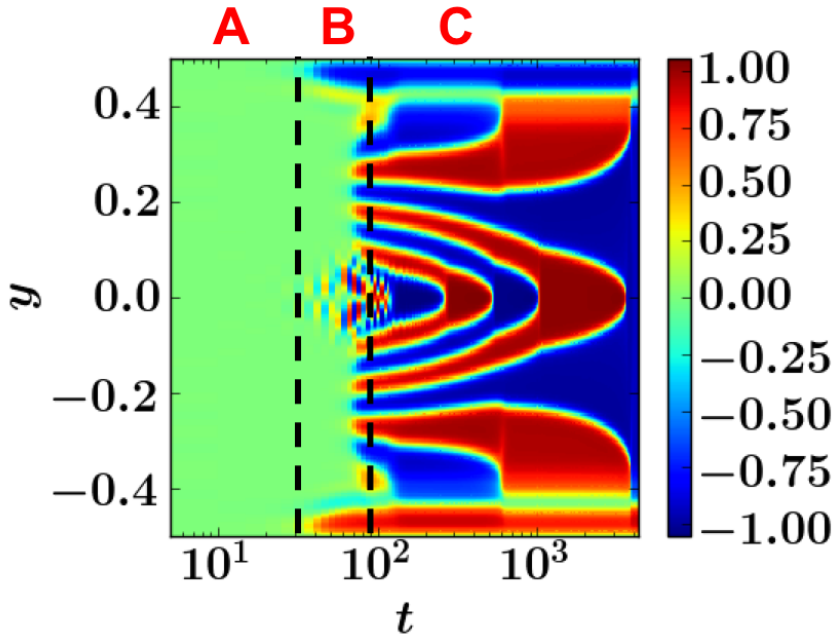

Figure 3.4: The evolution of ψ at $x = 0$ with time (Run2). The three stages are distiguished by black dashed lines, and marked as A, B, and C, respectively. In the target pattern stage (C), the merger process is shown as the corner of the "$>$" shape.

support a selected direction, it does not exhibit barrier propagation, as seen in models of drift-ZF staircases.

Fig. 3.2 (h) shows the final steady state. It resembles what is observed during the homogenization of magnetic potential A in MHD. The major difference is that the concentration field is $\psi \sim -1$ in the center of the eddy for the Cahn-Hilliard system, instead of $A \sim 0$ in MHD. This result implies that the concentration field is not conserved in our simulation, i.e., the red fluid is lost. This is acceptable, because the Dirichlet boundary conditions do not forbid the transport of matter in or out of the eddy. The choice of this boundary condition is to allow comparisons to studies of flux expulsion.

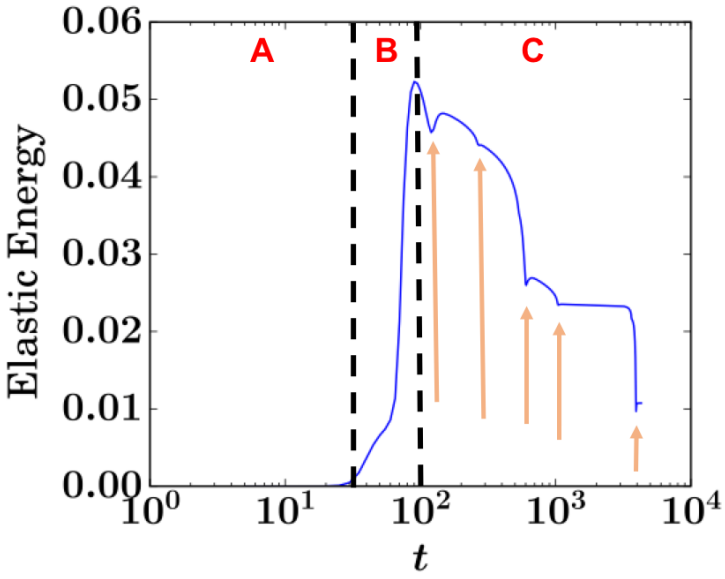

Figure 3.5: The time evolution of elastic energy (Run2). Note that logarithm scale is used for the t axis. A: the 'jelly roll' stage; B: the topological evolution stage; C: the target pattern stage. The dips marked by orange arrows are due to band mergers.

3.4 Time Evolution of the Elastic Energy

In our previous study [30], we stressed the analogy between 2D CHNS and 2D MHD. The energy in MHD consists of two parts: kinetic energy and magnetic energy. Similarly, we can also define the energy in the CHNS system to be the sum of kinetic energy E_K and elastic energy E_B [30]:

$$E_K = \int \frac{1}{2}\mathbf{v}^2 \, \mathrm{d}^2x \tag{3.3}$$

$$E_B = \int \frac{1}{2}\xi^2(\nabla\psi)^2 \, \mathrm{d}^2x \tag{3.4}$$

Note that this definition of energy differs from the energy commonly used in studies on the CHNS system ($E = \int[-\frac{1}{2}\psi^2 + \frac{1}{4}\psi^4 + \frac{1}{2}\xi^2(\nabla\psi)^2 + \frac{1}{2}\mathbf{v}^2]\,\mathrm{d}^2x$), but it makes it easier to compare to MHD studies. Since the velocity does not change with time in this study, the kinetic energy stays constant. The elastic energy E_B is the analogue of the magnetic energy in MHD. The time

evolution of elastic energy for a typical run is shown in Fig. 3.5. The 3 stages in the evolution are marked as A, B, and C, respectively.

In the 'jelly roll' pattern stage, the elastic energy increases but remains small compared to later stages. In the topology change stage, the elastic energy rises quickly and reaches a maximum value when the topology change is complete. Then, in the target pattern stage, the elastic energy decreases slowly and episodically. When band merger occurs, it appears as a local dip in the elastic energy time evolution plot. Examples of the dips are marked by orange arrows in Fig. 3.5. The time scales for band mergers can be obtained in the plot by measuring the time interval of the dips. The time scales for mergers are observed to be linear on the plot with a logarithm scale, so they are exponential on a linear scale. Note that in our normalization, the eddy turnover time is 1. The band merger time scales differ for each occurrence, but they all are exponentially long relative to the eddy turnover time.

3.5 The effects of D and ξ

In order to observe the phenomena presented above, there is a necessary range of parameters. Ch should be small, so long as the interface width is resolved ($\xi > h_0$, where h_0 is the mesh size). This is because we are interested in cases where the interface width is small compared to the system size. Pe should be large, so long as the cell's boundary layer is resolved ($L_{BL} > h_0$, where L_{BL} is the width of the boundary layer in ψ at the inner edge of the cell). In MHD, one expects to observe expulsion phenomenon when the magnetic Reynolds number Rm is large. Analogously, in the Cahn-Hilliard system, we are interested in the large Pe regime. Similar to the MHD case for which $L_{BL} \sim \mathrm{Rm}^{-1/3} L_0$, the width of the boundary layer in the Cahn-Hilliard system is estimated to be $L_{BL} \sim \mathrm{Pe}^{-1/5}\mathrm{Ch}^{3/5} L_0$. Thus the condition for resolution of L_{BL} is $\mathrm{Pe}^{1/5}\mathrm{Ch}^{-3/5}(\frac{h_0}{L_0}) < 1$. This expression is obtained by calculating the mixing time scale of the shear + dissipation hybrid case $t_{mix}^{-1} \sim \mathrm{Pe}^{-1/5}\mathrm{Ch}^{2/5} t_0^{-1}$. Note that in the Cahn-Hilliard case, the

dissipation is the hyper-diffusion, and the ratio of convection to hyper-diffusion is $\mathrm{Pe}/\mathrm{Ch}^2$.

A parameter scan of Pe and Ch is shown in Fig. 3.6. The elastic energy evolution exhibits the same trend discussed above, and all values of Pe and Ch pass through the same three stages. A characteristic time scale in this system is the time to reach the maximum elastic energy τ. τ is shown to scale as $\tau \sim \mathrm{Pe}^{1.05\pm0.05}\mathrm{Ch}^{1.78\pm0.04}$ (Fig. 3.7). The error bars reflect only the standard deviations of the linear fits, and the errors from τ itself are not considered. This relationship can be approximately understood by dimensional analysis: $\tau \propto \xi^2/D$.

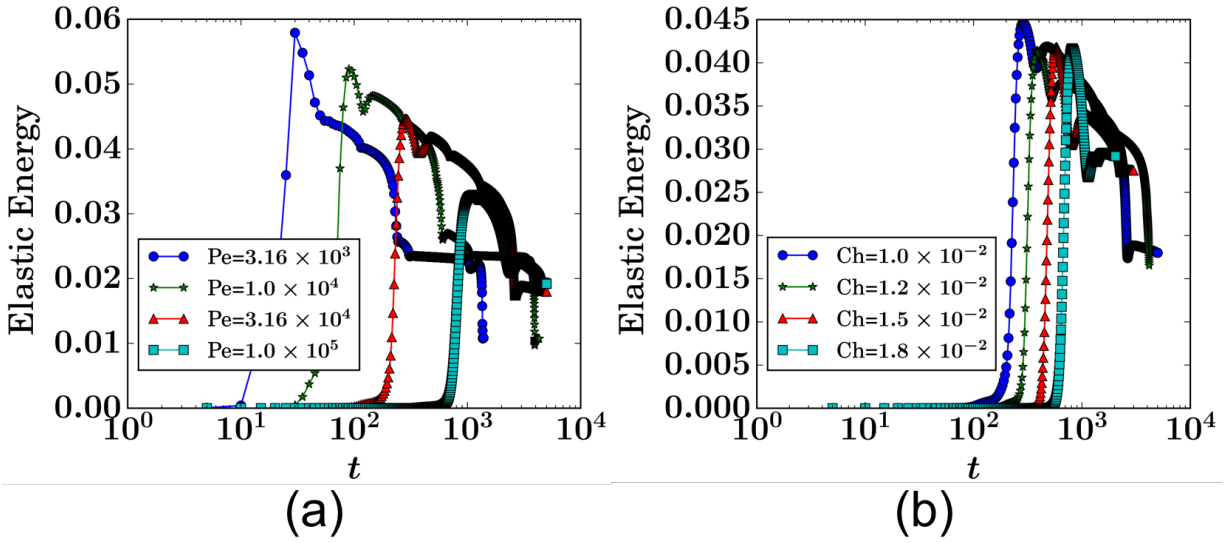

Figure 3.6: The time evolution of elastic energy for a range of Pe (a) and Ch (b).

3.6 Conclusion and Discussion

In summary, we have investigated the evolution of the concentration field of the Cahn-Hilliard system in the background of a single convective eddy, motivated by the analogy between CHNS and MHD. This study is an extension of the classic study of flux expulsion in 2D MHD and homogenization of potential vorticity in 2D fluids. We find there are three stages of the evolution: the 'jelly roll' pattern stage, the stage of topological evolution, and the target pattern stage. The target bands are metastable: they merge with each other on a time scale exponentially

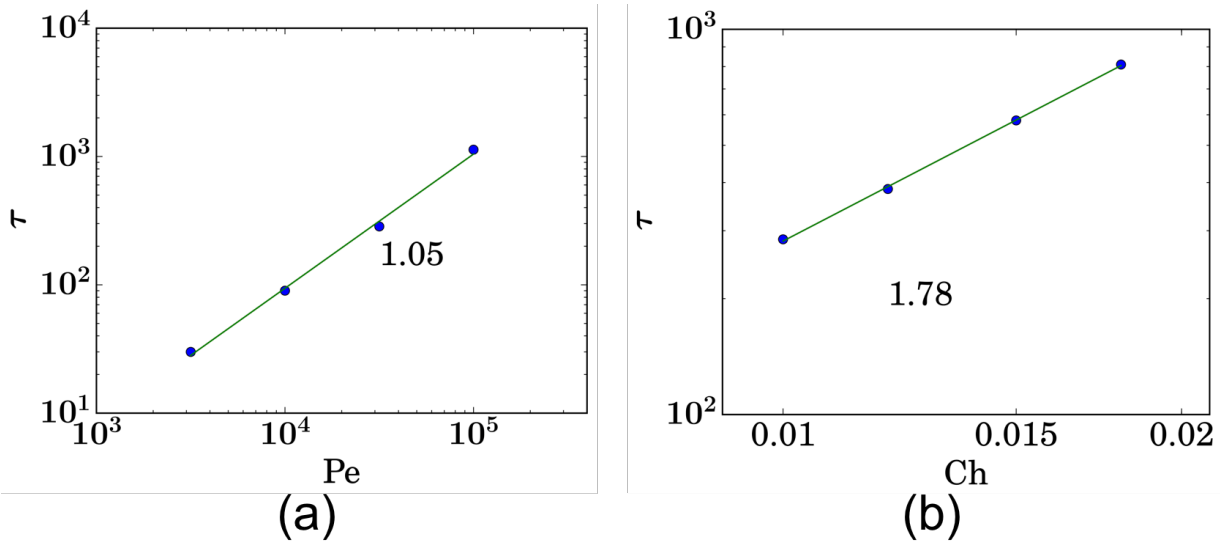

Figure 3.7: The relationship between the time to reach the maximum elastic energy τ and the dimensionless parameters Pe (a) and Ch (b).

long relative to the eddy turnover time. Band merger occurrences are associated with dips in the elastic energy evolution. The time scale for target pattern evolution and band merger is extended by the imposed shear flow of the eddy. Such flows slow down the merger of bands that is known to occur in, and is natural to, the Cahn-Hilliard system. The band merger process is similar to the drift-ZF staircases in the confined plasma turbulence. The major difference from flux expulsion in MHD is the metastable target pattern stage before reaching the steady homogenized state. Compared to the homogenization of the potential vorticity system, the evolution of the passive scalar in the Cahn-Hilliard system contains additional multi-stage physics, and it exhibits richer dynamics on the long time scale. We also found the time to reach the maximum elastic energy τ is $\tau \sim \mathrm{Pe}^{1.05\pm0.05}\mathrm{Ch}^{1.78\pm0.04}$. In future work, we will investigate the evolution of the concentration field with the back reaction on the fluid dynamics.

Acknowledgements

We thank David W. Hughes for stimulating discussions and Los Alamos National Laboratory for its hospitality and help with computing resources. This research was supported by the US Department of Energy, Office of Science, Office of Fusion Energy Sciences, under Award No. DE-FG02-04ER54738 and CMTFO Award No. DE-SC0008378.

Chapter 3 is a reprint of the material as it appears in X. Fan, P.H. Diamond, L. Chacón, "Formation and evolution of target patterns in Cahn-Hilliard flows", *Phys. Rev. E (Rap. Comm.)*, 96 (4), 041101, 2017. The dissertation author was the primary investigator and author of this paper.

Chapter 4

Spontaneous Transport Barriers Quench Turbulent Resistivity in 2D MHD

This Letter identifies the physical mechanism for the quench of turbulent resistivity in 2D MHD. Without an imposed, ordered magnetic field, a multi-scale, blob-and-barrier structure of magnetic potential forms spontaneously. Magnetic energy is concentrated in thin, linear barriers, located at the interstices between blobs. The barriers quench the transport and kinematic decay of magnetic energy. The local transport bifurcation underlying barrier formation is linked to the inverse cascade of $\langle A^2 \rangle$ and negative resistivity, which induce local bistability. For small scale forcing, spontaneous layering of the magnetic potential occurs, with barriers located at the interstices between layers. This structure is effectively a magnetic staircase.

4.1 Introduction

The evolution of mean quantities in turbulence is frequently modelled as a *transport process*, using ideas from the kinetic theory of gases. A classic example is that of Prandtl's theory of turbulent boundary layers, which first proposed the use of an eddy viscosity - based upon mixing

length theory - to calculate mean flow profiles at high Reynolds number. Magnetohydrodynamics (MHD) presents additional challenges, especially at high magnetic Reynolds number Rm. There, models based on transport theory concepts are central to our understanding of mean B ($\langle \mathbf{B} \rangle$) evolution in turbulent flows. Indeed, the well-known theory of mean field electrodynamics (Moffatt [71]) employs transport coefficients α, β - related to turbulent helicity and energy, respectively - to describe the growth and transport of a mean magnetic field. Such models are heavily utilized in dynamo theory - the study of how large scale fields are formed. The turbulent or "eddy" *resistivity*, η_T, is ubiquitous in these models (and corresponds to β above). While η_T is often taken as kinematic ($\eta_T \sim \eta_K \sim \sum_{\mathbf{k}} \langle \tilde{v}^2 \rangle_{\mathbf{k}} \tau_c$ where τ_c is the self-correlation time) for many applications, nonlinear dependence of η_T on magnetic field and potential has been observed in numerous simulations [16, 100, 99, 15, 3, 62, 7, 33, 70, 56, 93, 94, 57, 51, 53, 52, 98, 29, 59, 67]. Such nonlinearity arises from the fact that the magnetic fields alter the turbulent flows which scatter them. As this nonlinearity tends to reduce η_T relative to kinematic expectations, such trends are referred to as quenching. Rm dependent quenching – i.e. when the product $\mathrm{Rm}\langle \mathbf{B} \rangle^2$ enters – is of particular interest, as it signals that for the relevant case of high Rm, relatively weak fields can produce significant feedback on transport and evolution processes. Such Rm-dependent feedback has been associated with Alfvenization (i.e. the conversion of hydrodynamics turbulence to Alfven wave turbulence) and/or with the balance of magnetic helicity $\langle \mathbf{A} \cdot \mathbf{B} \rangle$ (i.e. in 3D) or $\langle A^2 \rangle$ (i.e. in 2D). Both arguments ultimately point to *memory*, due to the freezing-in law, as the origin of the quench. The quenching problem is also relevant to models of fast reconnection and impulsive energy release processes in MHD, as it constrains the size of (frequently invoked) anomalous dissipation [103, 102]. More generally, it is an important paradigm of the transport of an active scalar.

In a seminal paper [16] which broached the quenching question, Cattaneo and Vainshtein (CV) presented numerical simulations of 2D MHD turbulence which demonstrated that even a weak large scale magnetic field is sufficient to quench the turbulent transport of the active scalar

A (the magnetic potential). Based on ideas from mean field theory, CV suggested – and presented simulations to support – the idea that η_T is given by

$$\eta_T \sim \frac{\langle v^2 \rangle^{1/2} l}{1 + \frac{1}{\mu_0 \rho} \mathrm{Rm} \langle \mathbf{B} \rangle^2 / \langle v^2 \rangle} \tag{4.1}$$

The mean field $\langle \mathbf{B} \rangle$ here is estimated using:

$$|\langle \mathbf{B} \rangle| \sim \sqrt{\langle A^2 \rangle} / L_0 \tag{4.2}$$

where L_0 is system size. For $\frac{1}{\mu_0 \rho} \mathrm{Rm} \langle \mathbf{B} \rangle^2 / \langle v^2 \rangle < 1$, $\eta_T \sim \eta_K \sim \langle v^2 \rangle^{1/2} l$. While for $\frac{1}{\mu_0 \rho} \mathrm{Rm} \langle \mathbf{B} \rangle^2 / \langle v^2 \rangle > 1$, $\eta_T \ll \eta_K$, so η_T is quenched. It is important to note that, in view of Cowling's Theorem, suppression occurs only for a time of *limited duration*, without external forcing of A. After the afore mentioned suppression stage, rapid decay of the magnetic field occurs, and η_T reverts to η_K. The evolutions of E_B, E_K (magnetic and kinetic energy) and $\langle A^2 \rangle$ (mean square potential) are shown in Fig. 4.1 (a, b).

Equation (4.1) was also obtained analytically from statistical theory, assuming the presence of an imposed weak large scale field $\mathbf{B}_0$ (i.e. $\langle \mathbf{B} \rangle = \mathbf{B}_0$) [40, 41, 27, 26]. (Note the assumptions that $|\langle \mathbf{B} \rangle|$ is determined by root-mean-square A and the system size in CV.) The derivation made use of $\langle A^2 \rangle$ balance to constrain the turbulent resistivity [105, 85, 84]. Rm-dependence of the quench stems from the fact that $\langle A^2 \rangle$ is conserved up to resistive diffusion. This early work on resistivity quenching triggered a tidal wave of subsequent studies of nonlinear dynamo evolution and quenching.

In this Letter, we show that, without an imposed, ordered magnetic field, Rm-dependent quenching is intrinsically an intermittency phenomena, and can occur where a global mean field $\langle \mathbf{B} \rangle$ simply does not exist. Rather, turbulent resistivity quenching occurs due to intermittent *transport barriers*. A transport barrier is a localized region of mixing and transport significantly lower than the mean thereof, i.e. $\eta_{T,local} < \bar{\eta}_T$. These barriers are extended, thin, linear features,

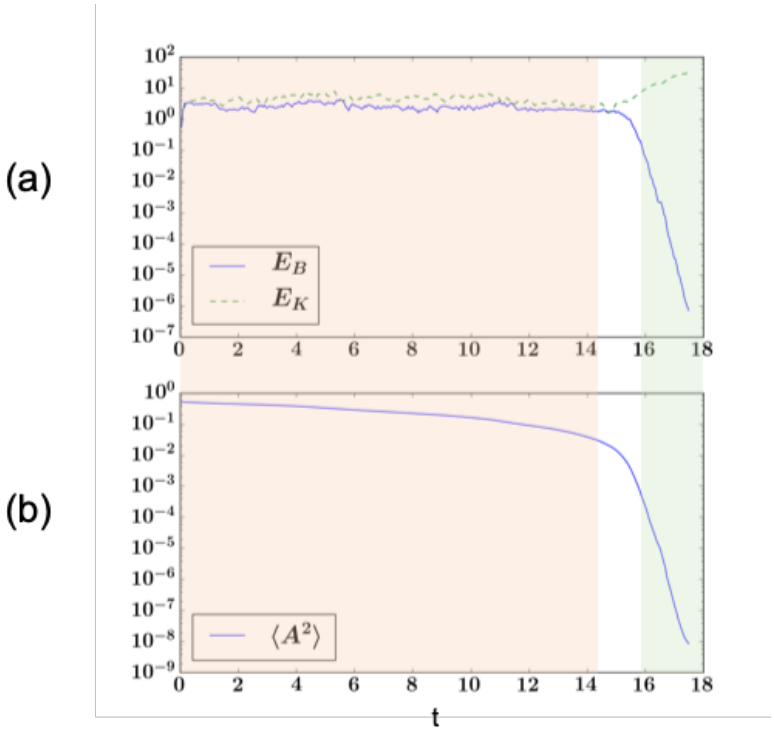

Figure 4.1: Time evolution of (a) magnetic energy E_B and kinetic energy E_K; (b) $\langle A^2 \rangle$ in Run1. The suppression stage is marked in orange, and the kinematic decay stage in green. The decay of E_B is slow in the suppression stage, which is consistent with previous studies. The decay of $\langle A^2 \rangle$ is also slow in the suppression stage, and is more smooth compared to E_B.

into which strong $\langle B^2 \rangle$ is concentrated. The barriers are formed by the $\langle B^2 \rangle$ feedback on scalar transport, specifically by magnetic flux coalescence. Thus, transport quenching is manifestly not a mean field effect, as the structure of the field is more akin to a random network than to a smooth mean field. The barriers form in the interstices between blobs of $\langle A^2 \rangle$, which are formed by the inverse cascade of $\langle A^2 \rangle$. Overall, the magnetic potential and field have a structure of "blob-and-barrier" at large Rm, as shown in Fig. 4.2. In contrast to the assumptions of CV, the magnetic field exhibits *two* non-trivial scales, i.e. the blob size L_{blob} and the barrier width W, where $W \ll L_{blob}$. L_{blob} characterizes the magnetic potential while W characterizes the field intensity.

The A field in the blob-and-barrier structure of 2D MHD resembles the concentration contrast field ψ in the Cahn-Hilliard Navier-Stokes (CHNS) system [89, 30, 31, 32, 77].

4.2 Analysis: global

In this Letter, the 2D MHD equations are solved using direct numerical simulation [20, 19] with doubly periodic boundary condition:

$$\partial_t A + \mathbf{v} \cdot \nabla A = \eta \nabla^2 A \tag{4.3}$$

$$\partial_t \omega + \mathbf{v} \cdot \nabla \omega = \frac{1}{\mu_0 \rho} \mathbf{B} \cdot \nabla \nabla^2 A + \nu \nabla^2 \omega + f \tag{4.4}$$

Here ω is vorticity, η is resistivity, ν is viscosity, $\mu_0 \rho$ is magnetic permeability and density, and f is an isotropic homogeneous external forcing, with wave number k and magnitude f_0. The simulation box size is $L_0^2 = 1.0 \times 1.0$ with 1024×1024 resolution. The parameters used are summarized in Table. 4.1. The initial condition for the ω field is $\omega_I = 0$ everywhere; the initial condition for A field is a cosine function in Run1:

$$A_I(x, y) = A_0 \cos 2\pi x \tag{4.5}$$

Table 4.1: Initial conditions, k and Rm for the suppression stage. For all runs, $A_0 = 1.0$ and $f_0 = 30$.

Runs	Initial Condition	η	ν	$1/(\mu_0\rho)$	k	Rm
Run1	Bimodal	$1*10^{-4}$	$1*10^{-4}$	0.04	5	~ 500
Run2	Unimodal	$1*10^{-4}$	$1*10^{-4}$	0.04	5	~ 500
Run3	Bimodal	$1*10^{-4}$	$2*10^{-3}$	0.01	32	~ 150

The setup of Run1 differs from that of Ref. [16] only in the range of Rm studied.

Non-trivial blob-and-barrier structure is observed in real space at large Rm, and this structure forms quickly after a short transition period. Fig. 4.2 (a1) shows a snapshot of magnetic potential in the suppression stage for Run1. It consists of "blobs" (regions in red and blue) and interstices (green), and is very different from the initial condition, for which a mean field is relevant. Fig. 4.2 (a2) shows the B^2 field for the same run. The high B^2 regions (bright color) occur at the interstices of the A blobs, since $\mathbf{B} \equiv \hat{\mathbf{z}} \times \nabla A$. The interstices have a 1-dimensional shape. We call these 1-dimensional, high B^2 regions "barriers", because these are the regions where transport is strongly suppressed relative to the kinematic case η_K, due to locally strong B^2, as discussed below. One measure of this blob-and-barrier structure is the structure of the probability density function (PDF) of A. As is shown in Fig. 4.2 (a3), the PDF of A for Run1 during the suppression stage has two peaks, both at $A \neq 0$.

Notably, such a structure of the PDF also appears in the analogous CHNS system. Some binary fluid transfers from miscible phase to immiscible phase when the temperature dropped to below the corresponding critical temperature, and this second order phase transition is called spinodal decomposition. The Cahn-Hilliard Navier-Stokes (CHNS) equations describe a binary fluid undergoing spinodal decomposition:

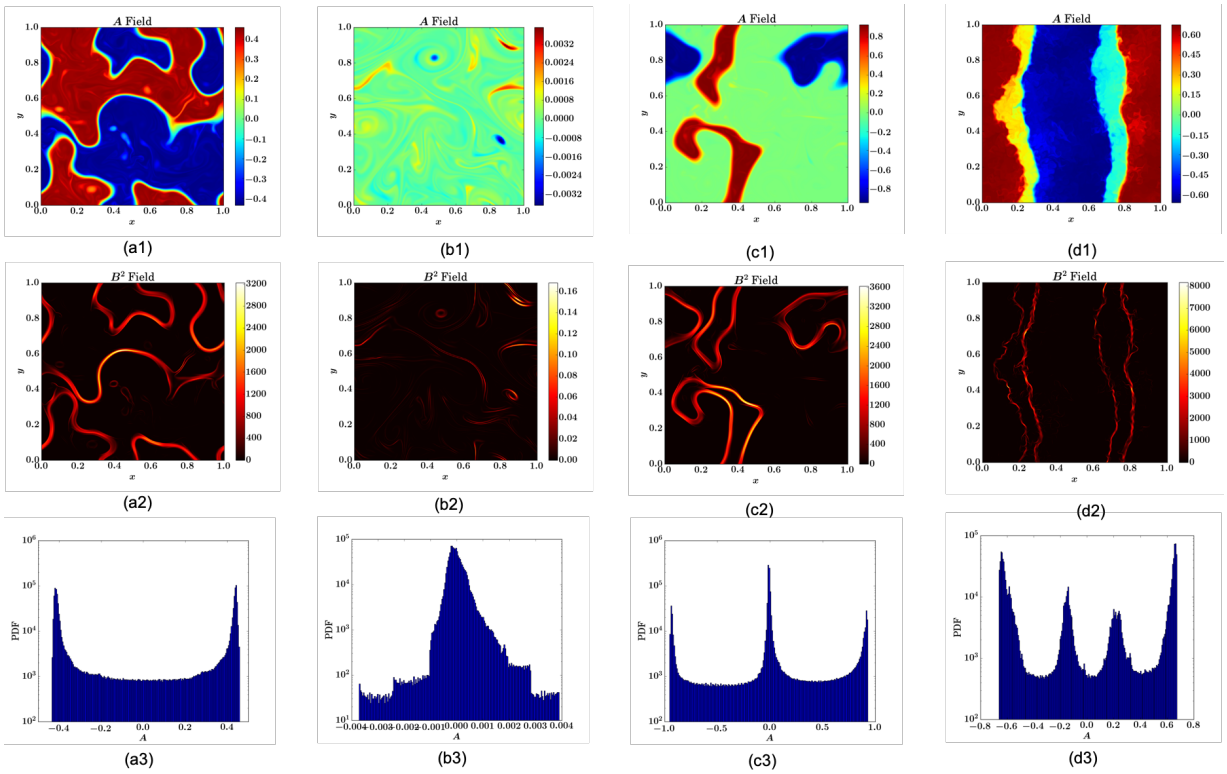

Figure 4.2: Row 1: A field snapshots; Row 2: $\langle B^2 \rangle$ field snapshots; Row 3: PDF of A. Column a: Run1 at $t = 10$ (suppression stage). The system exhibits blob-and-barrier feature, and the PDF of A is bimodal. Column b: Run1 at $t = 17$ (kinematic decay stage). The distribution of the fields are trivial. Column c: Run2 at $t = 10$. Two peaks still arise on the PDF of A even though its initial condition is unimodal. Column d: Run3 at $t = 4.5$. The system exhibits staircases feature, and the PDF of A has multiple peaks.

$$\partial_t \psi + \mathbf{v} \cdot \nabla \psi = D\nabla^2(-\psi + \psi^3 - \xi^2 \nabla^2 \psi) \tag{4.6}$$

$$\partial_t \omega + \mathbf{v} \cdot \nabla \omega = \frac{\xi^2}{\rho} \mathbf{B}_\psi \cdot \nabla \nabla^2 \psi + \nu \nabla^2 \omega \tag{4.7}$$

$$\mathbf{v} = \hat{\mathbf{z}} \times \nabla \phi, \ \omega = \nabla^2 \phi \tag{4.8}$$

$$\mathbf{B}_\psi = \hat{\mathbf{z}} \times \nabla \psi, \ j_\psi = \xi^2 \nabla^2 \psi \tag{4.9}$$

where $\psi = \frac{\rho_A - \rho_B}{\rho_A + \rho_B}$ is the local relative concentration, and ξ is a coefficient describing the strength of the surface tension interaction.

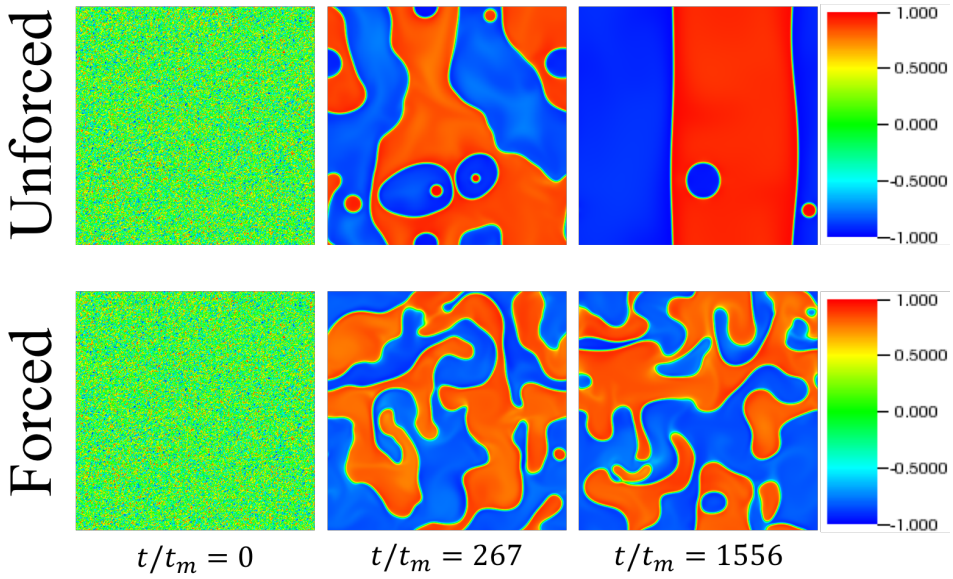

Figure 4.3: Some typical screenshots for the ψ field in the 2D CHNS system. Reprint from [30].

2D CHNS and 2D MHD are both active scalar systems. The two systems are analogous, and the correspondence of the physics quantities between the two systems are summarized in Table. 4.2. The comparison and contrast of some most important features are summarized in Table. 4.3 and Table. 4.4. See Ref. [30, 31, 32] for more details about turbulence in 2D CHNS.

In comparison with the blob-and-barrier structure described above, in the kinematic decay

Table 4.2: The correspondence between 2D MHD and the 2D CHNS system. Reprint from [30].

	2D MHD	2D CHNS
Magnetic Potential	A	ψ
Magnetic Field	$\mathbf{B}$	$\mathbf{B}_\psi$
Current	j	j_ψ
Diffusivity	η	D
Interaction strength	$\frac{1}{\mu_0}$	ξ^2

Table 4.3: Comparison of 2D MHD and the 2D CHNS system. Reprint from [30].

	2D MHD	2D CHNS
Ideal Quadratic Conserved Quantities	Conservation of E, H^A and H^C	Conservation of E, H^Ψ and H^C
Role of elastic waves	Alfven wave couples $\mathbf{v}$ with $\mathbf{B}$	CHNS linear elastic wave couples $\mathbf{v}$ with $\mathbf{B}_\psi$
Origin of elasticity	Magnetic field induces elasticity	Surface tension induces elasticity
Origin of the inverse cascades	The coalescence of magnetic flux blobs	The coalescence of blobs of the same species
The inverse cascades	Inverse cascade of H^A	Inverse cascade of H^Ψ
Power law of spectra	$H_k^A \sim k^{-7/3}$	$H_k^\Psi \sim k^{-7/3}$

Table 4.4: Contrast of 2D MHD and the 2D CHNS system. Reprint from [30].

	2D MHD	2D CHNS
Diffusion	A simple positive diffusion term	A negative, a self nonlinear, and a hyper-diffusion term
Range of potential	No restriction for range of A	$\psi \in [-1, 1]$
Interface Packing Fraction	Not far from 50%	Small
Back reaction	$\mathbf{j} \times \mathbf{B}$ force can be significant	Back reaction is apparently limited
Kinetic energy spectrum	$E_k^K \sim k^{-3/2}$	$E_k^K \sim k^{-3}$
Suggestive cascade by E_k^K	Suggestive of direct energy cascade	Suggestive of direct enstrophy cascade

stage of Run1 (i.e. at later time, when the magnetic field is so weak that η_T reverts to η_K), the fields are well mixed and nontrivial real space structure is absent. No barriers are discernible in the decay stage. The corresponding PDF of A is a distribution for a passive scalar, with *one peak* at $A = 0$, as shown in Fig. 4.2 column (b).

The time evolution of PDF of A for Run1 (Fig. 4.4 (a)) has a horizontal "Y" shape. The PDF has two peaks initially, and the interval between the peaks decreases as the A field decays. The PDF changes from double peak to single peak as the system evolves from the suppression stage to the kinematic stage.

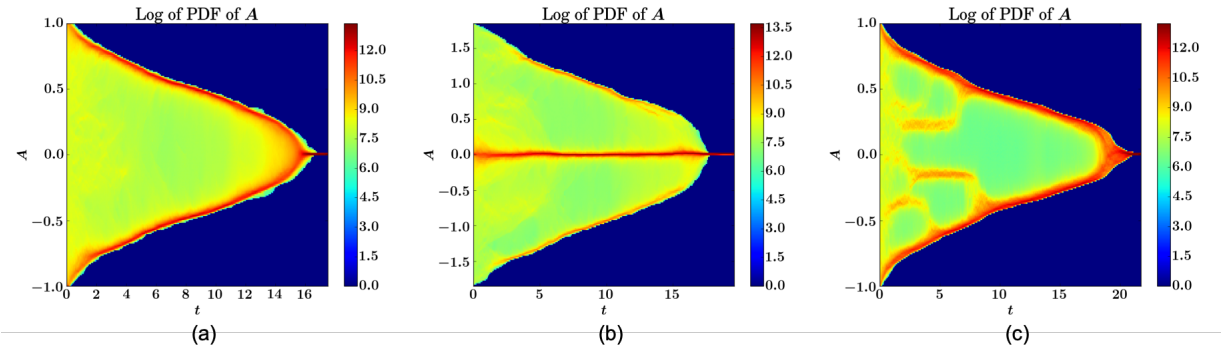

Figure 4.4: The time evolutions of PDF of A. (a) For Run1, the PDF is bimodal in the suppression stage, and ΔA between the two peaks reduces in time. The PDF becomes unimodal in the kinematic decay stage. (b) For Run2, two peaks at $A \neq 0$ still arise spontaneously given a unimodal initial condition. (c) For Run3, with external forcing at smaller scale, layering and coarsening can occur. See further explanations in the text.

Two quantities which characterize the field structure in the suppression stage are the *packing fraction* P, and *barrier width* W, defined below. In order to identify the barriers, we set a threshold on local field intensity, and define the barriers to be the regions where $B(x,y) > \sqrt{\langle B^2 \rangle} * 2$. The packing fraction P is defined as:

$$P \equiv \frac{\text{\# of grid points in barrier regions}}{\text{\# of total grid points}} \tag{4.10}$$

P is the fraction of the space where intensity exceeds the mean square value. The expression for the barrier width is $W \sim \Delta A / B_b$, where ΔA is the difference in A between adjacent blobs, and B_b

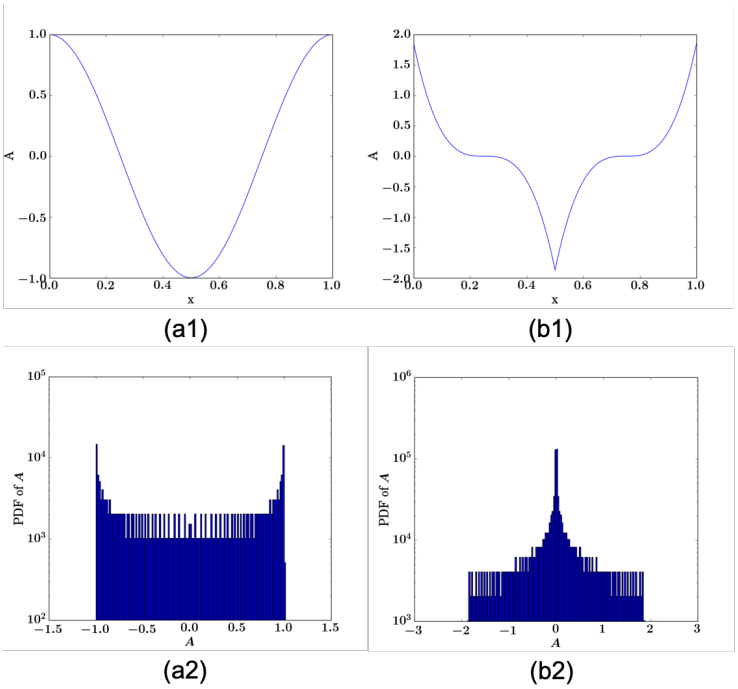

Figure 4.5: The initial conditions for A and their PDFs: (a) "Bimodal" for Run1 and Run3; (b) "Unimodal" for Run2.

is the magnitude of the magnetic field in the barrier regions. We use $\sqrt{\langle A^2 \rangle}$ to estimate ΔA for the bimodal PDF, such as for Run1. The narrow barriers contain most of the magnetic energy. For example, in Run1 at $t = 10$, the barriers occupy only $P = 9.9\%$ of the system space, but the magnetic field in these regions accounts for 80.7% of the magnetic energy. Therefore, we can use the magnetic energy in the barriers $\langle B_b^2 \rangle$ to approximate the total magnetic energy, i.e.:

$$\sum_{\text{barriers}} B_b^2 \sim \int \mathrm{d}^2 x B^2 \tag{4.11}$$

It follows that $\langle B_b^2 \rangle \sim \langle B^2 \rangle / P$. We can thus define W based on the arguments above as:

$$W^2 \equiv \langle A^2 \rangle / (\langle B^2 \rangle / P) \tag{4.12}$$

This definition of W can be justified by measuring the approximate barrier widths. The time

evolutions of P and W in Run1 are shown in Fig. 4.6. P stays at $0.08 \sim 0.10$ throughout the suppression stage. P starts to decline near the end of the suppression stage, and drops to the noise level in the kinematic decay stage. W decreases during the suppression stage, due mainly to the decrease in ΔA. It is important to note that the decline in P, which begins at $t \sim 13$, slightly *leads* the decay in magnetic energy, which begins at $t \sim 15$. This supports the notion that barriers, the population of which is measured by P, are responsible for the quenching of mixing and decay in the suppression stage.

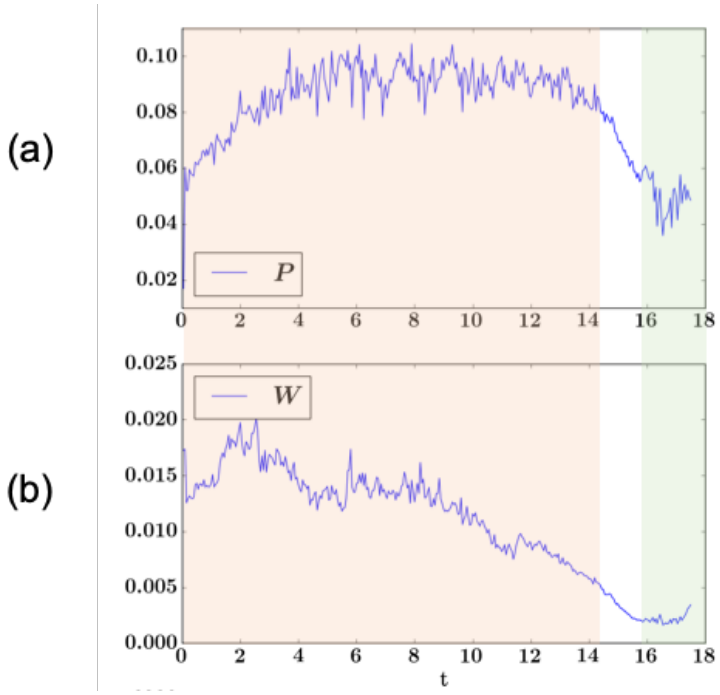

Figure 4.6: Time evolution of (a) packing fraction P; and (b) barrier width W in Run1.

One may question whether the bimodal PDF is due to the initial condition, since the cosine initial condition in Run1 is bimodal. The answer is no. In order to show this, a unimodal initial condition is constructed for Run2, such that the initial PDF of A has one peak at $A = 0$:

$$A_I(x,y) = A_0 * \begin{cases} -(x-0.25)^3 & 0 <= x < 1/2 \\ (x-0.75)^3 & 1/2 <= x < 1 \end{cases} \tag{4.13}$$

See Fig. 4.5 for the comparison between bimodal and unimodal initial condition. To make Run2 and Run1 have the same time duration of the suppression stage, the initial magnitude A_0 in Run2 is chosen such that the initial $\langle A^2 \rangle$ (not E_B!) is the same with Run1.

Fig. 4.2 column (c) shows a snapshot for Run2 at $t = 10$. The time evolution of the PDF of A for that case is shown in Fig. 4.4 (b). It is evident that, two non zero peaks in the PDF of A still arise, even if the initial condition is unimodal. The blob structure in A and the barrier structure in B^2 are also evident.

4.3 Analysis: local

One can easily see from the B^2 fields plots in Fig. 4.2 that, a large scale $\langle \mathbf{B} \rangle$ does not exist. Intermittent magnetic intensity, with low P, is a consequence of the blob-and-barrier structure. Therefore, the traditional approach of mean field theory, especially Eqn. (4.2), is neither applicable nor relevant. Globally, no theory exists for $\mathbf{B}_0 = 0$. Usual closure approaches appear useful when the averaging window is restricted to a suitable size, corresponding to a *localized region* within which a mean $\mathbf{B}$ exists. In order to derive an expression for the effective η_T for such a local region from dynamics, we extend the theory by [40, 41, 27, 26], and propose:

$$\eta_T = \frac{\langle v^2 \rangle^{1/2} l}{1 + \mathrm{Rm} \frac{1}{\mu_0 \rho} \langle \mathbf{B} \rangle^2 / \langle v^2 \rangle + \mathrm{Rm} \frac{1}{\mu_0 \rho} \frac{\langle A^2 \rangle}{L_{blob}^2} / \langle v^2 \rangle} \tag{4.14}$$

Here L_{blob} is the size of the large A blobs, i.e. the characteristic length scale for $\langle A^2 \rangle$. The derivation is shown below.

We start from:

$$\frac{1}{2} [\partial_t \langle A^2 \rangle + \langle \nabla \cdot (\mathbf{v} A^2) \rangle] = -\Gamma_A \frac{\partial \langle A \rangle}{\partial x} - \eta \langle B^2 \rangle \tag{4.15}$$

where $\Gamma_A = \langle v_x A \rangle$ is the spatial flux of A. In the past, only the $\Gamma_A \frac{\partial \langle A \rangle}{\partial x}$ term is kept in (4.15) to

balance $\eta\langle B^2\rangle$. However, in the absence of $\mathbf{B}_0$, $\Gamma_A \frac{\partial\langle A\rangle}{\partial x}$ term can be small, while the triplet term $\langle\nabla\cdot(\mathbf{v}A^2)\rangle$ can remain, if the average is taken over a window smaller than the system size L_0. Note the relevant scale l here is

$$l_d < W < l < L_0 \tag{4.16}$$

where l_d is the dissipation scale. Retaining all contributions, we have

$$\partial_t\langle A^2\rangle = -\langle\mathbf{v}A\rangle\cdot\nabla\langle A\rangle - \nabla\cdot\langle\mathbf{v}A^2\rangle - \eta\langle B^2\rangle \tag{4.17}$$

Now assume the fluxes are Fickian. Note that, in principle, there are two diffusion coefficients:

$$\langle\mathbf{v}A\rangle = -\eta_{T1}\nabla\langle A\rangle \tag{4.18}$$

$$\langle\mathbf{v}A^2\rangle = -\eta_{T2}\nabla\langle A^2\rangle \tag{4.19}$$

Plugging them in, we get

$$\partial_t\langle A^2\rangle = \eta_{T1}(\nabla\langle A\rangle)^2 + \nabla\eta_{T2}\cdot\nabla\langle A^2\rangle - \eta\langle B^2\rangle \tag{4.20}$$

The first term on the RHS is turbulent diffusion of $\langle A\rangle$, corresponding to the large scale magnetic field. The second term is the turbulent diffusion of $\langle A^2\rangle$, which controls decay in weak magnetic field. The third term is the usual collisional dissipation. In principle, $\eta_{T1}\neq\eta_{T2}$, though these two are related. Both terms are retained. For simplicity, we assume $\eta_{T1}=\eta_{T2}=\eta_T$. For a stationary state, we have

$$\langle B^2\rangle \sim \frac{\eta_T}{\eta}(\langle B\rangle^2 + \langle A^2\rangle/L_{blob}^2) \tag{4.21}$$

where L_{blob} is the blob size, the characteristic length scale for $\langle A^2\rangle$. By standard closure methods,

one can obtain an expression for η_T [85, 84]:

$$\eta_T = \sum_{\mathbf{k}} \tau_c [\langle v^2 \rangle_{\mathbf{k}} - \frac{1}{\mu_0 \rho} \langle B^2 \rangle_{\mathbf{k}}] \tag{4.22}$$

Plugging (4.21) into (4.22) yields Eqn. (4.14) proposed above. Detailed comparisons of Eqn. (4.14) with simulation results are nontrivial and will be left for a future paper.

Note that $L_{blob} \ll L_0$. In regions where no high intensity magnetic field is present, i.e. inside blobs, $\mathrm{Rm} \frac{1}{\mu_0 \rho} \langle B \rangle^2 / \langle v^2 \rangle$ is negligible. Yet transport is still reduced relative to kinematics by $\langle A^2 \rangle$, via the $\mathrm{Rm} \frac{1}{\mu_0 \rho} \frac{\langle A^2 \rangle}{L_{blob}^2} / \langle v^2 \rangle$ term. In the barrier regions where magnetic energy is large, $\mathrm{Rm} \frac{1}{\mu_0 \rho} \langle B \rangle^2 / \langle v^2 \rangle$ is dominant, since $\langle B^2 \rangle \gg \langle A^2 \rangle / L_{blob}^2$ for $P \ll 1$. Such regions – barriers – are where turbulent transport of A is most strongly suppressed.

A key question concerns how transport barriers form spontaneously in turbulent 2D MHD. We argue that transport barriers result from negative resistivity, driven by the inverse cascade of $\langle A^2 \rangle$. In Eqn. (4.22), the positive contribution to η_T is a consequence of turbulent mixing by fluid advection, while the second, negative, term is a consequence of flux coalescence. From the above, we see that the turbulent resistivity can go negative locally, where $\langle B^2 \rangle$ is strong. Of course, the system-averaged resistivity is positive, so the field decays, though slowly. Note though that a local negative contribution can trigger a feedback loop, i.e.: B^2 strong in a specific region $\rightarrow$ local η_T negative $\rightarrow$ local ∇A increases $\rightarrow$ local B^2 increases further. The feedback process saturates after the short transition period, as the inverse cascade of $\langle A^2 \rangle$ must ultimately deplete the small scales.

Another way to view this evolution is as a local transport bifurcation – see the spatially local S-shaped flux-gradient curve for A, shown in Fig. 4.7 for illustration, which follows from Eqn. (4.14). The S-curve describes a bi-stable system. Note there are two stable ranges with positive slope, and one unstable region between, with a negative slope (as for negative resistivity). This implies that barrier formation is a transport bifurcation, which occurs when local magnetic

intensity exceeds the threshold given by (4.22). This mechanism resembles a transport bifurcation in magnetically confined systems [1, 2]. Here, feedback via regions of locally intense B^2, rather than $\mathbf{E} \times \mathbf{B}$ shear, is the trigger for barrier formation.

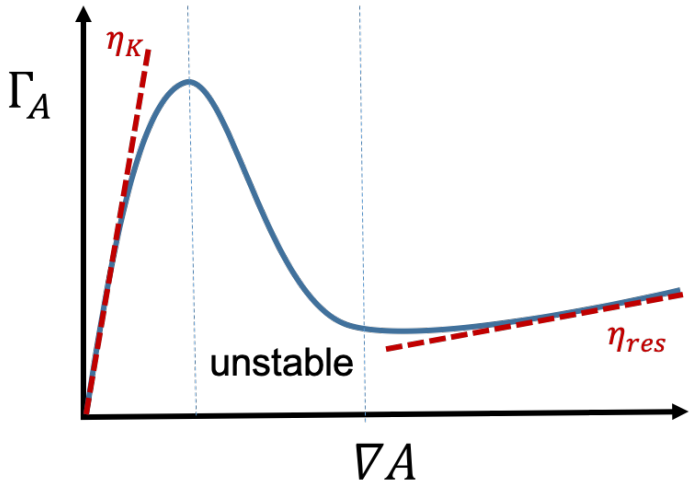

Figure 4.7: A sketch showing the relationship between flux Γ_A and ∇A. The total resistivity is $\eta_{tot} = \delta\Gamma_A/\delta\nabla A$, and is composed of turbulent and collisional parts $\eta_{tot} = \eta_T + \eta$. In the small B limit, $\eta_{tot} \sim \eta_K$; in the large B limit, the residual resistivity is $\eta_{res} \sim \frac{ul}{\mathrm{Rm}\frac{1}{\mu_0\rho}\langle B\rangle^2/\langle v^2\rangle + \mathrm{Rm}\frac{1}{\mu_0\rho}\frac{\langle A^2\rangle}{L_{blob}^2}/\langle v^2\rangle} + \eta$. The transition between the two limits is the transport bifurcation.

4.4 Layering of magnetic potential

Inhomogeneous mixing and bistability (of which negative viscosity is a symptom) are the key elements in the dynamics of layering (i.e. staircase formation) in many systems [3, 1, 2]. Given that, and the ubiquitous blob-and-barrier structure here, it is natural to ask if spontaneous layering can occur in 2D MHD. We answer in the affirmative – see Fig. 4.2 column (d). The initial condition in Run3 is the same bimodal one as for Run1. The key difference in parameters is the forcing scale, which is smaller here, i.e. $k = 32$ in Run3, rather than $k = 5$ for the other runs. As shown in Fig. 4.4 (c), the layered structure consists of regions of homogenized A, with small transition layers of sharp gradients in A (and thus B^2) between them. Layering thus induces

transport barriers. The layered structure persists for the duration of the suppression stage, but coarsens, as shown in Fig. 4.4 (c). Coarsening occurs by a sequence of blob mergers. Note that by $t \sim 4$ the staircase has coarsened to four transition layers. We note that closure theory for the evolution of $\langle A^2 \rangle_{\mathbf{k}}$ predict a positive turbulent hyper-resistivity along with the negative component of the turbulent resistivity [27, 26]. This implies that evolution equation for mean $\langle A \rangle$ has a structure much like the Cahn-Hilliard equation, the solutions of which are known to manifest mergers and coarsening [32].

4.5 Conclusions

In summary, we observe a blob-and-barrier real space structure in the decay of magnetic fields in turbulent 2D MHD. The magnetic field and the resulting barriers are highly intermittent, and cannot be treated by mean field theory. The turbulent resistivity is suppressed in the barriers, where the magnetic fields are strong. The barriers form at blob interstices. For small scale forcing, spontaneous layering of magnetic potential occurs due to inhomogeneous mixing. Barriers form between layers. The layered structure coarsens in time.

This analysis has implications beyond 2D. One line of development is to the quenching of transport of magnetic helicity and magnetic dynamo processes by spatially intermittent but locally strong magnetic fields. The other is to anomalous dissipation in anisotropically ordered 3D systems, such as reduced MHD, where the nonlinear dynamics are effectively two dimensional. These topics will be pursued in the future.

Acknowledgments

This research was supported by the US Department of Energy, Office of Science, Office of Fusion Energy Sciences, under Award No. DE-FG02-04ER54738 and CMTFO Award No.

DE-SC0008378.

Chapter 4 is a reprint of the material as it appears in Xiang Fan, P.H. Diamond, L. Chacón, "Spontaneous transport barriers quench turbulent resistivity in two-dimensional magnetohydrodynamics", *Phys. Rev. E (Rap. Comm.)*, 99 (4), 041201, 2019. The dissertation author was the primary investigator and author of this paper.

Chapter 5

Summary and Future Work

5.1 Summary

In this dissertation, we have studied 2D CHNS and 2D MHD as examples of active scalar turbulence systems, with emphasis on cascades and spectra, real space structure, and inhomogeneous mixing and transport. The key results are summarized below.

In Chapter 2, we analyze the similarities and differences between 2D CHNS and 2D MHD, and study cascades and spectra in 2D CHNS. The conserved quantities are analogous, and both systems exhibit dual cascades. Moreover, the CHNS system supports an elastic wave, which resembles the Alfven wave in MHD. The origin of the inverse cascade for 2D CHNS is the coalescence of blobs of concentration of the same species. Similarly, it is the coalescence of blobs of magnetic flux for 2D MHD. In 2D CHNS, smaller blobs progressively merge and become larger blobs. The blob size grows as $l \sim t^{2/3}$, until capped by the Hinze scale l_H. The Hinze scale is defined by the balance of turbulent kinetic energy and the elastic energy. An elastic range is observed from the dissipation scale up to Hinze scale $l_d < l < l_H$. In the elastic range, the spectrum for the inverse cascade of mean square concentration is $\langle \psi^2 \rangle_k \sim k^{-7/3}$, and the exponent $-7/3$ is the same for $\langle A^2 \rangle_k$ in 2D MHD. This power law can thus be understood by

the explanation used in 2D MHD. On the other hand, the exponent for the forward cascade is closer to -3 in 2D CHNS, not $-3/2$, as in 2D MHD. The exponent -3 suggests it is more like the forward enstrophy cascade in 2D Navier-Stokes turbulence rather than the forward energy cascade in 2D MHD. This result is plausible because it is observed that the back reaction of surface tension on the fluid is diminished as the blobs coalesce. The back reaction is localized in the interstices between blobs. The packing fraction of such regions decreases as blobs merge. In other words, the inverse cascade of $\langle \psi^2 \rangle$ modifies the forward cascade. The power law for the inverse $\langle \psi^2 \rangle$ cascade is observed to be more robust than the forward energy/enstrophy cascade in 2D CHNS, and it suggests that the inverse cascade is the more fundamental one in this system. This raises the interesting question of: what about other active scalar turbulent systems?

In Chapter 3, we investigated the kinematic evolution of the concentration field in the 2D Cahn-Hilliard system in a background of a single fixed eddy. The analogy between this and flux expulsion phenomenon in 2D MHD is noted and discussed. The concentration field first exhibits a "jelly roll" shape, then a topological change (reconnection) occurs, and the field morphs into a "target" shape, which means the bands are in the form of concentric annuli. The target pattern is metastable. The bands merge gradually, and the time scale of the mergers is exponentially long. The change in elastic energy is episodic during the target pattern stage. Dips in the energy evolution plot corresponds to the band mergers. A characteristic time scale in this system is the time to reach the maximum elastic energy. This time scale is shown to be approximately $\sim \xi^2/D$. The band merger process resembles step merger in drift-ZF staircases. The general lesson is that negative diffusion can lead to the formation of novel patterns in simple systems, and the formation of target pattern in single eddy mixing is a good example.

In Chapter 4, turbulent transport in active scalar systems is studied. We initially planned to first repeat the classic problem of suppression of turbulent transport in decaying 2D MHD turbulence for the purpose of code verification, and then study the corresponding phenomenon in 2D CHNS. However, in 2D MHD, a surprising new phenomenon appears for higher Rm, and

it is worth deeper investigation. Without an externally imposed large scale magnetic field, no well defined mean B is observed. Instead, a blob-and-barrier real space structure spontaneously emerges. The conventional understanding is based on mean field theory, which is not applicable in this case. The magnetic energy is concentrated in the barriers, which are located in the interstices between blobs of magnetic potential. The barriers are highly intermittent, and mixing of magnetic potential is inhomogeneous. The turbulent transport is quenched more heavily in the barrier regions where magnetic fields are strongest. The spontaneous formation of the barriers is due to negative diffusion, which ultimately follows from flux coalescence and the inverse cascade of $\langle A^2 \rangle$. For small scale external forcing (of the fluid), a layering (or staircase) of magnetic potential can occur, with barriers located in the interstices of layers. The layering is observed to coarsen in time. This layering can also be explained by a negative diffusion mechanism. Such a phenomenon is relevant to the $\mathbf{E} \times \mathbf{B}$ staircase in fusion studies.

In general, broader lessons for active scalar systems are learned beyond the specifics of 2D CHNS and 2D MHD. The studies in this dissertation illustrate that dual (or multiple) cascades can interact with each other, and one can modify another. One example is the inverse cascade of $\langle \psi^2 \rangle$ can reduce the region of active elastic back reaction and thus alter the forward cascade in 2D CHNS. We also show how a length scale, for example the Hinze scale in 2D CHNS, emerges from the balance of kinetic energy and elastic energy in blobby turbulence. This length scale is a result of competition between the blob coalescence process and the eddy breakup process. We learn how negative diffusion (flux/blob coalescence) can lead to novel real space structure in a simple system, for example the target pattern in 2D Cahn-Hilliard system. We also learn that negative resistivity can exist (though for a short time) in a simple system such as 2D MHD. This results in the formation of nontrivial real space structure, i.e. the blob-and-barrier structure and layering structure. More generally, we see that studying analogous but different systems can improve our understanding of all of them.

5.2 Future Work

In this dissertation, we mainly focused on two systems, 2D CHNS and 2D MHD as examples of elastic active scalar turbulence systems. Other similar systems can also be studied in this spirit, and be compared to these two in the future. For instance, the Oldroyd-B model for polymer solutions [74, 96, 24] is also an interesting active elastic system.

Another direction of future work is the extension of the transport study in MHD. An obvious extension is the numerical verification of the new η_T expression we proposed. For this, an approach like Lagrangian conditional averaging [39] may be required, because of the motion and evolution of the barriers. There are still a lot of important features remaining to be investigated, for instance: what determines the barrier width and packing fraction in 2D MHD turbulence? Why does layering appear when the forcing scale is small? What determines the step width, in the case of layering? The transport study may also be extended to 3D MHD, with a special note that the inverse cascade of $\langle A^2 \rangle$ in 2D will be replaced by the inverse cascade of $\langle \mathbf{A} \cdot \mathbf{B} \rangle$ in 3D. It will be interesting to investigate how these spatially intermittent, locally strong magnetic fields affect magnetic dynamo processes in 3D MHD. Turbulent transport in CHNS is also an interesting topic for future study. It is natural to extend the theory for MHD to CHNS, because of the many common properties appearing in both systems, especially the blob-and-barrier structure.

Some of our results can be potentially addressed by experiments. Although real physical systems are intrinsically 3D, there are experimental techniques to approximate 2D turbulence. Some widely used experimental realizations of 2D turbulence include thin electrically conducting layers, and soap films [10]. It is possible to further use a stirred binary fluid undergoing spinodal decomposition to realize 2D CHNS turbulence in experiments. It should be easier to take snapshots of the concentration field in 2D than in 3D. Experiments on 2D MHD in plasmas are difficult to realize in the lab. However, it is possible to do 2D MHD experiments on liquid metals [65, 86]. These, however, will have too low an Rm unless stirred vigorously (i.e. by an expensive

motor drive) or unless very large.

Bibliography

[1] Arash Ashourvan and P. H. Diamond. How mesoscopic staircases condense to macroscopic barriers in confined plasma turbulence. *Physical Review E*, 94(5):051202, November 2016. URL: https://link.aps.org/doi/10.1103/PhysRevE.94.051202.

[2] Arash Ashourvan and P. H. Diamond. On the emergence of macroscopic transport barriers from staircase structures. *Physics of Plasmas*, 24(1):012305, January 2017. URL: http://aip.scitation.org/doi/abs/10.1063/1.4973660.

[3] N. J. Balmforth, Stefan G. Llewellyn Smith, and W. R. Young. Dynamics of interfaces and layers in a stratified turbulent fluid. *Journal of Fluid Mechanics*, 355:329–358, January 1998. URL: https://www.cambridge.org/core/journals/journal-of-fluid-mechanics/article/dynamics-of-interfaces-and-layers-in-a-stratified-turbulent-fluid/3B3702F53603A440351FD17C7CCB92EF#.

[4] Ludovic Berthier, Jean-Louis Barrat, and Jorge Kurchan. Phase Separation in a Chaotic Flow. *Phys. Rev. Lett.*, 86(10):2014–2017, March 2001. URL: http://link.aps.org/doi/10.1103/PhysRevLett.86.2014.

[5] S. Berti, G. Boffetta, M. Cencini, and A. Vulpiani. Turbulence and Coarsening in Active and Passive Binary Mixtures. *Phys. Rev. Lett.*, 95(22):224501, November 2005. URL: http://link.aps.org/doi/10.1103/PhysRevLett.95.224501.

[6] D. Biskamp and U. Bremer. Dynamics and Statistics of Inverse Cascade Processes in 2d Magnetohydrodynamic Turbulence. *Phys. Rev. Lett.*, 72(24):3819–3822, June 1994. URL: http://link.aps.org/doi/10.1103/PhysRevLett.72.3819.

[7] D. Biskamp and E. Schwarz. On two-dimensional magnetohydrodynamic turbulence. *Physics of Plasmas (1994-present)*, 8(7):3282–3292, July 2001. URL: http://scitation.aip.org/content/aip/journal/pop/8/7/10.1063/1.1377611.

[8] Dieter Biskamp. *Magnetohydrodynamic Turbulence*. Cambridge University Press, June 2003. URL: https://books.google.com/books?id=6iDZWv2DC-EC&printsec=frontcover#v=onepage&q&f=false.

[9] J. A. Boedo, D. L. Rudakov, R. A. Moyer, G. R. McKee, R. J. Colchin, M. J. Schaffer, P. G. Stangeby, W. P. West, S. L. Allen, T. E. Evans, R. J. Fonck, E. M. Hollmann, S. Krasheninnikov, A. W. Leonard, W. Nevins, M. A. Mahdavi, G. D. Porter, G. R. Tynan, D. G. Whyte, and X. Xu. Transport by intermittency in the boundary of the DIII-D tokamak. *Physics of Plasmas*, 10(5):1670–1677, April 2003. URL: http://aip.scitation.org/doi/abs/10.1063/1.1563259.

[10] Guido Boffetta and Robert E. Ecke. Two-Dimensional Turbulence. *Annual Review of Fluid Mechanics*, 44(1):427–451, January 2012. URL: http://www.annualreviews.org/doi/abs/10.1146/annurev-fluid-120710-101240.

[11] SI Braginskii. Transport processes in a plasma. *Reviews of plasma physics*, 1, 1965. URL: http://adsabs.harvard.edu/abs/1965RvPP....1..205B.

[12] John W Cahn. On spinodal decomposition. *Acta Metallurgica*, 9(9):795–801, September 1961. URL: http://www.sciencedirect.com/science/article/pii/0001616061901821.

[13] John W. Cahn and John E. Hilliard. Free Energy of a Nonuniform System. I. Interfacial Free Energy. *The Journal of Chemical Physics*, 28(2):258–267, February 1958. URL: http://scitation.aip.org/content/aip/journal/jcp/28/2/10.1063/1.1744102.

[14] James A Carlson, Arthur Jaffe, and Andrew Wiles. *The millennium prize problems*. American Mathematical Society Providence, RI, 2006. URL: http://www.claymath.org/library/monographs/MPPc.pdf.

[15] Fausto Cattaneo. On the effects of a weak magnetic field on turbulent transport. *The Astrophysical Journal*, 434:200–205, 1994. URL: http://adsabs.harvard.edu/full/1994ApJ...434..200C.

[16] Faustro Cattaneo and Samuel Vainshtein. Suppression of Turbulent Transport by a Weak Magnetic Field. *The Astrophysical Journal*, 1991. URL: http://adsabs.harvard.edu/full/1991ApJ...376L..21C.

[17] Antonio Celani, Massimo Cencini, Andrea Mazzino, and Massimo Vergassola. Active versus Passive Scalar Turbulence. *Physical Review Letters*, 89(23):234502, November 2002. URL: http://link.aps.org/doi/10.1103/PhysRevLett.89.234502.

[18] Antonio Celani, Massimo Cencini, Andrea Mazzino, and Massimo Vergassola. Active and passive fields face to face. *New Journal of Physics*, 6:72–72, July 2004. URL: http://stacks.iop.org/1367-2630/6/i=1/a=072?key=crossref.69723c59e7bc48b4befc8586a59cec0d.

[19] L. Chacón and D.A. Knoll. A 2D High-β Hall MHD implicit nonlinear solver. *Journal of Computational Physics*, 188(2):573–592, July 2003. URL: http://linkinghub.elsevier.com/retrieve/pii/S0021999103001931.

[20] L. Chacón, D.A. Knoll, and J.M. Finn. An Implicit, Nonlinear Reduced Resistive MHD Solver. *Journal of Computational Physics*, 178(1):15–36, May 2002. URL: http://linkinghub.elsevier.com/retrieve/pii/S0021999102970154.

[21] L. Chacón, D.A. Knoll, and J.M. Finn. Hall MHD effects on the 2d Kelvin-Helmholtz/tearing instability. *Physics Letters A*, 308(2-3):187–197, February 2003. URL: http://linkinghub.elsevier.com/retrieve/pii/S0375960102018078.

[22] J. W. Connor and R. J. Hastie. Two fluid equations for resistive ballooning modes in axisymmetric toroidal plasmas. *Plasma Physics and Controlled Fusion*, 27(6):621, 1985. URL: http://stacks.iop.org/0741-3335/27/i=6/a=001.

[23] Charu Datt, Sumesh P. Thampi, and Rama Govindarajan. Morphological evolution of domains in spinodal decomposition. *Phys. Rev. E*, 91(1):010101, January 2015. URL: http://link.aps.org/doi/10.1103/PhysRevE.91.010101.

[24] P. G. De Gennes. Towards a scaling theory of drag reduction. *Physica A: Statistical Mechanics and its Applications*, 140(1):9–25, December 1986. URL: http://www.sciencedirect.com/science/article/pii/0378437186902001.

[25] P H Diamond, S-I Itoh, K Itoh, and T S Hahm. Zonal flows in plasmaa review. *Plasma Physics and Controlled Fusion*, 47(5):R35–R161, May 2005. URL: http://stacks.iop.org/0741-3335/47/i=5/a=R01?key=crossref.a4dceee0ba00403ce427a135a3569ce5.

[26] P. H. Diamond, Sanae-I. Itoh, and Kimitaka Itoh. *Modern Plasma Physics, Physical Kinetics of Turbulence Plasmas Vol. 1*. Cambridge University Press, 2010. URL: http://www.langtoninfo.com/web_content/9780521869201_frontmatter.pdf.

[27] P. H. Diamond, E. J. Kim, and D. W. Hughes. Self-consistent mean field electrodynamics in two and three dimensions. In *Fluid Dynamics and Dynamos in Astrophysics and Geophysics*, page 145. CRC Press, 2005. URL: https://books.google.com/books?id=PLNwoJ6qFoEC&lpg=PP1&pg=PA145#v=onepage&q&f=false.

[28] D. A. DIppolito, J. R. Myra, and S. J. Zweben. Convective transport by intermittent blob-filaments: Comparison of theory and experiment. *Physics of Plasmas*, 18(6):060501, June 2011. URL: http://aip.scitation.org/doi/abs/10.1063/1.3594609.

[29] Gregory L. Eyink, A. Lazarian, and E. T. Vishniac. FAST MAGNETIC RECONNECTION AND SPONTANEOUS STOCHASTICITY. *The Astrophysical Journal*, 743(1):51, November 2011. URL: https://doi.org/10.1088%2F0004-637x%2F743%2F1%2F51.

[30] Xiang Fan, P. H. Diamond, L. Chacón, and Hui Li. Cascades and spectra of a turbulent spinodal decomposition in two-dimensional symmetric binary liquid mixtures. *Physical Review Fluids*, 1(5):054403, September 2016. URL: http://link.aps.org/doi/10.1103/PhysRevFluids.1.054403.

[31] Xiang Fan, P. H. Diamond, and L. Chacn. Formation and evolution of target patterns in Cahn-Hilliard flows. *Physical Review E*, 96(4):041101, October 2017. URL: https://link.aps.org/doi/10.1103/PhysRevE.96.041101.

[32] Xiang Fan, P. H. Diamond, and L. Chacn. CHNS: A case study of turbulence in elastic media. *Physics of Plasmas*, 25(5):055702, March 2018. URL: https://aip.scitation.org/doi/full/10.1063/1.5016075.

[33] George B. Field and Eric G. Blackman. Dynamical Quenching of the 2 Dynamo. *The Astrophysical Journal*, 572(1):685, June 2002. URL: https://iopscience.iop.org/article/10.1086/340233/meta.

[34] U. Frisch, A. Pouquet, J. Léorat, and A. Mazure. Possibility of an inverse cascade of magnetic helicity in magnetohydrodynamic turbulence. *Journal of Fluid Mechanics*, 68(04):769–778, April 1975. URL: http://journals.cambridge.org/article_S002211207500122X.

[35] Uriel Frisch. *Turbulence: the legacy of AN Kolmogorov*. Cambridge university press, 1995. URL: https://books.google.com/books?id=K-Pf7RuYkf0C&printsec=frontcover#v=onepage&q&f=false.

[36] G. Fuchert, G. Birkenmeier, M. Ramisch, and U. Stroth. Characterization of the blob generation region and blobby transport in a stellarator. *Plasma Physics and Controlled Fusion*, 58(5):054005, 2016. URL: http://stacks.iop.org/0741-3335/58/i=5/a=054005.

[37] H. Furukawa. Spinodal decomposition of two-dimensional fluid mixtures: A spectral analysis of droplet growth. *Phys. Rev. E*, 61(2):1423–1431, February 2000. URL: http://link.aps.org/doi/10.1103/PhysRevE.61.1423.

[38] Andrew D. Gilbert, Joanne Mason, and Steven M. Tobias. Flux expulsion with dynamics. *Journal of Fluid Mechanics*, 791:568–588, March 2016. URL: https://www.cambridge.org/core/journals/journal-of-fluid-mechanics/article/flux-expulsion-with-dynamics/0936A7CDF7F23929806AF926681780EC.

[39] D. Grasso, F. Califano, F. Pegoraro, and F. Porcelli. Phase mixing and island saturation in hamiltonian reconnection. *Phys. Rev. Lett.*, 86:5051–5054, May 2001. URL: https://link.aps.org/doi/10.1103/PhysRevLett.86.5051.

[40] A. V. Gruzinov and P. H. Diamond. Self-consistent theory of mean-field electrodynamics. *Physical Review Letters*, 72(11):1651–1653, March 1994. URL: https://link.aps.org/doi/10.1103/PhysRevLett.72.1651.

[41] A. V. Gruzinov and P. H. Diamond. Nonlinear mean field electrodynamics of turbulent dynamos. *Physics of Plasmas*, 3(5):1853–1857, May 1996. URL: https://aip.scitation.org/doi/10.1063/1.871981.

[42] Francisco Guilln-Gonzlez and Giordano Tierra. Second order schemes and time-step adaptivity for AllenCahn and CahnHilliard models. *Computers & Mathematics with Applications*, 68(8):821–846, October 2014. URL: http://www.sciencedirect.com/science/article/pii/S0898122114003320.

[43] Akira Hasegawa and Kunioki Mima. Pseudothreedimensional turbulence in magnetized nonuniform plasma. *The Physics of Fluids*, 21(1):87–92, January 1978. URL: http://aip.scitation.org/doi/abs/10.1063/1.862083.

[44] Akira Hasegawa and Masahiro Wakatani. Plasma Edge Turbulence. *Physical Review Letters*, 50(9):682–686, February 1983. URL: https://link.aps.org/doi/10.1103/PhysRevLett.50.682.

[45] Akira Hasegawa and Masahiro Wakatani. Self-organization of electrostatic turbulence in a cylindrical plasma. *Physical Review Letters*, 59(14):1581–1584, October 1987. URL: https://link.aps.org/doi/10.1103/PhysRevLett.59.1581.

[46] Takeji Hashimoto, Katsuo Matsuzaka, Elisha Moses, and Akira Onuki. String Phase in Phase-Separating Fluids under Shear Flow. *Physical Review Letters*, 74(1):126–129, January 1995. URL: http://link.aps.org/doi/10.1103/PhysRevLett.74.126.

[47] Takeji Hashimoto, Tomoaki Takebe, and Koji Asakawa. Phase transition of polymer mixtures under simple shear flow. *Physica A: Statistical Mechanics and its Applications*, 194(1):338–351, March 1993. URL: http://www.sciencedirect.com/science/article/pii/037843719390367D.

[48] R. J. Hastie, J. J. Ramos, and F. Porcelli. Drift ballooning instabilities in tokamak edge plasmas. *Physics of Plasmas*, 10(11):4405–4412, October 2003. URL: http://aip.scitation.org/doi/10.1063/1.1612499.

[49] J. O. Hinze. Fundamentals of the hydrodynamic mechanism of splitting in dispersion processes. *AIChE J.*, 1(3):289–295, September 1955. URL: http://onlinelibrary.wiley.com/doi/10.1002/aic.690010303/abstract.

[50] P Iroshnikov. Turbulence of a Conducting Fluid in a Strong Magnetic Field. *Soviet Astronomy*, 1964. URL: http://adsabs.harvard.edu/full/1964SvA.....7..566I.

[51] Shane R. Keating and P. H. Diamond. Turbulent Diffusion of Magnetic Fields in Two-Dimensional Magnetohydrodynamic Turbulence with Stable Stratification. *Physical Review Letters*, 99(22):224502, November 2007. URL: https://link.aps.org/doi/10.1103/PhysRevLett.99.224502.

[52] Shane R. Keating and P. H. Diamond. Turbulent resistivity in wavy two-dimensional magnetohydrodynamic turbulence. *Journal of Fluid Mechanics*, 595:173–202, January 2008. URL: https://doi.org/10.1017/S002211200700941X.

[53] Shane R. Keating, L. J. Silvers, and P. H. Diamond. On Cross-Phase and the Quenching of the Turbulent Diffusion of Magnetic Fields in Two Dimensions. *The Astrophysical Journal Letters*, 678(2):L137, 2008. URL: http://stacks.iop.org/1538-4357/678/i=2/a=L137.

[54] V. M. Kendon, J-C. Desplat, P. Bladon, and M. E. Cates. 3d Spinodal Decomposition in the Inertial Regime. *Phys. Rev. Lett.*, 83(3):576–579, July 1999. URL: http://link.aps.org/doi/10.1103/PhysRevLett.83.576.

[55] Vivien M. Kendon, Michael E. Cates, Ignacio Pagonabarraga, J.-C. Desplat, and Peter Bladon. Inertial effects in three-dimensional spinodal decomposition of a symmetric binary fluid mixture: a lattice Boltzmann study. *Journal of Fluid Mechanics*, 440:147–203, August 2001. URL: http://journals.cambridge.org/article_S0022112001004682.

[56] Eun-jin Kim. Consistent Theory of Turbulent Transport in Two-Dimensional Magnetohydrodynamics. *Physical Review Letters*, 96(8):084504, March 2006. URL: https://link.aps.org/doi/10.1103/PhysRevLett.96.084504.

[57] Nathan Kleeorin and Igor Rogachevskii. Nonlinear turbulent magnetic diffusion and effective drift velocity of a large-scale magnetic field in two-dimensional magnetohydrodynamic turbulence. *Physical Review E*, 75(6):066315, June 2007. URL: https://link.aps.org/doi/10.1103/PhysRevE.75.066315.

[58] A. Kolmogorov. The Local Structure of Turbulence in Incompressible Viscous Fluid for Very Large Reynolds' Numbers. *Akademiia Nauk SSSR Doklady*, 30:301–305, 1941. URL: http://adsabs.harvard.edu/abs/1941DoSSR..30..301K.

[59] Todor Kondi, David W. Hughes, and Steven M. Tobias. The Decay of a Weak Large-scale Magnetic Field in Two-dimensional Turbulence. *The Astrophysical Journal*, 823(2):111, 2016. URL: http://stacks.iop.org/0004-637X/823/i=2/a=111.

[60] Robert H. Kraichnan. Inertial-Range Spectrum of Hydromagnetic Turbulence. *Physics of Fluids*, 8(7):1385, 1965. URL: http://scitation.aip.org/content/aip/journal/pof1/8/7/10.1063/1.1761412.

[61] Robert H Kraichnan. Inertial ranges in two-dimensional turbulence. *The Physics of Fluids*, 10(7):1417–1423, 1967. URL: https://aip.scitation.org/doi/10.1063/1.1762301.

[62] A. Lazarian and Ethan T. Vishniac. Reconnection in a Weakly Stochastic Field. *The Astrophysical Journal*, 517(2):700–718, June 1999. URL: https://doi.org/10.1086%2F307233.

[63] J. C. Li and P. H. Diamond. Negative viscosity from negative compressibility and axial flow shear stiffness in a straight magnetic field. *Physics of Plasmas*, 24(3):032117, March 2017. URL: http://aip.scitation.org/doi/abs/10.1063/1.4978956.

[64] J. C. Li, P. H. Diamond, X. Q. Xu, and G. R. Tynan. Dynamics of intrinsic axial flows in unsheared, uniform magnetic fields. *Physics of Plasmas*, 23(5):052311, May 2016. URL: http://aip.scitation.org/doi/10.1063/1.4950830.

[65] O Lielausis. Dynamo theory and liquid metal mhd experiments. *Astronomische Nachrichten*, 315(4):303–317, 1994. URL: https://onlinelibrary.wiley.com/doi/abs/10.1002/asna.2103150407.

[66] Ju Liu, Luca Dedè, John A Evans, Micheal J Borden, and Thomas J. R. Hughes. Isogeometric analysis of the advective CahnHilliard equation: Spinodal decomposition under shear flow. *Journal of Computational Physics*, 242:321–350, June 2013. URL: http://www.sciencedirect.com/science/article/pii/S0021999113001186.

[67] J. Mak, S. D. Griffiths, and D. W. Hughes. Vortex disruption by magnetohydrodynamic feedback. *Physical Review Fluids*, 2(11):113701, November 2017. URL: https://link.aps.org/doi/10.1103/PhysRevFluids.2.113701.

[68] W. H. Matthaeus, A. Pouquet, P. D. Mininni, P. Dmitruk, and B. Breech. Rapid Alignment of Velocity and Magnetic Field in Magnetohydrodynamic Turbulence. *Phys. Rev. Lett.*, 100(8):085003, February 2008. URL: http://link.aps.org/doi/10.1103/PhysRevLett.100.085003.

[69] N. Mattor and P. H. Diamond. Momentum and thermal transport in neutralbeamheated tokamaks. *The Physics of Fluids*, 31(5):1180–1189, May 1988. URL: http://aip.scitation.org/doi/abs/10.1063/1.866747.

[70] Pablo D. Mininni, David C. Montgomery, and Annick G. Pouquet. A numerical study of the alpha model for two-dimensional magnetohydrodynamic turbulent flows. *Physics of Fluids*, 17(3):035112, March 2005. URL: https://aip.scitation.org/doi/abs/10.1063/1.1863260.

[71] H. K. Moffatt. *Magnetic field generation in electrically conducting fluids*. Cambridge University Press, 1983. URL: https://books.google.com/books/about/Magnetic_Field_Generation_in_Electricall.html?id=cAo4AAAAIAAJ.

[72] H. K. Moffatt and H. Kamkar. On the time-scale associated with flux expulsion. *Stellar and Planetary Magnetism (ed. AM Soward)*, pages 91–97, 1983. URL: http://www.igf.fuw.edu.pl/KB/HKM/PDF/HKM_045.pdf.

[73] Lennon Ó Náraigh and Jean-Luc Thiffeault. Bubbles and filaments: Stirring a Cahn-Hilliard fluid. *Phys. Rev. E*, 75(1):016216, January 2007. URL: http://link.aps.org/doi/10.1103/PhysRevE.75.016216.

[74] JG Oldroyd. On the formulation of rheological equations of state. *Proceedings of the Royal Society of London. Series A. Mathematical and Physical Sciences*, 200(1063):523–541, 1950. URL: https://royalsocietypublishing.org/doi/abs/10.1098/rspa.1950.0035.

[75] Nairita Pal, Prasad Perlekar, Anupam Gupta, and Rahul Pandit. Binary-Fluid Turbulence: Signatures of Multifractal Droplet Dynamics and Dissipation Reduction. *arXiv:1512.09331 [cond-mat, physics:physics]*, December 2015. arXiv: 1512.09331. URL: http://arxiv.org/abs/1512.09331.

[76] Nairita Pal, Prasad Perlekar, Anupam Gupta, and Rahul Pandit. Binary-fluid turbulence: Signatures of multifractal droplet dynamics and dissipation reduction. *Physical Review E*, 93(6):063115, June 2016. URL: https://link.aps.org/doi/10.1103/PhysRevE.93.063115.

[77] Rahul Pandit, Debarghya Banerjee, Akshay Bhatnagar, Marc Brachet, Anupam Gupta, Dhrubaditya Mitra, Nairita Pal, Prasad Perlekar, Samriddhi Sankar Ray, Vishwanath Shukla, and Dario Vincenzi. An overview of the statistical properties of two-dimensional turbulence in fluids with particles, conducting fluids, fluids with polymer additives, binary-fluid mixtures, and superfluids. *Physics of Fluids*, 29(11):111112, October 2017. URL: http://aip.scitation.org/doi/abs/10.1063/1.4986802.

[78] Prasad Perlekar, Roberto Benzi, Herman J. H. Clercx, David R. Nelson, and Federico Toschi. Spinodal Decomposition in Homogeneous and Isotropic Turbulence. *Physical Review Letters*, 112(1):014502, January 2014. URL: http://link.aps.org/doi/10.1103/PhysRevLett.112.014502.

[79] Prasad Perlekar, Luca Biferale, Mauro Sbragaglia, Sudhir Srivastava, and Federico Toschi. Droplet size distribution in homogeneous isotropic turbulence. *Physics of Fluids*, 24(6):065101, June 2012. URL: http://scitation.aip.org/content/aip/journal/pof2/24/6/10.1063/1.4719144.

[80] Prasad Perlekar, Nairita Pal, and Rahul Pandit. Two-dimensional Turbulence in Symmetric Binary-Fluid Mixtures: Coarsening Arrest by the Inverse Cascade. *arXiv:1506.08524 [cond-mat, physics:physics]*, June 2015. arXiv: 1506.08524. URL: http://arxiv.org/abs/1506.08524.

[81] Prasad Perlekar, Nairita Pal, and Rahul Pandit. Two-dimensional Turbulence in Symmetric Binary-Fluid Mixtures: Coarsening Arrest by the Inverse Cascade. *Scientific Reports*, 7:44589, March 2017. URL: http://www.nature.com/srep/2017/170321/srep44589/full/srep44589.html.

[82] Stephen B Pope and Stephen B Pope. *Turbulent flows*. Cambridge university press, 2000. URL: https://books.google.com/books?id=HZsTw9SMx-0C&printsec=frontcover#v=onepage&q&f=false.

[83] David Porter. *Phase Transformations in Metals and Alloys*. 1981.

[84] A. Pouquet. On two-dimensional magnetohydrodynamic turbulence. *Journal of Fluid Mechanics*, 88(01):1–16, 1978. URL: https://aip.scitation.org/doi/10.1063/1.1377611.

[85] A. Pouquet, U. Frisch, and J. L'eorat. Strong MHD helical turbulence and the nonlinear dynamo effect. *Journal of Fluid Mechanics*, 77(02):321–354, 1976. URL: http://journals.cambridge.org/abstract_S0022112076002140.

[86] Kian Rahbarnia, Benjamin P Brown, Mike M Clark, Elliot J Kaplan, Mark D Nornberg, Alex M Rasmus, Nicholas Zane Taylor, Cary B Forest, Frank Jenko, Angelo Limone, et al.

Direct observation of the turbulent emf and transport of magnetic field in a liquid sodium experiment. *The Astrophysical Journal*, 759(2):80, 2012. URL: https://iopscience.iop.org/article/10.1088/0004-637X/759/2/80.

[87] P. B. Rhines and W. R. Young. How rapidly is a passive scalar mixed within closed streamlines? *Journal of Fluid Mechanics*, 133:133–145, 1983. URL: http://journals.cambridge.org/article_S0022112083001822.

[88] Peter B. Rhines and William R. Young. Homogenization of potential vorticity in planetary gyres. *Journal of Fluid Mechanics*, 122:347–367, September 1982. URL: http://journals.cambridge.org/article_S0022112082002250.

[89] Ricardo Ruiz and David R. Nelson. Turbulence in binary fluid mixtures. *Physical Review A*, 23(6):3224, 1981. URL: http://journals.aps.org/pra/abstract/10.1103/PhysRevA.23.3224.

[90] S. Servidio, W. H. Matthaeus, M. A. Shay, P. A. Cassak, and P. Dmitruk. Magnetic Reconnection in Two-Dimensional Magnetohydrodynamic Turbulence. *Phys. Rev. Lett.*, 102(11):115003, March 2009. URL: http://link.aps.org/doi/10.1103/PhysRevLett.102.115003.

[91] Boris I Shraiman and Eric D Siggia. Scalar turbulence. *Nature*, 405(6787):639, 2000. URL: https://www.nature.com/articles/35015000.

[92] Eric D. Siggia. Late stages of spinodal decomposition in binary mixtures. *Phys. Rev. A*, 20(2):595–605, August 1979. URL: http://link.aps.org/doi/10.1103/PhysRevA.20.595.

[93] L. J. Silvers. Dynamic effects of a magnetic field on diffusion in a chaotic flow. *Physics Letters A*, 334(5):400–405, January 2005. URL: http://www.sciencedirect.com/science/article/pii/S0375960104016408.

[94] L. J. Silvers. On the choice of boundary conditions when studying the turbulent diffusion of magnetic fields. *Monthly Notices of the Royal Astronomical Society*, 367(3):1155–1162, April 2006. URL: https://academic.oup.com/mnras/article/367/3/1155/1040944/On-the-choice-of-boundary-conditions-when-studying.

[95] Victor P. Starr. *Physics of Negative Viscosity Phenomena*. McGraw-Hill, 1968. URL: http://agris.fao.org/agris-search/search.do?recordID=US201300315890.

[96] M. Tabor and P. G. de Gennes. A Cascade Theory of Drag Reduction. *EPL*, 2(7):519, 1986. URL: http://stacks.iop.org/0295-5075/2/i=7/a=005.

[97] G. Tierra and F. Guilln-Gonzlez. Numerical Methods for Solving the CahnHilliard Equation and Its Applicability to Related Energy-Based Models. *Arch Computat Methods Eng*, pages 1–21, May 2014. URL: http://link.springer.com/article/10.1007/s11831-014-9112-1.

[98] Steven M. Tobias, Patrick H. Diamond, and David W. Hughes. -Plane Magnetohydrodynamic Turbulence in the Solar Tachocline. *ApJ*, 667(1):L113, 2007. URL: http://stacks.iop.org/1538-4357/667/i=1/a=L113.

[99] Samuel Vainshtein and Faustro Cattaneo. Nonlinear Restrictions on Dynamo Action. *The Astrophysical Journal*, 1992. URL: http://articles.adsabs.harvard.edu/full/1992ApJ...393..165V.

[100] Samuel I. Vainshtein and Robert Rosner. On turbulent diffusion of magnetic fields and the loss of magnetic flux from stars. *The Astrophysical Journal*, 376:199–203, July 1991. URL: http://adsabs.harvard.edu/abs/1991ApJ...376..199V.

[101] N. O. Weiss. The Expulsion of Magnetic Flux by Eddies. *Proceedings of the Royal Society of London A: Mathematical, Physical and Engineering Sciences*, 293(1434):310–328, August 1966. URL: http://rspa.royalsocietypublishing.org/content/293/1434/310.

[102] P. W. Xi, X. Q. Xu, and P. H. Diamond. The impact of pedestal turbulence and electron inertia on edge-localized-mode crashes. *Physics of Plasmas*, 21(5):056110, May 2014. URL: https://aip.scitation.org/doi/abs/10.1063/1.4875332.

[103] P.W. Xi, X.Q. Xu, and P.H. Diamond. Phase Dynamics Criterion for Fast Relaxation of High-Confinement-Mode Plasmas. *Physical Review Letters*, 112(8):085001, February 2014. URL: https://link.aps.org/doi/10.1103/PhysRevLett.112.085001.

[104] Ling Zang. Mse 5034 & 6034 lecture 22. Spinodal Decomposition: Part 1: general description and practical implications. URL: https://pubweb.eng.utah.edu/~lzang/images/lecture-22.pdf.

[105] Ya B. Zeldovich. The magnetic field in the two-dimensional motion of a conducting turbulent fluid. *Sov. Phys. JETP*, 4:460–462, 1957. URL: http://jetp.ac.ru/cgi-bin/dn/e_051_03_0493.pdf.